Title
Bistable Electroactive Polymer Material Innovations and Device Explorations

Author
Qiu, Yu

Publication Date
2019

Peer reviewed|Thesis/dissertation

UNIVERSITY OF CALIFORNIA

Los Angeles

Bistable Electroactive Polymer Material Innovations and Device Explorations

A dissertation submitted in partial satisfaction of the requirements of the degree Doctoral of Philosophy in Materials Science and Engineering

by

Yu Qiu

2019

ABSTRACT OF THE DISSERTATION

Bistable Electroactive Polymer Material Innovations and Device Explorations

by

Yu Qiu

Doctor of Philosophy in Materials Science and Engineering

University of California, Los Angeles, 2019

Professor Qibing Pei, Chair

Smart materials are defined as materials that can change their properties to adapt the versatile surrounding environment. Variable stiffness polymer (VSP) represents a highly interesting class of smart material. VSPs change their stiffness in response to the environmental cues such as temperature, light, moisture, magnetic field, etc. Temperature-stimulated VSPs stand out due to their dry and compact formfactor that doesn't require bulky external stimulus sources. Typically, the VSPs, which can also be attributed to shape memory polymers, exhibit a modulus change as high as a few hundred folds across glass transition temperature. The polymer could assume specific rigid shapes at working conditions but can be programed to different ones via deforming at an elevated temperature. Moreover, the stiffness tunability enables VSP to adapt in different working conditions. As one representative of the intelligent polymeric systems, VSPs

have gained significant interest in wearable electronics, bio-inspired robotics and human-assistive devices in recent years. However, the use of most VSPs is limited by the wide glass transition temperature band, especially in human-contact applications. Moreover, the exploration of VSPs has mainly focused on manipulating the polymer network for multiple temporary shapes transition and large elastic energy storage. Little work has been done to increase the stiffness variation, which is vital for VSP's adaptiveness.

The phase-changing bistable electroactive polymer (BSEP) is a unique VSP we synthesized. The BSEP can adjust its modulus over 3000-fold within a narrow temperature band. The stiffness tunability is realized by reversibly crystallizing and melting of nanocrystalline in the polymer network. Unlike most glass transition VSPs, which have a broad transition temperature band of over 30 °C, BSEP possesses a sharp phase transition within 10 °C and a tunable inflection point between 30-50 °C. Such narrow transition band and low inflection point reduce thermal energy consumption and ensure the use of BSEP in human-contact and in-body applications.

This dissertation summarizes important research in material properties explorations (one chapter) and novel devices (two chapters) based on BSEPs. Advancements related to highly compliant and efficient Joule heating electrodes --- a crucial component of VSP devices are also covered. The main body of the dissertation comprises three chapters. The first chapter depicts the research in BSEP's mechanical property engineering. We introduced reversible cross-links and modified the BSEP formulation to achieve high mechanical strain and stress for improved toughness. We also synthesized a composite combining BSEP and bacterial cellulose nanofibrils, resulting in a material with ultrawide tunable stiffness range from tens of kPa to 1 GPa. Such wide stiffness range grants the BSEP more potential applications in various conditions. The second chapter describes a refreshable tactile display using the BSEP and a stretchable serpentine Joule heating electrode. The reported tactile device utilizes the stiffness variation of BSEP to achieve large pixel displacement, high blocking force and compact formfactor with low

activation voltage. The work could open a path to building compact, user-friendly and cost-effective tactile devices for variety of important applications. The third chapter presents a highly sensitive capacitive touch sensor based on the BSEP as a self-conformable smart skin. The device combines the properties of variable stiffness BSEP and touch sensor, which grants the sensor the ability of adapting on various surfaces and in different working conditions. The device integrates sensing and adaptiveness to mimic human skin and presents a novel platform in wearable electronics on epidermis or next generation robotics.

The dissertation of Yu Qiu is approved.

Dwight C. Streit

Ali Mosleh

Yong Chen

Qibing Pei, Committee Chair

University of California, Los Angeles

2019

TABLE OF CONTENT

LIST OF FIGURES

LIST OF TABLES

ACKNOLEDGEMENT

I would like to give my sincerest thanks to my adviser, Professor Qibing Pei, for his precious guidance and financial support during my Ph.D. study. Professor Pei has not only provided me inspiration ideas in research, but also taught me how to lean, think, and work in a scientific way. These are precious advices that will guide me in my future life.

Also, I would like to thank Professor Dwight C. Streit, Professor Ali Mosleh, Professor Christopher S. Lynch, and Professor Yong Chen for serving as my committee members and their inspiring comments.

Especially, I would like to thank Dr. Xiaofeng Liu, Dr. Rujun Ma, Dr. Yuan Meng, Dr. Kwing Tong, Dr. Fangchao Zhao, Dr. Zhi Ren, and Dr. Wei Hu for teaching me research fundamental skills in the lab. Without their training, my research could be far slower and more challenging. I would also like to give my thanks to Mr. Roger (hongxiang) Zhao, Mr. Jason (Zhixin) Xie, Ms. Yu Xie, Mr. Ziyang Zhang, Ms. Erin Askounis, Mr. Zhou Li, Mr. Hexing Yin, Mr. Kareem Youssef, Ms. Zihang Peng, Mr. Roshan Plamthottam, Ms. Jianghan Wu, Mr. Hanxiang Wu, Mr. Jiacheng Fan, Mr. Hao Yu, Ms. Yayun Liu, Mr. Haolun Wang, Ms. Fangyi Guan and other lab colleagues for their help and valuable discussion. Thank you all for being such a good friend. I would thank Ms. Sabrina (Zhiyun) Lu for working together with me in Chapter 3. I also want to thank Dr. James Holbery and Dr. Siyuan Ma from Microsoft and other group members from Applied Science Group in Microsoft for flourishing scientific ideas in Chapter 4. The opportunities of working with those highly intelligent people during my internships there provided me with the insight of industry world and ideas in career planning.

A big thanks to my family, Dr. Weikun Xiao, Mr. Jiancai Qiu, Ms. Aijun Hao, Mr. Fan Xiao, Ms. Yu Gu, for their selfless support and encouragement. Special thanks to my lovely cats, Pumpkin and Oreo. Thank you for being with me all the time.

VITA

2013 B. E.

Polymer Materials and Engineering,

Beijing University of Chemical Technology

PUBLICATIONS

Qiu, Y., Ma, S., Holbery, J., and Pei, Q. (2019), "A Self-Conformable Smart Skin with Sensing and Shape Memory Functions" Under review.

Qiu, Y., Zhang, E., Plamthottam R., and Pei, Q. (2019), "Dielectric elastomer artificial muscle: materials innovations and device explorations" *ACC. Chem. Res.* 52 (2), 316-325.

Qiu, Y., Askounis, E., Guan, F., Peng, Z., Xiao, W., and Pei, Q. (2019), "Dual stimuli-responsive polymer nanocomposite with ultra-wide tunable stiffness range triggered by temperature and humidity" Under review.

Qiu, Y., Lu, Z., and Pei, Q. (2018), "Refreshable Tactile Display based on a Bistable Electroactive Polymer and Stretchable Serpentine Joule Heating electrode." *ACS Appl. Mater. Interfaces*, 10 (29), 24807-24815.

Pei, Q., **Qiu, Y**. (2018), "Refreshable Tactile Display Using Bistable Electroactive Polymer and Deformable Serpentine Electrode", *UC Case No. 2018-435-1*.

Qiu, Y., Ren, Z., Hu, W., Liu, C., and Pei, Q. (2016), "Bistable Electroactive Polymer with Sharp Rigid-to-Rubbery Phase Transition." *Electroactive Polymer Actuators and Devices (EAPAD)*. 9798, 97981U.

Zhang, Y., Zhao, Y., Wu, D., Xue, J., **Qiu, Y.**, Liao, M., Pei, Q., Yang, Y., Goorsky, M., He, X. (2019), "Homogeneous Freestanding Luminescent Perovskite Organogel with Superior Water Stability" Under review.

Xu, Y., Sun, M., Rico, R., Khodambashi, R., Peet, M., Fisher, R., Marvi, H., Berman, S., **Qiu, Y.**, Peng, Z., Aukes, D., He, X. (2019) "Self-motion-sensing Microrobots Based on Stretchable Conductive Photothermally Responsive Hydrogel" Under review.

Chapter 1. Introduction and Dissertation Objectives

1.1.An overview of variable stiffness polymers

Traditional synthetic materials are usually designed and manufactured to have certain fixed mechanical properties that satisfy functional criteria and economic constraints defined by a specific application. For example, the bulletproof vest, made from Kevlar fiber-reinforced composite, has ultrahigh tensile strength and can be used as body armor or aircraft structural part.[1] Steel, which possesses a Young's modulus as high as 200 GPa, is able to provide structural support for most buildings. Rubber band is elastic and stretchable and can be used to tie the hair or strap multiple objects. Silicones have mechanical stiffness close to biological tissues, thus, are widely used in plastic surgeries and management of hypertrophic scarring.[2,3] Those materials have been served well to achieve specific functions for commercial applications. However, in some real-world situations, tunable mechanical properties are desired for materials to be used in applications with changeable working conditions such as in biomedicine, soft robotics, structural engineering, and wearable electronics.

Smart material with tunable properties to adapt versatile outside environment has emerged as a novel material for the engineering field. Variable stiffness polymers (VSPs) represent a highly interesting class of smart materials. VSPs show great potential in adapting changeable working conditions and are highly favored in some applications which require intelligent material system. For example, the morphing structure in smart aircraft where both high stiffness for structural load bearing and low stiffness for configuration change to achieve optimal aerodynamic benefit are required.[4] VSPs are also favored in soft robotic dexterous manipulation.[5] The force required to grasp an egg or tighten a screw is different, which requires materials with tunable stiffness for tunable force output. Another use is in wearable electronics

or exoskeletons. The material should show flexibility to not impede natural body motion, while needs to be stiffened to provide tactile feedback or robotic assistance during operation.

1.2.Natural VSPs

Nature provides good examples of such material systems. As adaption mechanisms, many natural materials show exceptional changes in their stiffness during loading conditions or under new external environments. These changes can be very slow or fast in time. For instance, a slow stiffness variation can be found in plants where diffusion of water for swelling and shrinking are *generally* responsible for the long time changes (Figure 1-1a).[6,7] A much faster stiffness variation can be found in many echinoderms such as Cucumaria frondosa (a sea cucumber) (Figure 1-1b).[8] The stiffening mechanism is enabled by the reinforcement of rigid, high-aspect ratio collagen fibrils in a low-modulus matrix, which creates considerable survival advantages for the sea cucumbers. The stiffness can be softened through decoupling of the nanofibrils modulated by soluble macromolecules from neutrally controlled effector cells. A more familiar example of natural variable stiffness material would be our skeletal muscle.[9,10] Our skeletal muscle can adjust its stiffness via contraction and relaxing, resulting in controllable force output for various body motions.

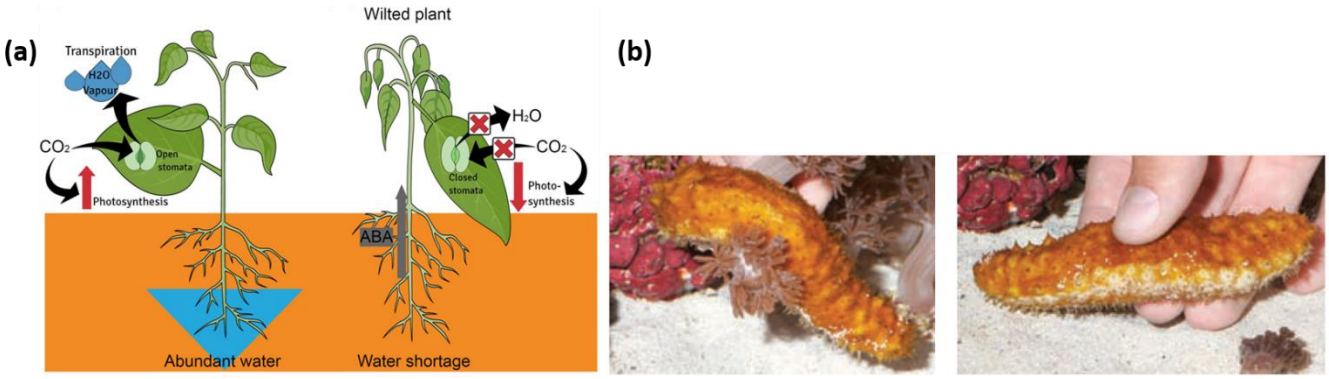

Figure 1-1. (a) Stiffness change of the plant stem due to water stress. Adopted from ref 7. (b) Pictures of a sea cucumber in relaxed (left) and stiffened (right) state. Adopted from ref 8.

All these strategies employed by nature to develop variable stiffness materials are especially inspiring in engineering field. Numerous biologically inspired VSPs have been synthesized for various applications. The strategies can be mainly divided into reversible cross-links or dynamic bonds, insertion or subtraction of external media, and phase transition.

1.3.Synthetic VSPs with dynamic bonds

In the theory of rubber elasticity[11], the tensile modulus *Y* of an ideal elastomer at small strain is determined by:

$$Y = \frac{3\rho RT}{\overline{M_C}} \tag{1-1}$$

Where ρ is the density of the elastomer, R is the gas constant (8.31 J/K-mol),T is the absolute temperature, and $\overline{M_C}$ is the average molecular weight of chain segments between crosslinking sites.[11] $\overline{M_C}$ is related to the polymer chain segment length and characterizes the crosslinking density of an elastomer network, where a larger $\overline{M_C}$ represents a lower crosslinking density. As indicated in Equation (1-1), polymer stiffness is closely related to the chain segment length. Thus, using dynamic bonds to change the chain segment length, or crosslinking density, make the polymer's stiffness adjustable.

1.3.1 Reversible covalent bonds: Diels-Alder reaction

Diels-Alder (DA) reaction offers an effective method to form thermo-reversible covalent bonds, and has been widely utilized in self-healing materials thanks to the good reversibility of the DA reaction.[12,13] Among DA pair, furan derivatives as the diene and maleimide derivatives as the dienophile have drawn great attention due to the fact that they possess a moderate reaction temperature for the forming and breaking of the DA bonds.[14] Hu et al. synthesized polyacrylic-based VSPs that combined furan-maleimide DA adduct moieties (PADA) for tunable stiffness (Figure 1-2a).[15] The furan-maleimide adducts can repeatedly break and reform through a DA reaction, altering the cross-linking density and the elastic moduli. The polymer showed an incremental and reversible modulus change between 0.17 (PADA-4-s) and 0.52 MPa (PADA-4-r) (Figure 1-2b). The stiffness variation of PADA was used to perform different properties where the soft state polymer showed a large electric actuation strain of 35% area expansion at 80 MV/m, while the rigid state polymer achieved high force output of 0.55 MPa at 104 MV/m (Figure 1-2c).[15]

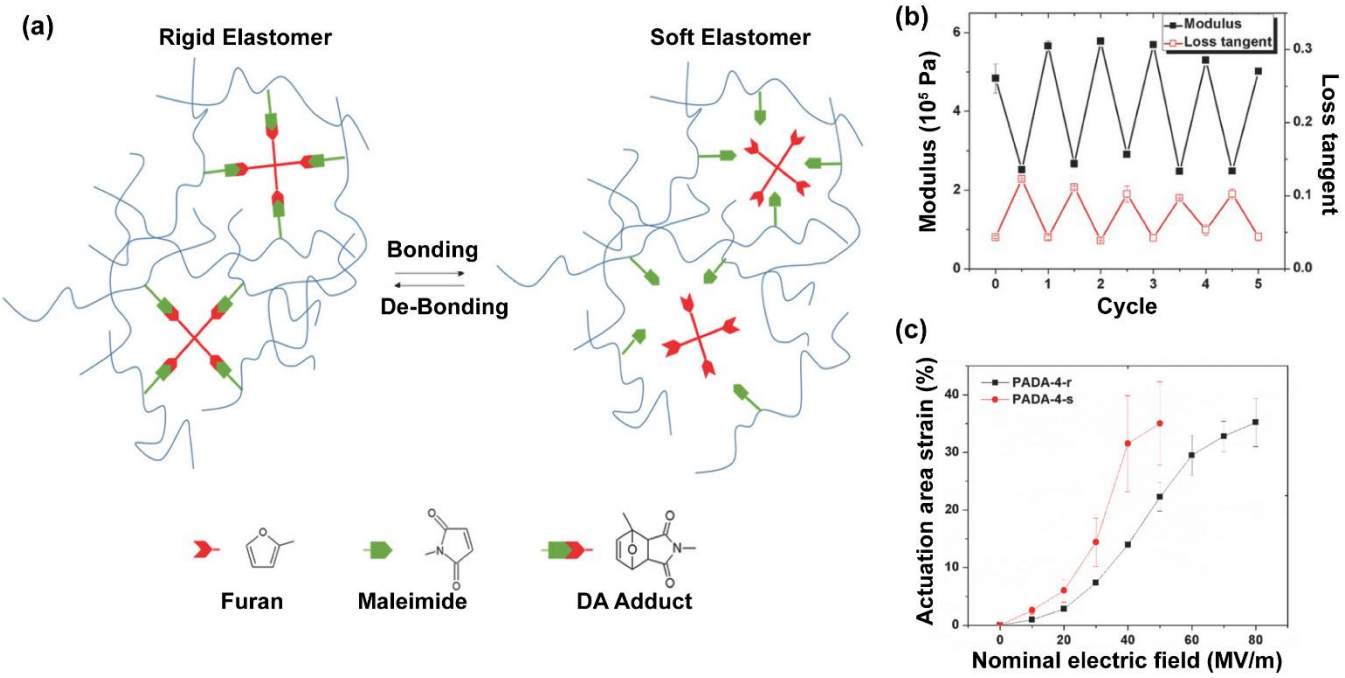

Figure 1-2. Variable stiffness polyacrylate with Diels-Alder bonds. (a) Polyacrylate crosslinked by a thermo-reversible Diels-Alder reaction. (b) Cyclic thermal treatment for modulus reversibility. (c) Areal actuation strain in the soft (PADA-4-s) and rigid (PADA-4-r) state at different electric fields. Adopted from Ref 15.

1.3.2 Reversible non-covalent bonds: hydrogen bonding interaction

Reversible non-covalent bonds, such as hydrogen bonds, also show promises in adjusting the stiffness of polymers.[16–18] Hydrogen bond is one of the most important of all directional intermolecular interactions. Its dissociation energy span more than two orders of magnitude (from about 0.2 to 40 kcal/mol), which is sensitive to temperature or moisture change in the environment. Polymer systems associated with rich hydrogen bonding interactions can demonstrate tunable stiffness due to the dissociation or disrupt of hydrogen bonds. Li et al. reported a lightly crosslinked elastomer with reversible hydrogen bonding groups, ureidopyrimidinone (UPy), can effectively adjust its modulus from about 30 kPa to 15 kPa.[18] The modulus drops with temperature increases, which can be attributed to the hydrogen bonds interactions. At low temperatures, hydrogen bonds act as non-covalent crosslinks and contribute to the storage modulus. At high temperature, hydrogen bonds dissociate, resulting in decreased storage modulus. Another work was reported by Chen et al. in which a moisture-sensitive polymer containing pyridine unit and UPy.[16] It was suggested that the pyridine based molecular shows response to the moisture, thus, serves as a "switch" for hydrogen bonding coupling and dissociation.

1.4.Synthetic VSPs with exchangeable soft media

Another mechanism of administrating the modulus is through controlling the absorption and subtraction of external soft media. As an example, a sponge in the complete dry state can be very rigid, like a chunk of plastic, while a wet or damp sponge is very soft and flexible. The change in the stiffness is due the swelling and deswelling of water. Inspired by this, scientist have investigated polymer system which involves adding filler materials that attract the soft media absorption or designing stimulus switches that can govern the external solvent exchange.

1.4.1. Polypyrrole

Conjugated polymer, such as polypyrrole, have long been studied as an electroactive polymer (EAP) actuator for artificial muscle applications.[19–21] During electrochemical oxidation, charge is removed from the polypyrrole's backbone. Ions from a surrounding electrolyte enter or leave the polymer, serving to maintain charge balance. In the process of changing oxidation state, stiffness, conductivity, optical absorption, permeability, hydrophobicity, and stored charge all change in a controllable manner, enabling transistors, filters, capacitors, and batteries, among other devices, to be constructed.[22] Although the study of polypyrrole has been mainly focused on serving as electroactive polymer, the stiffness variation can be observed during the actuation.[23,24] Pytel et al. conducted an in situ observation of the dynamic elastic modulus of polypyrrole in actions.[25] The modulus was found to be determined by the level of ion swelling. The elastic modulus decreases during the net influx of ions into the bulk polymer and increases as the ions are expelled. The stiffness variation was observed to have up to 3× change upon actuation.[25] Awareness of the variation in modulus is critical to develop the mechanics and loading conditions of polypyrrole-based actuators, as well as understanding the theoretical and practical active stresses and strains one can achieve in a given electrochemical environment.

1.4.2. Pnipam

Poly(N-isopropyl-acrylamide) (PNIPAm) hydrogel is a typical thermosensitive hydrogel with tunable stiffness, which grants it the name "intelligent hydrogel".[26] The unique coil-to-globule transition of PNIPAm chains at lower critical solution temperature (LCST) allows the large temperature-responsive phase transition of the hydrogel and exchange of large amount of water. PNIPAm is characterized by hydrophilic amide (-CONH-) and hydrophobic propyl (-$CH(CH_3)_2$) moieties in the polymer structure. As shown in Figure1-3, when the temperature is low, the hydrophilic amide group is solvated by the water molecules, resulting in low stiffness. When the temperature is elevated, the hydrogen bonding interaction is weakened, and subsequently, the interactions among the hydrophobic propyl groups dominate. The interactions of propyl groups drive the water molecules to be expelled from the hydrogel, resulting in a volume phase transition (VPT) and an increase of the stiffness.[27] The Young's modulus change of PNIPAm was first reported in 1998 by Takigawa et al., where the material possesses a modulus of 9.8 kPa at room temperature and equilibrium state, while at elevated temperature and collapsed state, the modulus of PNIPAm increases to 180 kPa.[27] The change in mechanical behavior enables PNIPAm based hydrogels many capabilities including controllable bending/unbending movement, targeting drug delivering, and shape memory property.[28]

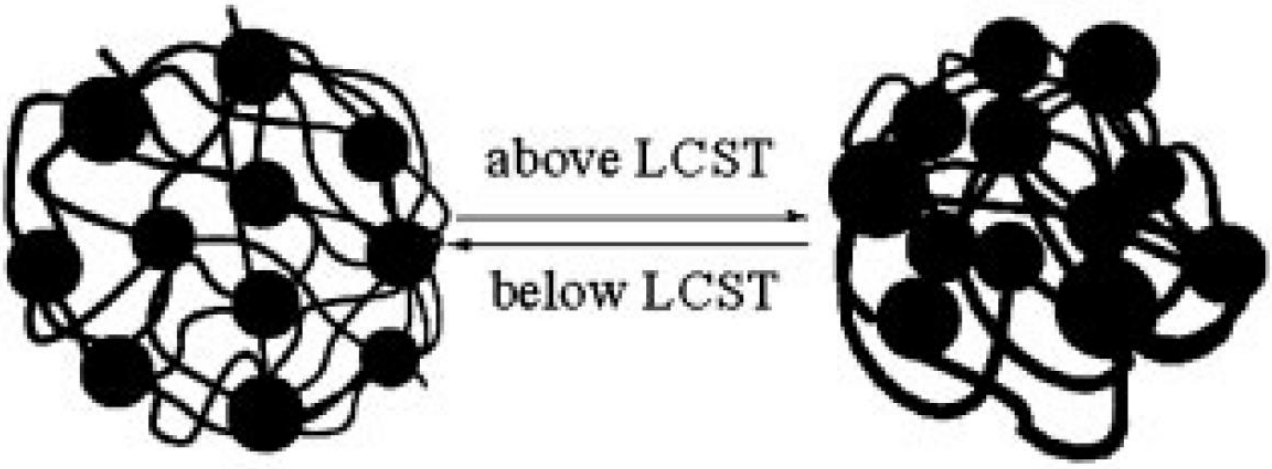

Figure 1-3. Demonstration of PNIPAm swell and de-swell with temperature below and above the LCST respectively. Adopted from ref 26.

1.4.3. Cellulose nanocomposite

Cellulose reinforced nanocomposites have been heavily exploited by Professor Christoph Weder and his team. The materials' design is inspired by the sea cucumber which regulates its stiffness by controlling the stress transfer between adjacent collagen fibrils through transiently established interactions.[8] Professor Weder and the team designed a composite system that comprises cellulose nanofibers and elastomer matrix (Figure 1-4).[8,29,30] The first series of nanocomposites investigated is based on a rubbery ethylene oxide-epichlorohydrin copolymer (EO-EPI) into which a rigid cellulose nanofiber network was incorporated. The soft EO-EPI possesses a low modulus, while the rigid cellulose nanofibers exhibit stiffness as high as 143 GPa due to the high density of strongly interacting surface hydroxyl groups. The resulting composite shows high stiffness due to the self-interactions within cellulose network. Decreased stiffness can be achieved during the process of hydration when the self-interaction is "switched off" by

competitive binding with a hydrogen-bond-forming solvent (Figure 1-4). The composite exhibited a reversible reduction in tensile modulus by a factor 40 from 800 to 20 MPa.[8] A deeper discussion on cellulose reinforced nanocomposites will be discussed in the next chapter.

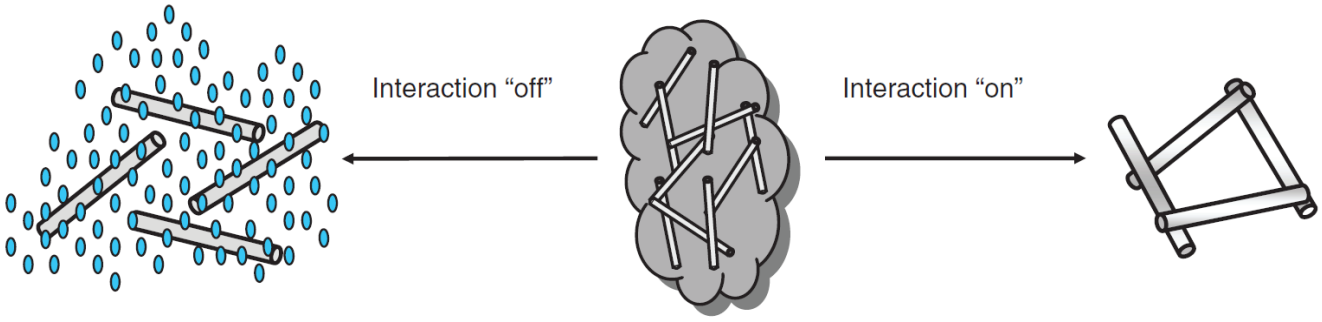

Figure 1-4. Schematic illustration of stiffness changing mechanism of cellulose whisker composite. Adopted from ref 8.

1.5.Synthetic VSPs with phase transition

Compare to the previously discussed VSPs that require exchange with external soft media, phase transition VSPs are more favored in compact and dry systems. This category of VSPs is most investigated and covers semi-crystalline polymers, glass transition polymers, and magneto-rheological elastomers.

1.5.1 Semi-crystalline polymer

The switch for tuning the stiffness of a semi-crystalline polymer is its melting temperature (Tm). Typically, the semi-crystalline polymer provides large chain mobility in the soft state, resulting in faster stiffness change and higher elasticity compare to other phase transition VSPs.[31] The most investigated semi-crystalline VSP system can be classified into three types: (1) polyolefins, for example, the crosslinked

polyethylene[32,33]; (2) polyethers, such as polyurethane (PU) block copolymers[34]; (3) polyesters, in particular poly(ε-caprolactone) (PCL)[35,36]. Among them, PCL, which features low melting temperature close to body temperature, is the most heavily investigated one. In the case for determine the transition temperature for semi-crystalline VSPs, the soft block plays the most crucible role, especially for PCL based polymers.[31] Thus, by controlling the molecular weight of PCL segment in PCL-PU block polymer[37] or controlling the size of crosslinker in PCL polymer network[35], the transition temperature can be adjusted to close to body temperature (Figure 1-5). The storage modulus of PCL network VSP changes from about 650 MPa at room temperature to about 40 MPa at body temperature.[35] Additionally, PCL based VSPs showed excellent biodegradability and biocompatibility, which grants their uses in biomedical applications.[38,39]

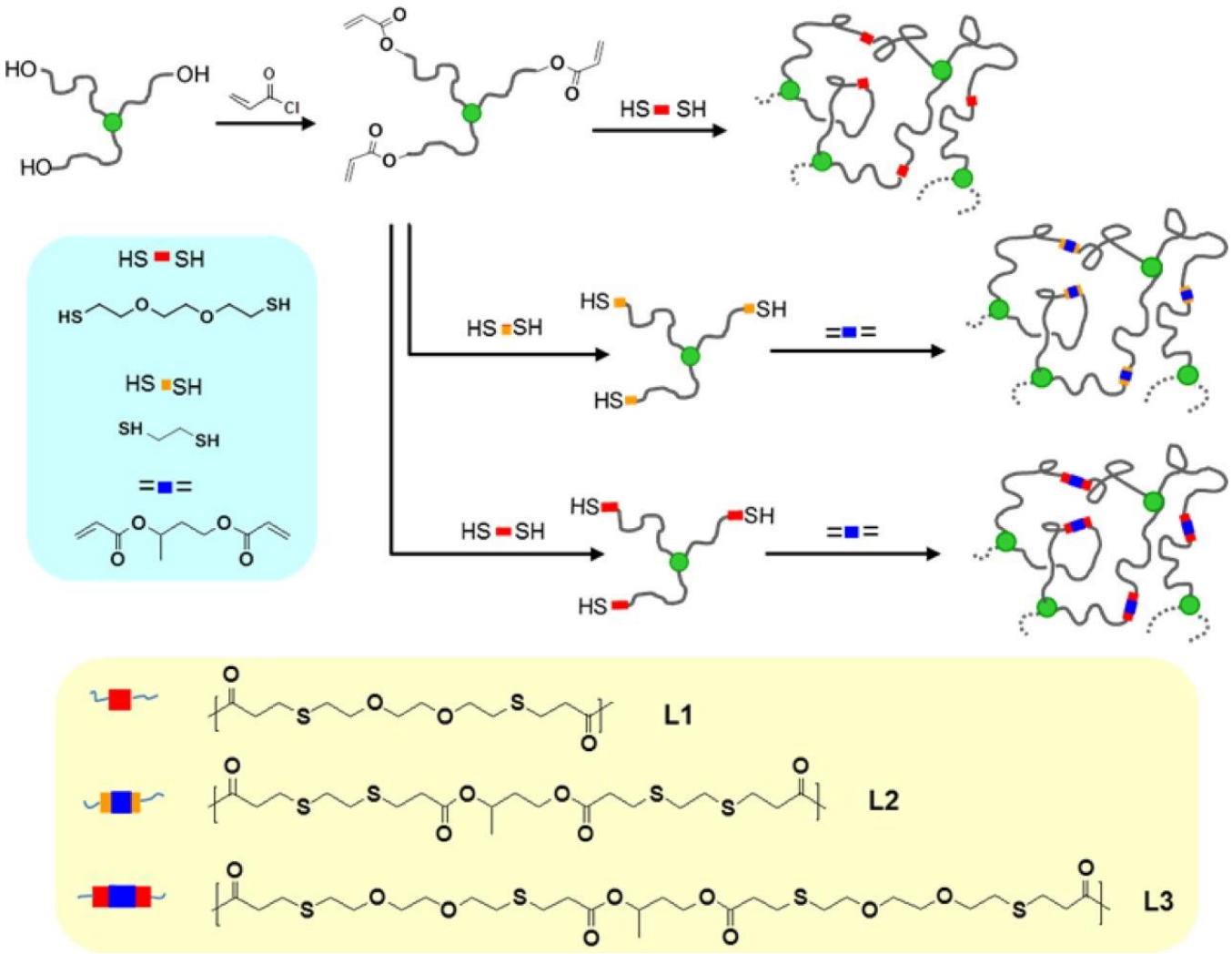

Figure 1-5. Scheme showing network formation with identical PCL cores but different lengths of non-crystalline spacers, L1-L3. Adopted from Ref 35.

1.5.2 Glass transition polymer

VSPs with glass transition switch reveal relative slow stiffness variation compared with Tm-based VSPs due to their broader glass transition interval, which hinders their application where immediate stiffness change is required. Many shape memory polymers fit into this category[40,41], and they have become more attractive in biomedical areas. Slow stiffness change results in slow shape recovery for shape memory

polymers. Such behavior is favored in certain clinical treatments, like Invisalign orthodontic techniques.[42,43] Sharp et al. reported the use of a slow self-deploying Tg-based VSP as neuronal electrode.[44] The polymer possesses a storage modulus as high as 1 GPa at room temperature, and gradually reduces its modulus to 10 MPa at temperature above Tg.[44] The slow stiffness change limits the self-deploying rate for avoiding insertion-induced tissue damage.

1.5.3 magneto-rheological elastomer

Magnetically-induced VSPs are of great interest for medical applications because the materials can be actuated to adjust the stiffness by a non-contact remote mode. A magnetorheological (MR) material is an intelligent material in which rheological properties can be controlled by a magnetic field. It is widely known that the viscosity of a MR fluid changes with application of magnetic field. In the case of a MR solid, the stiffness changes due to the cohesive forces between magnetically polarized particles.[45] Many MR materials have shown changeable stiffness using different soft materials as matrix such as hydrogel[46], polyurethane[47], and nitrile rubber[48,49]. More recently, Mitsumata et al reported a magnetic polyurethane elastomer exhibiting a reversible change of the storage modulus by a factor of 277 upon a magnetic field of 500 mT.[50] The magnetic polyurethane contains 29% (in volume) of carbonyl iron particles and showed a low storage modulus of about 6.45 kPa. With the application of magnetic field, the magnetic particles aligned and form a chain structure, resulting in high storage modulus of 1.55 MPa. The modulus was then dropped to 17.6 kPa when the magnetic field was turned off.[50] Despite the large stiffness difference MR elastomers can achieve, long term stability and reversibility is challenging in this field.

1.6.Bistable electroactive polymer as novel VSP

Bistable electroactive polymers are unique VSPs our group recently invented (Figure 1-6a). BSEPs outperform many other VSPs due to their outstanding performances in mechanical stretchability, tunable stiffness range, as well as suitable transition temperature band. BSEPs were first synthesized for use as dielectric elastomer actuators (DEAs) (Figure 1-6b). DEAs are deformable capacitors. They consist of a thin elastomeric film coated on both sides with compliant electrodes. When an electric field is applied, the electrostatic attraction between opposite charges on the two electrodes generates an electrostatic pressure on the film. This pressure forces the film to contract in thickness and expand in area, and thus, electrical energy is converted into mechanical work.[51] DEAs usually require a low elastic modulus to generate high actuation strain, they lack the stiffness required for structural applications. In addition, DEAs require a continuously applied field to maintain actuation, which consumes energy and reduces device lifetime. We synthesized BSEPs that combine the properties of variable stiffness polymers and DEAs, allowing for rigid-to-rigid actuation.[52–55] At room temperature, BSEPs behave like rigid plastics, but when above their transition temperature (T_r), they enter a rubbery state and can actuate like a DE (Figure 1-6a). Once the temperature is below the T_r, the bias voltage can be removed, and the actuated deformation is preserved. The BSEPs can thus be actuated to variable stable rigid shapes without external energy input to maintain the new shapes.

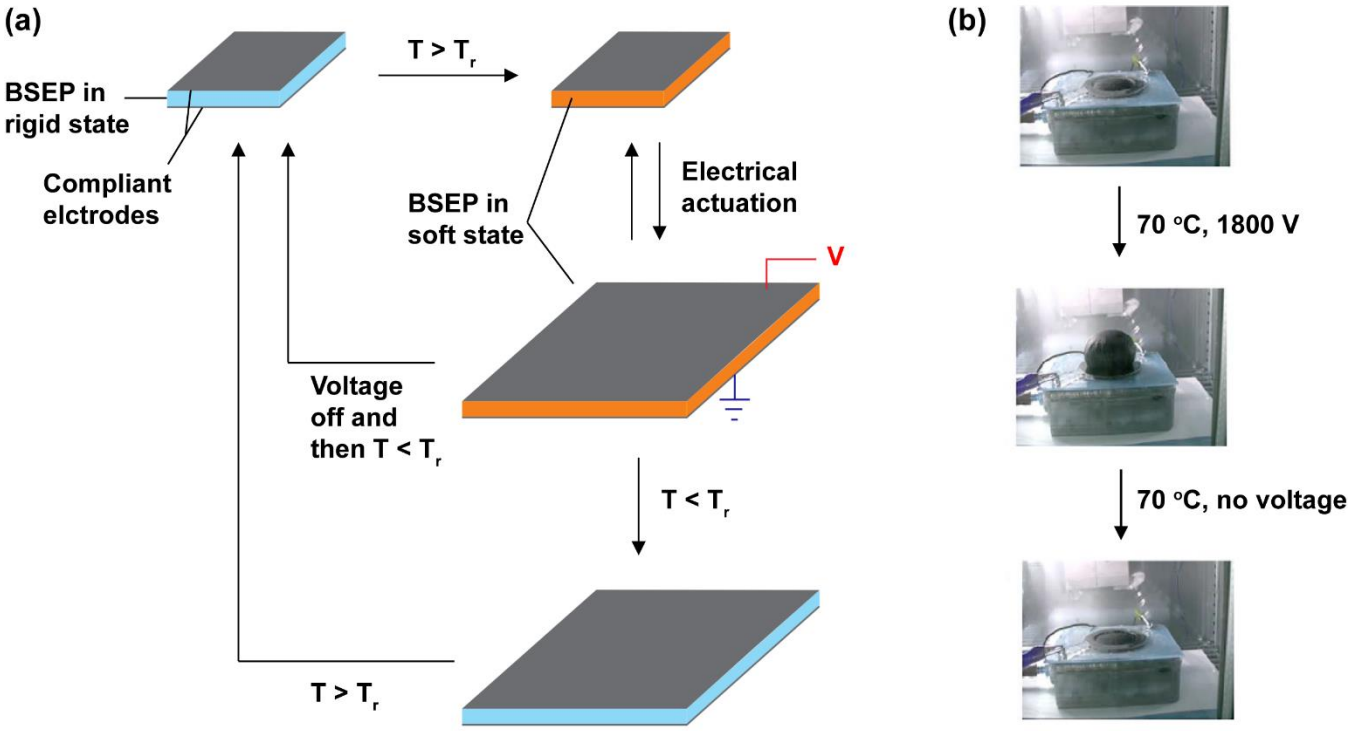

Figure 1-6. BSEP as DE actuators. (a) Working mechanism of a BSEP-based actuator. Adopted from ref 51. (b) Performance of diaphragm actuators using a glass transition BSEP. Adapted from ref 52.

BSEPs are categorized into two groups based on their physical states: glass transition BSEPs[52,53] (Figure 1-7a) and phase-changing BSEPs[54–56] (Figure 1-7b). The first glass transition BSEP we introduced was a linear thermoplastic poly(tert-butyl acrylate) (PTBA).[52] It exhibited a storage modulus change from 1.5 GPa at room temperature to 0.42 MPa at 70 °C (Figure 1-7c).[52] Although the PTBA successfully demonstrated controlled, reversible stiffness change and enough strength for serious mechanical loads, the modulus was not consistent at high temperature. The modulus of linear PTBA continuously decreased with increased temperature in the softened state, which resulted in non-uniform actuation and decreased mechanical strength caused by temperature fluctuations. Niu et al. resolved those issues by crosslinking the PTBA and introducing a second monomer to create an IPN.[53] The crosslinked PTBA-IPN had a constant modulus in the rubbery state and a stiffness change from 1 GPa to 1 MPa (Figure 1-7c, 1-7d).

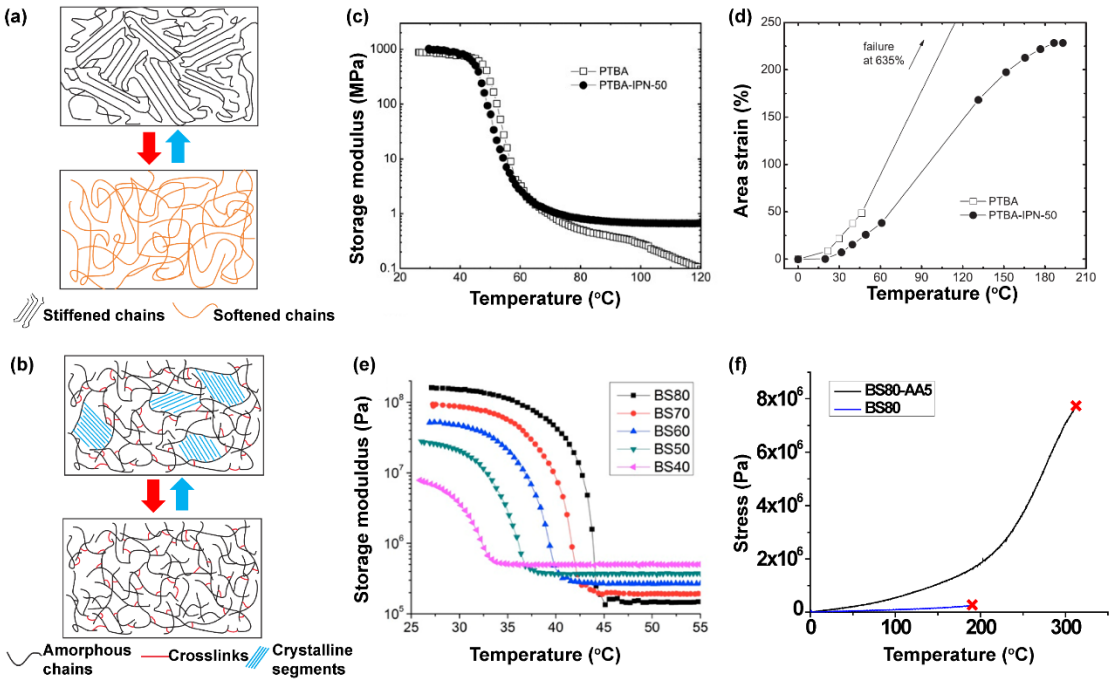

Figure 1-7. Improvements in the mechanical and dielectric properties of BSEP materials. (a) Illustration of the stiffness change of a glass transition BSEP and (b) phase-changing BSEP. Adopted from ref 51. (c) Comparison in modulus-temperature profile and (d) dielectric actuation performance between linear PTBA and crosslinked PTBA-IPN. Adopted from ref 53. (e) Temperature dependence of phase-changing BSEP (BSxx) moduli. Adopted from ref 54. (f) Stress-strain response of BS80-AA5 and BS80 at 50 °C. Adopted from ref 55.

The phase-changing BSEPs, introduced by Ren et al.[54], exhibit drastically narrowed T_r bands to a 10 °C range (Figure 1-7e) and lower inflection point below 50 °C, which is ideal for human-contact applications.[55] The phase changing BSEP mainly comprises of stearyl acrylate (SA) and long chain urethane diacrylate (UDA) and forms a crosslinked polymer network. The narrow transition band results from the rapid crystallization and melting of SA moieties in the polymer network. By varying the ratio between SA and UDA, the modulus and the temperature inflection point can be adjusted to fit in various

applications. With the formula of SA : UDA = 80 : 20, a large storage modulus change of ~1000 fold from 200 MPa to 0.2 MPa can thus be obtained.

1.7. Motivation of this dissertation

Table 1-1. Summary of variable stiffness polymers

Mechanism	Stimuli	VSP name	E_{rigid}	E_{soft}	E_{rigid}/E_{soft}	Reference
Reversible bonds	Diels-Alder reaction	Polyacrylate (Diels-Alder)	0.52 MPa	0.17 MPa	3.1	15
	Hydrogen bond	Ureidopyrimidinone	30 kPa	15 kPa	2	18
External soft media exchange	Redox reaction	PF_6^- doped Polypyrrole	300 MPa	100 MPa	3	25
	Redox reaction	Polypyrrole in $LiClO_4$	310 MPa	180 MPa	1.7	24
	Redox reaction	Polypyrrole in KCl	3.4 GPa	1.4 GPa	2.4	23
	water	Poly(N-isopropyl-acrylamide)	180 kPa	9.8 kPa	18.4	27
	water	EO-EPI cellulose whisker composite	880 MPa	20 MPa	44	8

	water	PVAc cellulose whisker composite	5.3 GPa	12.7 MPa	417	29
Phase transition	Magnetic field	Magnetic polyurethane	1.55 MPa	6.45 kPa	277	50
	Glass transition	Polyurethane block copolymer	2250 MPa	500 MPa	4.5	34
	Glass transition	Epoxy (DP7.1)	1 GPa	10 MPa	100	44
	Glass transition	Poly (tert butyl acrylate)	1.5 GPa	0.42 MPa (not consistent)	N/A	52
	Glass transition	PTBA-IPN	1 GPa	1 MPa	1,000	53
	Melting	poly(ε-caprolactone)	650 MPa	40 MPa	16.3	35
	Melting	BS80	200 MPa	0.2 MPa	1,000	54
	Melting	BS80-AA5	300 MPa	0.1 MPa	3,000	55 (Chapter 3)
Phase transition and external	Melting and water	BC-BSEP composite	1 GPa	40 kPa	30,000	(Chapter 2)

soft media exchange						

Table 1-1 summarizes the reported important variable stiffness polymers. The stiffness range of most synthetic materials can be roughly divided into three parts, including soft region (from 0 - 100 kPa), flexible region (100 kPa - 100 MPa), and rigid region (100 MPa - 10 GPa). A wider stiffness range may grant the material with more opportunities to be used in various areas. For example, a modulus in the GPa range ensures structural supporting or load bearing properties for the material. A MPa-region modulus has moderate stiffness, and usually brings flexibility to the material, such as in the case for most elastomers. A material with modulus in the kPa range matches the modulus of many bio-tissues, and has the opportunity to be used in biologically-related areas. As demonstrated in the Table 1-1, most VSPs with notable tunable stiffness range, including our BSEPs, fall into the flexible and rigid regions. Few VSPs have shown the ability of adjusting the modulus into the soft region which is closely related to biomedical applications. The polymers that have the variable stiffness range in the soft region are mainly hydrogel-based materials. Those hydrogels lack enough mechanical strength for use in many applications that involve stretching or load bearing. Thus, there is a need to develop a new VSP or improve the BSEP for enlarged tunable stiffness range that covers from soft region to rigid region, while maintaining good mechanical properties.

A suitable driving mechanism as well as proper application ideas are required to best utilize the stiffness-variable property of the VSPs. The previously reported BSEPs were mainly used as dielectric elastomer actuators (DEAs) which require high voltage (several kV) for actuation. Such high voltage is dangerous in applications that involve human contact. Although, the BSEP actuator showed privilege over other DEAs by separating the high voltage elements from operator due to its stiffness-variable property, the

concerns for high voltage were not eliminated. Thus, suitable and safe driving mechanisms are favored for BSEP to be used in many applications, which includes the adjustment of stiffness and actuation method.

1.8. Scope and layout of the dissertation

This dissertation consists of five chapters:

Chapter 1 gives the introduction of the background of the variable stiffness polymer. The importance of VSPs in adapting changeable working conditions and certain applications is stated. It then followed by an overview of VSPs in the field by dividing them into three types based on the different variable stiffness mechanisms. The chapter also includes a description of bistable electroactive polymers and their advantages over other VSPs.

Chapter 2 describes the fabrication of bacterial cellulose reinforced BSEP nanocomposite for ultra-wide stiffness tunable range. The composite combines the temperature-responsive phase transition nature from BSEP and water-responsive coupling-decoupling nature from BC filler, resulting in a composite with stiffness change of 25,000 times from nearly 1 GPa to 40 kPa.

Chapter 3 introduces a refreshable tactile display based on BSEP and a stretchable Joule heating electrode in serpentine pattern. The device exploits the large stiffness change of the BSEP polymer and large-strain deformation of the polymer at the softened state, resulting in a high-resolution tactile display that can exert large stroke and provide high blocking force.

Chapter 4 discusses a self-conformable smart skin based on BSEP that has sensing and variable stiffness functions. BSEP based capacitive touch sensor exhibited excellent sensing performance in imitate contact to human skin. The embedded compliant heater element grants the device with the ability to accommodate

irregular surfaces. The integrated multifunctional device mimics the sensing and adaptiveness of human skin and has the potential to be used in areas such as wearable electronics and smart skin for next generation robotics.

1.9.Reference

(1) Yang, H. H.; Yang, H. H. Kevlar Aramid Fiber. *New York Wiley* **1993**, 26–40.

(2) Mullison, E. G. Silicones and Their Uses in Plastic Surgery. *Arch. Otolaryngol.* **1965**, *81* (3), 264–269.

(3) Moustris, G. P.; Hiridis, S. C.; Deliparaschos, K. M.; Konstantinidis, K. M. Evolution of Autnomous and Semi-Autnomous Robotic Surgical Systems: A Review of the Literature. *Int. J. Med. Robot.* **2011**, *7* (April), 375–392.

(4) Sun, J.; Guan, Q.; Liu, Y.; Leng, J. Morphing Aircraft Based on Smart Materials and Structures: A State-of-the-Art Review. *Journal of Intelligent Material Systems and Structures*. 2016.

(5) Okamura, A. M.; Smaby, N.; Cutkosky, M. R. An Overview of Dexterous Manipulation. *Robot. Autom. 2000. Proceedings. ICRA '00. IEEE Int. Conf.* **2000**, *1* (April), 255–262 vol.1.

(6) Fratzl, P.; Barth, F. G. Biomaterial Systems for Mechanosensing and Actuation. *Nature*. 2009.

(7) Vyver, C. V. D.; Peter, S. How Do Plants Deal with Dry Days? *Front. Young Minds* **2017**, *5* (58).

(8) Capadona, J. R.; Shanmuganathan, K.; Tyler, D. J.; Rowan, S. J.; Weder, C. Stimuli-Responsive Polymer Nanocomposites Inspired by the Sea Cucumber Dermis. *Science.* **2008**.

(9) Gollhofer, A.; Schmidtbleicher, D.; Dietz, V. Regulation of Muscle Stiffness in Human

Locomotion. *Int. J. Sports Med.* **1984**.

(10) Sinkjær, T.; Toft, E.; Andreassen, S.; Hornemann, B. C. Muscle Stiffness in Human Ankle Dorsiflexors: Intrinsic and Reflex Components. *J. Neurophysiol.* **1988**.

(11) Brazel, C. S.; Rosen, S. L. *Fundamental Principles of Polymeric Materials*; 2012.

(12) Li, J.; Liang, J.; Li, L.; Ren, F.; Hu, W.; Li, J.; Qi, S.; Pei, Q. Healable Capacitive Touch Screen Sensors Based on Transparent Composite Electrodes Comprising Silver Nanowires and a Furan/Maleimide Diels-Alder Cycloaddition Polymer. *ACS Nano* **2014**.

(13) Liu, Y. L.; Chuo, T. W. Self-Healing Polymers Based on Thermally Reversible Diels-Alder Chemistry. *Polymer Chemistry*. 2013.

(14) Chen, X.; Dan, M. A.; Ono, K.; Mal, A.; Shen, H.; Nutt, S. R.; Sheran, K.; Wudl, F. A Thermally Re-Mendable Cross-Linked Polymeric Material. *Science.* **2002**, *295* (5560), 1698–1702.

(15) Hu, W.; Ren, Z.; Li, J.; Askounis, E.; Xie, Z.; Pei, Q. New Dielectric Elastomers with Variable Moduli. *Adv. Funct. Mater.* **2015**, *25* (30), 4827–4836.

(16) Chen, S.; Hu, J.; Yuen, C. wah; Chan, L. Novel Moisture-Sensitive Shape Memory Polyurethanes Containing Pyridine Moieties. *Polymer (Guildf).* **2009**.

(17) Hu, X.; Zhou, J.; Vatankhah-Varnosfaderani, M.; Daniel, W. F. M.; Li, Q.; Zhushma, A. P.; Dobrynin, A. V.; Sheiko, S. S. Programming Temporal Shapeshifting. *Nat. Commun.* **2016**, *7* (May), 1–7.

(18) Li, J.; Viveros, J. A.; Wrue, M. H.; Anthamatten, M. Shape-Memory Effects in Polymer Networks Containing Reversibly Associating Side-Groups. *Adv. Mater.* **2007**.

(19) Hutchison, A. S.; Lewis, T. W.; Moulton, S. E.; Spinks, G. M.; Wallace, G. G. Development of

Polypyrrole-Based Electromechanical Actuators. *Synth. Met.* **2000**.

(20) Spinks, G. M.; Liu, L.; Wallace, G. G.; Zhou, D. Strain Response from Polypyrrole Actuators under Load. *Adv. Funct. Mater.* **2002**.

(21) Zhou, D.; Spinks, G. M.; Wallace, G. G.; Tiyapiboonchaiya, C.; MacFarlane, D. R.; Forsyth, M.; Sun, J. Solid State Actuators Based on Polypyrrole and Polymer-in-Ionic Liquid Electrolytes. In *Electrochimica Acta*; 2003.

(22) Skot(1) Skotheim, T. A.; Reynolds, J. R. Handbook of Conducting Polymers: Conjugated Polymers Processing and Applications; 2007.heim, T. A.; Reynolds, J. R. *Handbook of Conducting Polymers: Conjugated Polymers Processing and Applications*; 2007.

(23) Murray, P.; Spinks, G. M.; Wallace, G. G.; Burford, R. P. Electrochemical Induced Ductile—Brittle Transition in Tosylate-Doped (PTS) Polypyrrole. *Synth. Met.* **2002**.

(24) Otero, T. F.; López Cascales, J. J.; Vázquez Arenas, G. Mechanical Characterization of Free-Standing Polypyrrole Film. *Mater. Sci. Eng. C* **2007**.

(25) Pytel, R. Z.; Thomas, E. L.; Hunter, I. W. In Situ Observation of Dynamic Elastic Modulus in Polypyrrole Actuators. *Polymer (Guildf).* **2008**.

(26) Hirokawa, Y.; Tanaka, T. Volume Phase Transition in a Nonionic Gel. *J. Chem. Phys.* **1984**.

(27) Takigawa, T.; Yamawaki, T.; Takahashi, K.; Masuda, T. Change in Young's Modulus of Poly(N-Isopropylacrylamide) Gels by Volume Phase Transition. *Polym. Gels Networks* **1998**, *5* (6), 585–589.

(28) Haq, M. A.; Su, Y.; Wang, D. Mechanical Properties of PNIPAM Based Hydrogels: A Review. *Materials Science and Engineering C*. 2017.

(29) Hess, A.; Dunning, J.; Harris, J.; Capadona, J. R.; Shanmuganathan, K.; Rowan, S. J.; Weder, C.; Tyler, D. J.; Zorman, C. A. A Bio-Inspired, Chemo-Responsive Polymer Nanocomposite for Mechanically Dynamic Microsystems. In *TRANSDUCERS 2009 - 15th International Conference on Solid-State Sensors, Actuators and Microsystems*; 2009.

(30) Mendez, J.; Annamalai, P. K.; Eichhorn, S. J.; Rusli, R.; Rowan, S. J.; Foster, E. J.; Weder, C. Bioinspired Mechanically Adaptive Polymer Nanocomposites with Water-Activated Shape-Memory Effect. *Macromolecules* **2011**.

(31) Liu, C.; Qin, H.; Mather, P. T. Review of Progress in Shape-Memory Polymers. *J. Mater. Chem.* **2007**.

(32) Morshedian, J.; Khonakdar, H. A.; Mehrabzadeh, M.; Eslami, H. Preparation and Properties of Heat-Shrinkable Cross-Linked Low-Density Polyethylene. *Adv. Polym. Technol.* **2003**.

(33) Kolesov, I. S.; Kratz, K.; Lendlein, A.; Radusch, H. J. Kinetics and Dynamics of Thermally-Induced Shape-Memory Behavior of Crosslinked Short-Chain Branched Polyethylenes. *Polymer (Guildf).* **2009**.

(34) Lee, B. S.; Chun, B. C.; Chung, Y. C.; Sul, K. Il; Cho, J. W. Structure and Thermomechanical Properties of Polyurethane Block Copolymers with Shape Memory Effect. *Macromolecules* **2001**.

(35) Meng, Y.; Jiang, J.; Anthamatten, M. Body Temperature Triggered Shape-Memory Polymers with High Elastic Energy Storage Capacity. *J. Polym. Sci. Part B Polym. Phys.* **2016**, *54* (14), 1397–1404.

(36) Kim, B. K.; Lee, S. Y.; Xu, M. Polyurethanes Having Shape Memory Effects. *Polymer (Guildf).* **1996**.

(37) Ping, P.; Wang, W.; Chen, X.; Jing, X. Poly(ε-Caprolactone) Polyurethane and Its Shape-Memory Property. *Biomacromolecules* **2005**.

(38) Lendlein, A.; Langer, R. Biodegradable, Elastic Shape-Memory Polymers for Potential Biomedical Applications. *Science.* **2002**.

(39) Feng, Y.; Behl, M.; Kelch, S.; Lendlein, A. Biodegradable Multiblock Copolymers Based on Oligodepsipeptides with Shape-Memory Properties. *Macromol. Biosci.* **2009**.

(40) Mather, P. T.; Luo, X.; Rousseau, I. A. Shape Memory Polymer Research. *Annu. Rev. Mater. Res.* **2009**.

(41) Behl, M.; Lendlein, A. Shape-Memory Polymers. *Mater. Today* **2007**.

(42) Melkos, A. B. Advances in Digital Technology and Orthodontics: A Reference to the Invisalign Method. *Med. Sci. Monit.* **2005**.

(43) Burstone, C. J. Variable-Modulus Orthodontics. *Am. J. Orthod.* **1981**.

(44) Sharp, A. A.; Panchawagh, H. V.; Ortega, A.; Artale, R.; Richardson-Burns, S.; Finch, D. S.; Gall, K.; Mahajan, R. L.; Restrepo, D. Toward a Self-Deploying Shape Memory Polymer Neuronal Electrode. *J. Neural Eng.* **2006**.

(45) Shiga, T.; Okada, A.; Kurauchi, T. Magnetroviscoelastic Behavior of Composite Gels. *J. Appl. Polym. Sci.* **1995**.

(46) Mitsumata, T.; Ikeda, K.; Gong, J. P.; Osada, Y.; Szabó, D.; Zrínyi, M. Magnetism and Compressive Modulus of Magnetic Fluid Containing Gels. *J. Appl. Phys.* **1999**.

(47) Mitsumata, T.; Okazaki, T. Magnetization-Induced Reduction in Dynamic Modulus of Polyurethane Elastomers Loaded with Ferrite. *Japanese J. Appl. Physics, Part 1 Regul. Pap.*

Short Notes Rev. Pap. **2007**.

(48) Lokander, M.; Stenberg, B. Improving the Magnetorheological Effect in Isotropic Magnetorheological Rubber Materials. *Polym. Test.* **2003**.

(49) Lokander, M.; Stenberg, B. Performance of Isotropic Magnetorheological Rubber Materials. *Polym. Test.* **2003**.

(50) Mitsumata, T.; Ohori, S. Magnetic Polyurethane Elastomers with Wide Range Modulation of Elasticity. *Polym. Chem.* **2011**.

(51) Qiu, Y.; Zhang, E.; Plamthottam, R.; Pei, Q. Dielectric Elastomer Artificial Muscle: Materials Innovations and Device Explorations. *Acc. Chem. Res.* **2019**, *52* (2), 316–325.

(52) Yu, Z.; Yuan, W.; Brochu, P.; Chen, B.; Liu, Z.; Pei, Q. Large-Strain, Rigid-to-Rigid Deformation of Bistable Electroactive Polymers. *Appl. Phys. Lett.* **2009**, *95* (19), 21–24.

(53) Niu, X.; Yang, X.; Brochu, P.; Stoyanov, H.; Yun, S.; Yu, Z.; Pei, Q. Bistable Large-Strain Actuation of Interpenetrating Polymer Networks. *Adv. Mater.* **2012**, *24* (48), 6513–6519.

(54) Ren, Z.; Hu, W.; Liu, C.; Li, S.; Niu, X.; Pei, Q. Phase-Changing Bistable Electroactive Polymer Exhibiting Sharp Rigid-to-Rubbery Transition. *Macromolecules* **2016**, *49* (1), 134–140.

(55) Qiu, Y.; Lu, Z.; Pei, Q. Refreshable Tactile Display Based on a Bistable Electroactive Polymer and a Stretchable Serpentine Joule Heating Electrode. *ACS Appl. Mater. Interfaces* **2018**, *10*, 24807–24815.

(56) Qiu, Y.; Ren, Z.; Hu, W.; Liu, C.; Pei, Q. Bistable Electroactive Polymer with Sharp Rigid-to-Rubbery Phase Transition. In *Electroactive Polymer Actuators and Devices (EAPAD) 2016*; 2016; p 97981U.

Chapter 2. Dual stimuli-responsive polymer nanocomposite with ultra-wide tunable range triggered by water and temperature

2.1. Background of this study

Smart materials which change their mechanical properties "on command", such as upon exposure to a pre-defined stimulus in a highly controllable and reversible manner, are attractive for countless technologically relevant applications. In the research of designing variable stiffness polymers, choosing a suitable stimulus method is vital for use in different applications. VSPs with reversible covalent bonds induced from Diels-Alder reaction can be used as self-healing component in electronic displays for prolonged lifetime.[1] The phase-changing VSP with adjustable transition temperature, such as bistable electroactive polymer, finds its application in wide range of areas like soft robotics, wearable electronics, human-assistive machine, etc.[2,3] The cellulose reinforced nanocomposite is suitable for applications that involve water or solvent, like under-water robots and in body devices.[4] Aside from choosing proper stimulus method, enlarging the stiffness tunability range is also important for giving the material more opportunities to be used in different areas. As summarized in Chapter 1, the cellulose reinforced composite and phase-changing BSEP demonstrated largest modulus change with 330-fold [5] and 3000-fold [3] respectively.

2.1.1 Cellulose reinforced composite

The cellulose reinforced nanocomposite was extensively exploited by Professor Christoph Weder and his team.[6] The work was first inspired by the sea cucumbers of which the mechanism responsible for the

morphing mechanical properties displayed by the inner dermis. Many echinoderms, such as sea cucumber and starfish, share the ability to rapidly and reversibly alter the stiffness of their connective tissue, which creates significant survival advantages.[7] Such stiffness tunability has been proved to be enabled from reversible associations among collagen fibrils that are rigid and have high aspect ratio.[8] The stiffness of the composite reinforced by the interactions among collagen fibrils through hydrogen bonding. These interactions can be regulated by a hydrogen-bond-forming solvent via competing binding. The Weder group utilized low-modulus synthetic polymer as the matrix and cellulose nanofibers as the rigid filler to fabricate variable stiffness composites.

The first generation of percolating cellulose whisker nanocomposite was based on a 1:1 ethyleneoxide/epichlorohydrin copolymer (EO-EPI) matrix, which possesses a low storage modulus of 3.7 MPa (neat polymer).[4] With the addition of cellulose whisker, the storage modulus increased to around 880 MPa at a whisker content of about 19 vol%.[4] Upon exposure to water, the composite exhibited a modulus reduction to 20 MPa.[4] To further enlarge the stiffness variation, the percolating network of cellulose whiskers were incorporated into a glass transition polymer, such as poly(vinyl acetate) (PVAc).[5] PVAc is a thermal responsive polymer with glass transition temperature from 60 – 80 °C. An increase in the stiffness variation band was observed for the composites. The PVAc based composite exhibited a storage modulus of 5.3 GPa at room temperature and dry state with 16.5 vol% of cellulose whisker content.[5] The modulus decreased to 12.7 MPa when the material was heated above the glass transition temperature of PVAc and immersed into water.[5] The stiffness tunability range increased 10 times compare to the previous work. However, the transition temperature of the PVAc appears too high for many applications that involve human contact. In addition, the modulus of the composite in the soft end is still relatively high in comparison with epidermis or bio-tissues, which limits its usage in some biomedical or wearable electronics applications.

2.1.2 Bacterial cellulose

Bacterial cellulose (BC) received ample attention due to its numerous great properties such as large length-to-diameter aspect ratio, high porosity, biodegradability, excellent biological affinity, and high water-holding capacity.[9] Formed by repeated connection of glucose building blocks, BC possesses abundant surface hydroxyl groups forming plentiful inter- and intra-molecular hydrogen bonds. Bacterial cellulose has the same molecular formula as plant cellulose, but with unique and sophisticated three-dimensional porous network structure, consisting of continuous nanofibers. Each nanofiber is a bundle of cellulose microfibrils (Figure 2-1).[10] From previous research and some commercialized products, BC and its derivatives have shown tremendous potential in field like biomedical, electronics, and food industrial.[9,10] Due to the poor stress-bearing capability of BC, it is often fabricated into composite. BC owns a highly porous nature arrangement of fibrils, which allows infiltration of another material to form a matrix.[10] The formation of composite material provide additional properties to BC while preserve its own biological and physiochemical properties.

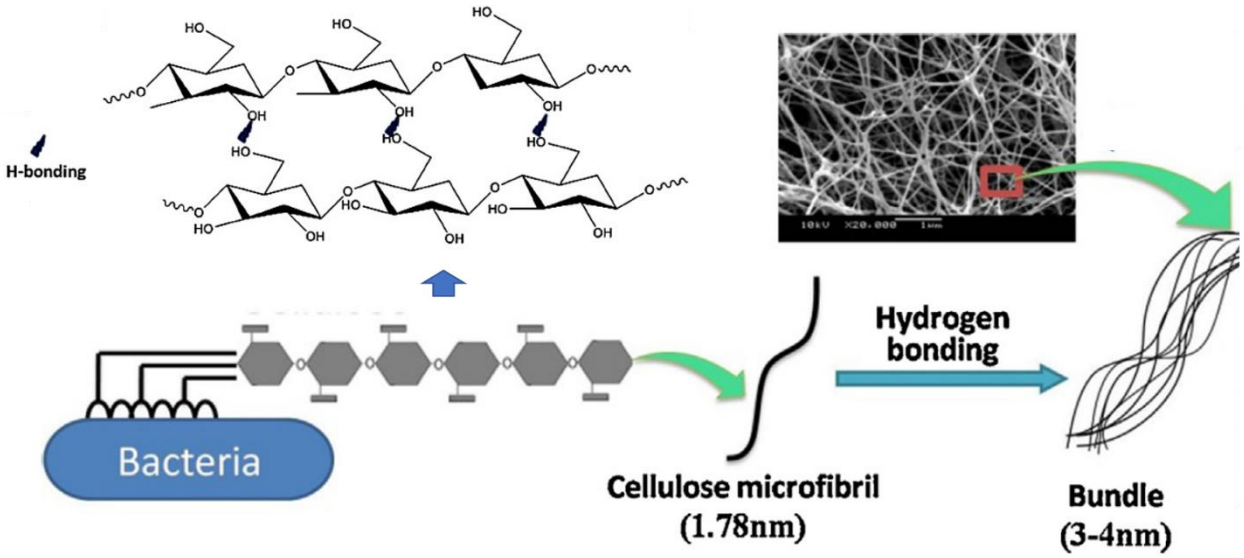

Figure 2-1. Illustration of the chemical structure and the production of bacterial cellulose. Adopted from ref 10.

2.1.3 Bacterial cellulose reinforced BSEP nanocomposite

In this work, we present a novel composite that combines the stiffness variation mechanism from cellulose nanofibers and phase-changing BSEP to achieve ultrawide modulus regulation range (Figure 2-2). The composite utilizes phase changing BSEP, with sharp transition temperature tuned to around human body temperature, as the matrix material. Bacterial cellulose nanofibers form a percolative network in the matrix, resulting in a significant mechanical reinforcement with a storage modulus as high as 1 GPa. Upon heating and water-exposure, the BSEP matrix softened, while the hydrophilic cellulose network forms water channels for the composite to absorb water molecules. With the plasticized effect from water molecules, the stiffness of the softened BSEP further reduces to 40 kPa. The BC-BSEP composite exhibits a large stiffness change of 25,000-fold with dual stimulus of temperature and water. The composites also show good biocompatibility, which grants their potential application in biomedical area.

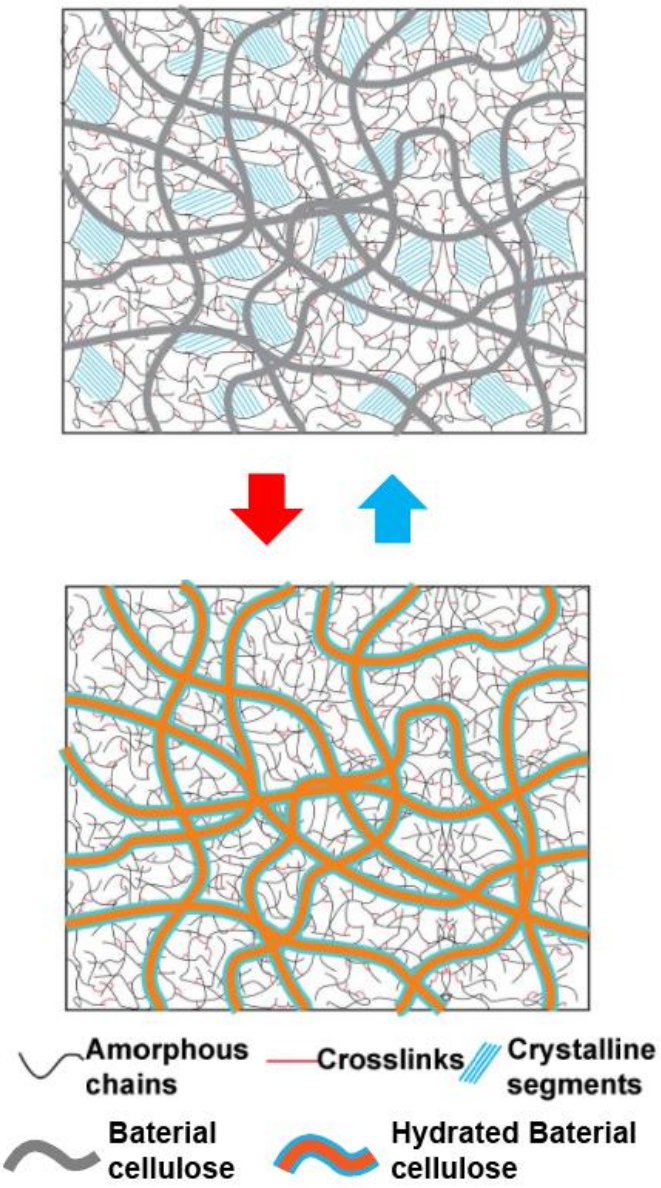

Figure 2-2. Stiffness changing mechanism of the BC-BSEP composite.

2.2. Experimental design

2.2.1 Raw materials

Urethane diacrylate (UDA, catalog name: CN9021), SR9035, and SR415 were obtained from SARTOMER and used as received. Stearyl acrylate (SA), trimethylolpropane triacrylate (TMPTA), acrylic acid (AA), 2-carboxyethyl acrylate (CEA), 2,2-Dimethoxy-2-phenylacetophenone (DMPA), benzophenone (BP), and isopropyl alcohol (IPA) were purchased from Sigma-Aldrich and used as received. Hexadecyl acrylate (HA) was purchased from Tokyo Chemical Industry Co., LTD. and used as received. Bacterial cellulose was obtained from Hannan Yeguo Foods Co., Ltd.

2.2.2 Preparation of BSEP prepolymer solution and thin film fabrication

Table 2-1. Formulations of different BSEPs.

	SA (part in weight)	HA (part in weight)	UDA (part in weight)	AA (part in weight)	CEA (part in weight)	DMPA (part in weight)	BP (part in weight)
BS-AA5	80	0	20	5	0	0.25	0.125
BS-AA10	80	0	20	10	0	0.25	0.125
BS-AA15	80	0	20	15	0	0.25	0.125
BS-CEA5	80	0	20	0	5	0.25	0.125
BS-CEA10	80	0	20	0	10	0.25	0.125
BS-CEA15	80	0	20	0	15	0.25	0.125
BS1H7	10	70	20	0	10	0.25	0.125
BS4H4	40	40	20	0	10	0.25	0.125

BS7H1	70	10	20	0	10	0.25	0.125

The BSEP prepolymer solutions was made by mixing the components listed in the Table 2-1 at 50 °C. To make a BSEP thin film, the prepolymer solution was then injected between a pair of glass slides on a hot plate with two strips of tape as spacers. The thickness of the liquid layer was defined by the thickness of the spacers. In the device assembling, 90 μm thick spacers were used to fabricate the BSEP film. Next, the prepolymer was cured through a UV curing conveyor equipped with a Fusion 300S type "H" UV curing bulb for about 3min. Then the film can be gently peeled off the glass slide after it cooled down to room temperature.

2.2.3 Preparation of bacterial cellulose aerogel

The bacterial cellulose was first dissolved in boiling deionized water with different contents. The solutions were bath sonicated for 30 min to degas and form uniform aqueous solutions. The solutions were then carefully poured into plastic petri dishes and sealed using Petri Seal ™. Next, the petri dishes were placed in Nalgene® Mr. Frost® Cryo 1 °C (Thermo Scientific ™) freezing containers filled with IPA and placed in a -80 °C freezer. The simple to use system is designed to achieve a rate of cooling very close to -1 °C/minute for uniform freezing process. Finally, the frozen cellulose solution was freeze-dried overnight to sublimate the water molecules. The resulting cellulose aerogel forms a 3D percolative network with porous structure. The pore size is determined by the concentration of the BC aqueous solution. Thicker solution results in denser aerogel.

2.2.4 Fabrication of BC-BSEP nanocomposite

The freeze-dried BC aerogel was first immersed in a BSEP prepolymer solution at 50 °C. The porous structure makes the BSEP prepolymer solution to be absorbed by the BC foam, filling out most of the pores inside the aerogel. The system was then transferred into a vacuum oven with the temperature and the pressure to be set at 50 °C and -100 kPa respectively. The use of vacuum oven was to help the infiltration of the BSEP prepolymer solution into the BC network. Next, the fully soaked BC foam was compressed between two glass substrates into a thin film, and the BSEP prepolymer was cured under UV exposure. Finally, the composite film can be gently peeled off after the BSEP matrix cooled down to room temperature.

2.2.5 Biocompatibility test for BC-BSEP composite

All cell culture materials were purchased from ThermoFisher Scientific. To ensure normal cellular growth and low cytotoxicity of the materials, cell viability test was carried out according to ISO 10993-5.[11] In a certified A2 biosafety cabinet, BSEP matrix and BC-BSEP composite were placed at bottoms of a standard 12-well cell culture plate. A Total of 100,000 NIH3T3 mouse fibroblast cells were seeded in each well and cultured in Dulbecco's modified eagle medium with 10% fetal bovine serum plus 1% penicillin. The cell cultures were placed in 37 °C and 5% CO_2 cell incubator for 72 hrs. At the end of 72 hrs., LIVE/DEADTM assay working solution (Catalog number L3224) was prepared in phosphate buffered saline and warmed to 37 °C in heated water bath. Cell culture medium was replaced with the prepared working solution and incubated in 37 °C and 5% CO_2 for another 30 mins. At last, all samples were imaged with Zeiss Axio-Observer microscope (Carl Zeiss). All fluorescent/phase contrast images within the same comparison groups were imaged with same parameters, and all samples within each comparison group were prepared and processed together.

2.3. Results and discussion

2.3.1 Composite fabrication design

The reported composite material consists of hydrophobic BSEP matrix and hydrophilic bacterial cellulose filler, which combines the tunable stiffness mechanisms from temperature induced phase changing and water induced hydrogen bonds decoupling. However, an inevitable difficulty remains in the way of overcoming the rejection between BSEP matrix and BC filler due to their differences in the hydrophilicity. The reported two main methods of combining hydrophilic cellulose with hydrophobic polymer matrixes include chemical surface modification and template approach.[10,12,13] The chemical modification usually involves carbocymethylated, acetylated, phosphorylated, and modified by other graft copolymerization and crosslinking reaction to obtain series of BC derivatives.[10] The introduction of new functional groups to the BC structure can endow BC with hydrophobicity for better compatibility with polymer matrix. However, the addition of functional groups also affects the water holding capacity of BC, which may result in decreased water uptake and limit the stiffness variation range. The template approach typically involves the use of a common solvent, such as tetrahydrofuran (THF), that is both miscible with water and can dissolve many organic polymers or monomers.[13] It starts with the formation of cellulose organogel through a solvent-exchange sol-gel process. Then, soak the organogel in polymer/monomer-THF solution to let the polymer/monomer molecules diffuse into the cellulose gel. However, such approach limits the use of matrix material to a kind that needs to be dissolved in the common solvent. In addition, it is not suitable for fabricating thin film composite.

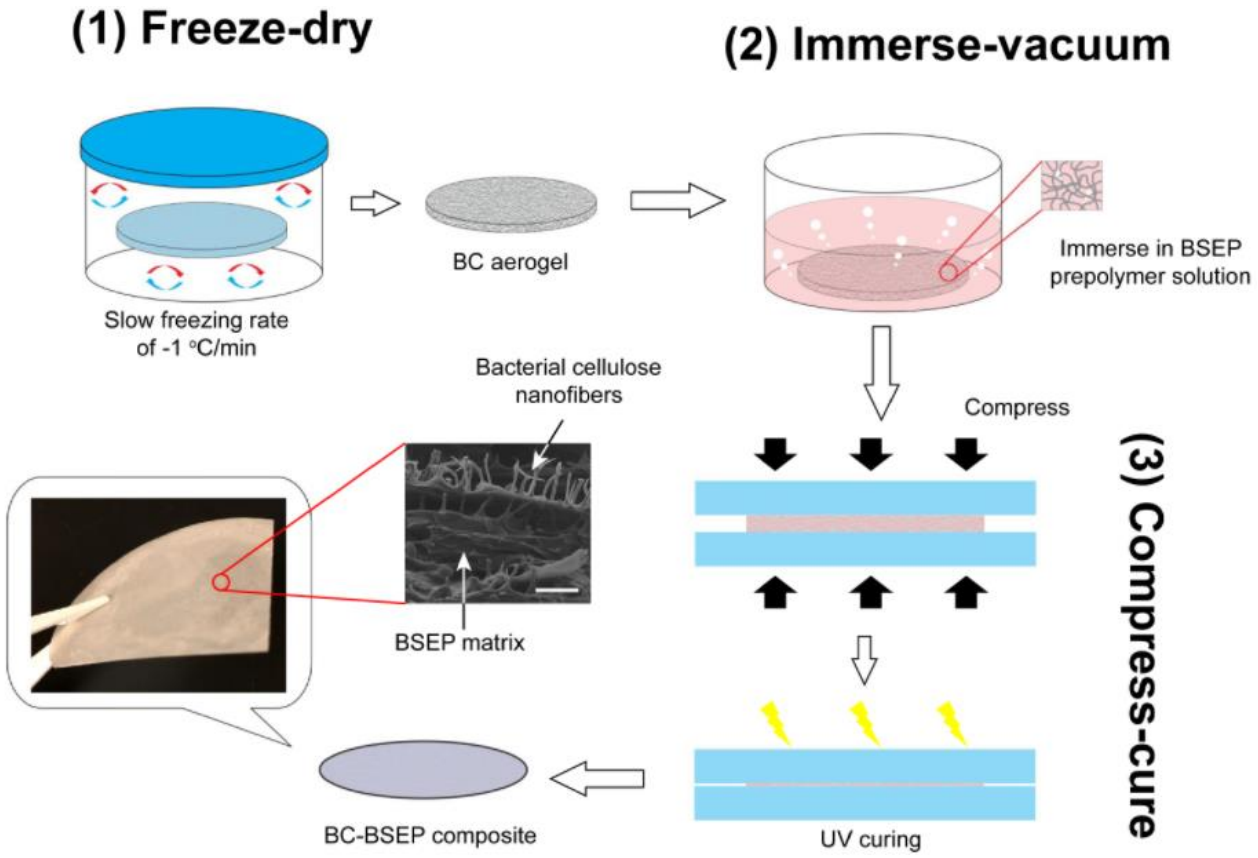

Figure 2-3. Fabrication process of the composite material.

Here, we introduce a fabrication method that can effectively combine the matrix and filler materials with different hydrophilicity into a uniform thin film composite. Such procedure includes three main steps: (1) freeze-dry, (2) immerse-vacuum, (3) compress-cure (Figure 2-3). The process starts with creating a 3D percolative network of bacterial cellulose as the skeleton structure for the composite via freeze-drying frozen BC aqueous solution. The key of obtaining a uniform BC aerogel is by controlling the crystallization of water molecules to form a frozen BC solution with uniformly distributed ice crystallites. It can be achieved by slow-freezing aqueous solution that has been degassed. The ununiform freezing is mainly caused by the air bubbles trapped in the solution (Figure 2-4a). Utilizing boiling water will help reduce the air trapped in water. The following sonication further eliminates the air bubbles in the solution. In addition, the freezing process was carried out in the Mr. Frosty ™ freezing container that is designed

to have a slow freezing rate of -1 °C/min. The slow freezing enables dissipation of air bubbles in the process. As demonstrated in Figure 2-4b, the resulting BC aerogel showed much more uniform structure compared to the one that was frozen in a traditional way. After the immersion of BC aerogel in BSEP prepolymer solution, the vacuum process is vital to force the incompatible BSEP prepolymer solution to infiltrate into the BC network. The low pressure in the vacuum oven can effectively "pump" the air inside the BC network and force the diffusion of the BSEP prepolymer solution. The resulting BC-BSEP "sponge" was compressed into thin film configuration and cured under UV. The three-step procedure offers a simple and effective way to fabricate a uniform cellulose composite with the matrix and filler materials having different hydrophilicity, while not sacrificing any functions for both BC and BSEP.

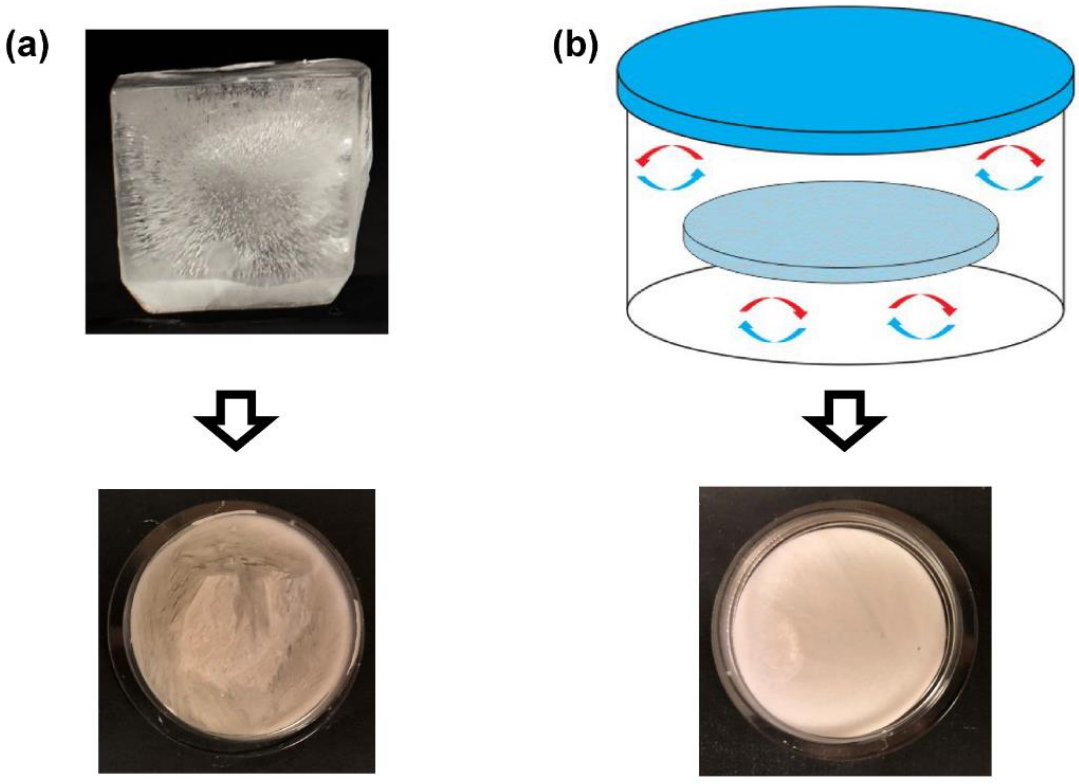

Figure 2-4. Illustration and pictures demonstration of ununiformly (a) and uniformly (b) frozen BC solution using traditional freezing procedure and slow freezing procedure respectively.

2.3.2 Mechanical modification of BSEP

Due to the low stress bearing property of bacterial cellulose, it is important for the BSEP matrix to have good mechanical behavior for high toughness composite. For the BSEP system, one way to increase the toughness of the material is to introduce a small molecule crosslinker. Ren et al. reported that the addition of small amount of trimethylolpropane triacrylate (TMPTA) can effectively increase the tensile strength of the BSEP material. However, due to the limited extension of TMPTA, the stretchability of the material was also largely reduced. To resolve this problem, crosslinkers, such as SR9035 and SR415, with multiple functional groups and longer connecting chains were investigated (Figure 2-5a). The detailed formulation can be found in Table 2-2. As shown in Figure 2-5b, the crosslinkers resulted in limited strengthening effect in the BSEP system. Thus, reversible crosslinker, such as hydrogen bond, was utilized. The hydrogen bond interaction acts as physical crosslinker that can repetitively break and reform to release the stress concentration and resist crack propagation without constraining the maximum elongation of the polymer. In addition, the hydrogen bonds can also interact with cellulose for enhanced mechanical property. Acrylic acid appears to be a suitable candidate because of the high hydrogen bond strength of 30 kJ/mol[14] and the acrylic functional group that can be polymerized into BSEP system. The strengthening effect of AA is enormous. The maximum elongation increased from 807% for BSEP without small molecule crosslinker to 1051% and 1073% for BS-AA10 and BS-AA15 respectively. The tensile strength is also increased to 1.4 MPa (BS-AA10) and 2.1 MPa (BS-AA15) with the true stress calculated to be 16 MPa and 25 MPa respectively (Figure 2-5c).

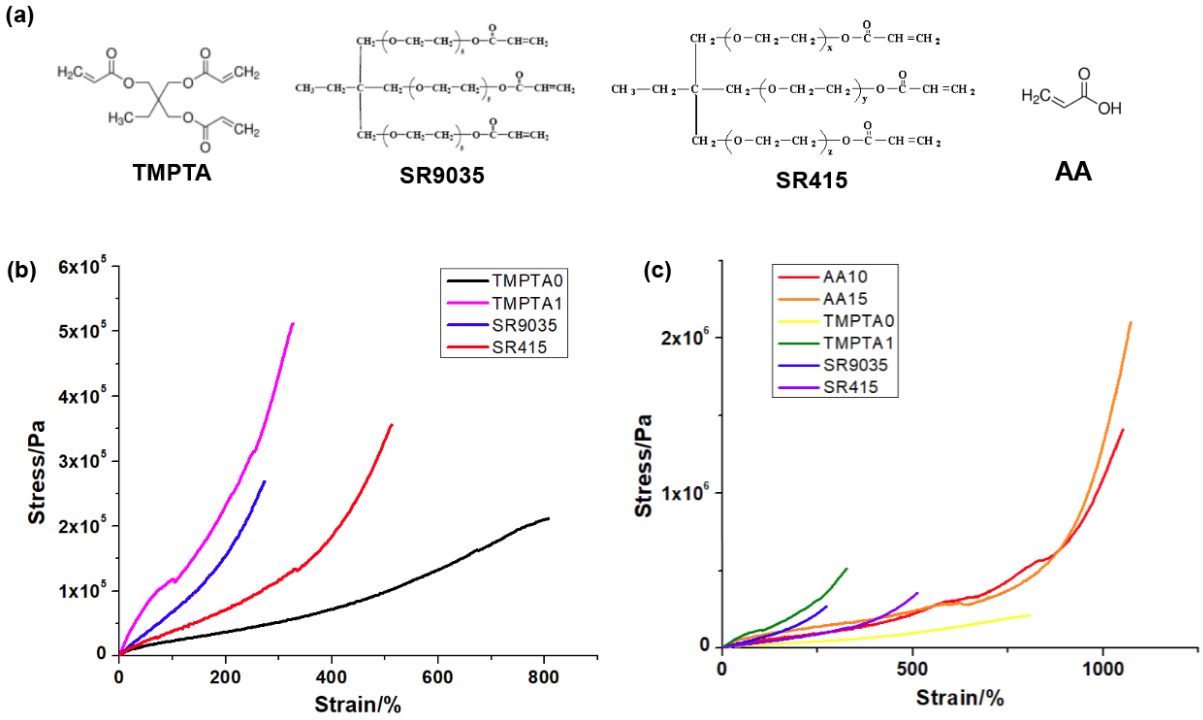

Figure 2-5. (a) Chemical structure of different small molecule crosslinkers. (b-c) Stress-strain behavior comparison of the BSEP materials with addition of different kinds of crosslinkers.

Table 2-2. Formulations of BSEP prepolymers with different kinds of crosslinkers.

	SA (part in weight)	HA (part in weight)	UDA (part in weight)	Crosslinker (part in weight)	DMPA (part in weight)	BP (part in weight)	AA (part in weight)
TMPTA0	10	70	20	0	0.25	0.125	0
TMPTA1	10	70	20	1	0.25	0.125	0
SR9035	10	70	20	1	0.25	0.125	0
SR415	10	70	20	1	0.25	0.125	0

AA10	10	70	20	0	0.25	0.125	10
AA15	10	70	20	0	0.25	0.125	15

However, the use of AA is not suitable for the fabrication of BC-BSEP composite. Due to the low boiling point of 141 °C in ambient atmosphere, most of the AA will evaporate during the vacuum process. Thus, carboxyethyl acrylic was used to substitute AA in the BSEP formula due to the high boiling point of 103 °C at 19 mmHg. CEA has the same hydrogen bond strength of 30 kJ/mol as AA[14], it can effectively strengthen the BSEP (Figure 2-6). BS80, which is the one without any CEA, has a strain at break of 191% and a tensile strength of 0.26 MPa. With the strengthening effect from CEA, the maximum elongation reached to around 900%, and the true tensile strength was 2.4 MPa (BS-CEA5), 3.4 MPa (BS-CEA10), and 4.7 MPa (BS-CEA15). The toughness of CEA based BSEP is slightly lower than AA based BSEP. The reason may be the limited miscibility in the BSEP prepolymer solution due to the higher molecular weight of CEA. Based on that, BS-CEA10 was used in the following experiments, because it strengthens the BSEP material while creates stable prepolymer solution without phase separation.

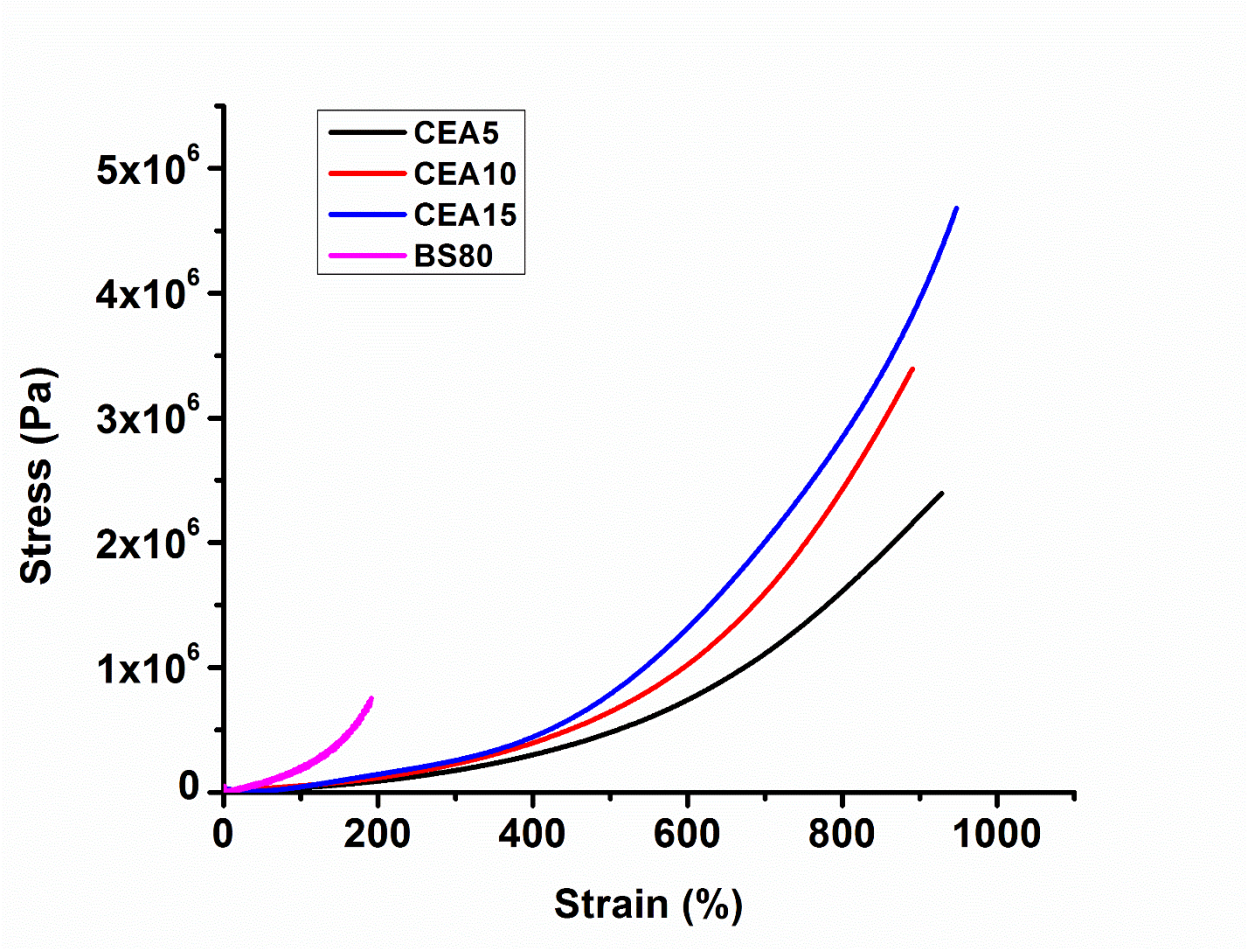

Figure 2-6. Stress-strain behavior of BSEPs with different amount of CEA. The arrows indicate the rapture of the polymer film in the tensile test.

Adjustable transition temperature is another intriguing property of BSEP material. Ren et al. reported a way of adjusting the transition temperature by varying the ratio between SA and UDA. By doing that, the tunable stiffness range of BSEP decreases for lower transition temperature. Here, we used a mixture of stearyl acrylate and hexadecyl acrylate for adjusting the transition temperature, while keeping the ratio between long chain acylate and UDA constant at 80 : 20. Due to the difference in the melting temperature of SA and HA, the Tr of the BSEPs can be easily adjusted from 30 to 50 °C with sharp transition and large

stiffness change (Figure 2-7). Transition temperature below 30 °C or above 50 °C may not be able to hold the deformed shapes at room temperature or be applicable in devices involve human contact. The BSEPs possess a storage modulus as high as around 100-200 MPa at room temperature. The modulus drastically decreases to around 10-30 kPa, resulting in around 5,000-fold change in the stiffness (Figure 2-7).

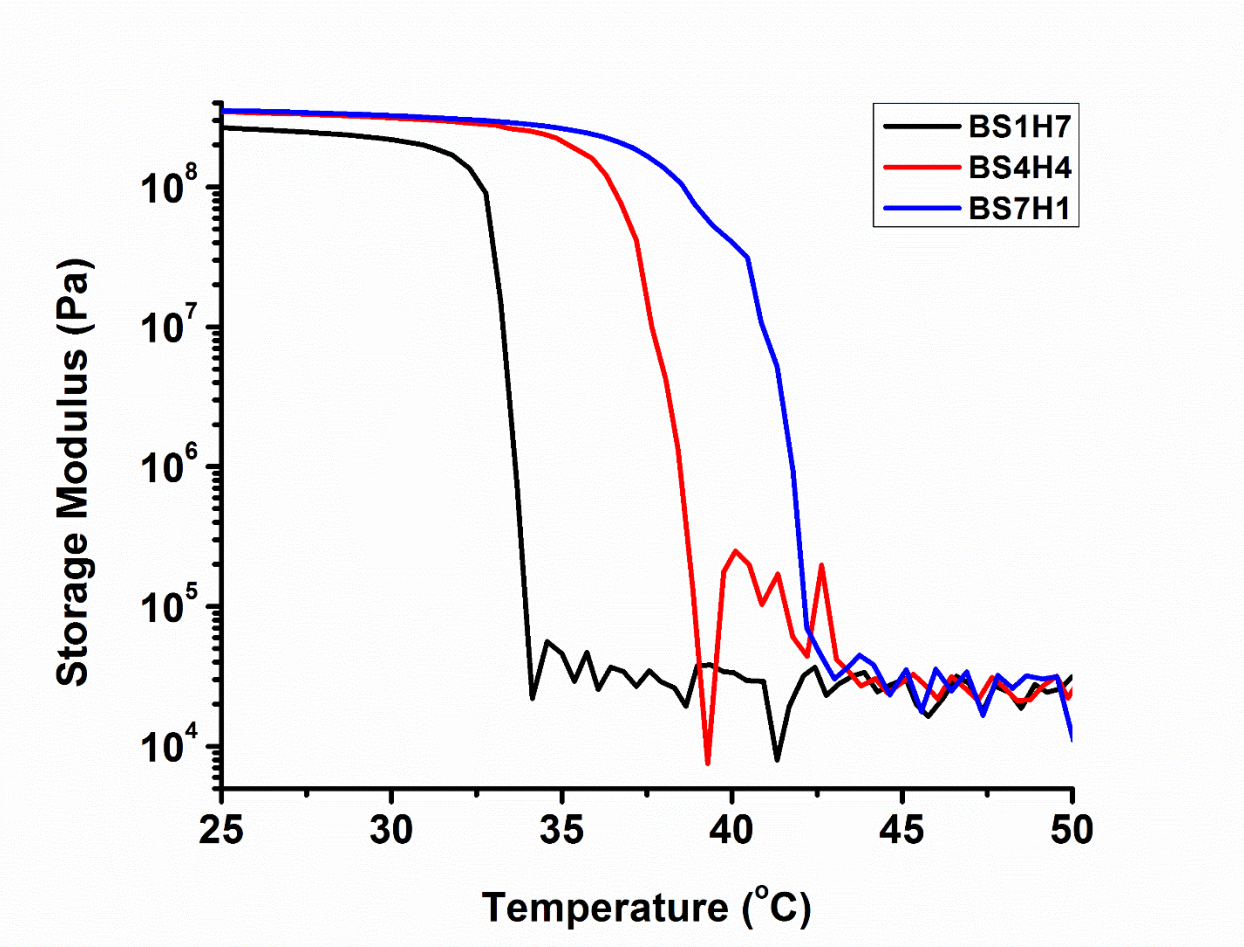

Figure 2-7. Storage modulus versus temperature curve of the BSEPs with transition temperature below, at, and above body temperature.

2.3.3 Bacterial cellulose

Bacterial cellulose is a fascinating and renewable natural nanomaterial. A condensed BC film, which is fabricated via evaporating BC aqueous solution, possesses a density as high as 1188.4mg/ml. By making the BC aerogel, the BC forms porous network structure, resulting in largely reduced density. The BC aerogel forms highly porous structure and can be compressed into thin film (Figure 2-8a). The density of the aerogel is determined by the concentration of BC in the aqueous solution. By changing the concentration from 0.7 wt% to 2 wt%, the density of the resulting aerogels increases. And the results are listed in the Table 2-3. Such density is the key parameter determining the BC content in the composite. With lower density, the free volume in the BC aerogel is larger, resulting in higher amount of BSEP prepolymer diffused into the BC network (Figure 2-8b). Thus, the filler content is lower.

Table 2-3. Densities of BC aerogels resulted from BC solutions with different concentrations.

	Concentration (wt%)	Density (mg/ml)
BC_{sol}-1	0.7	9.36
BC_{sol}-2	1	13.37
BC_{sol}-3	1.5	20.06
BC_{sol}-4	2	26.74

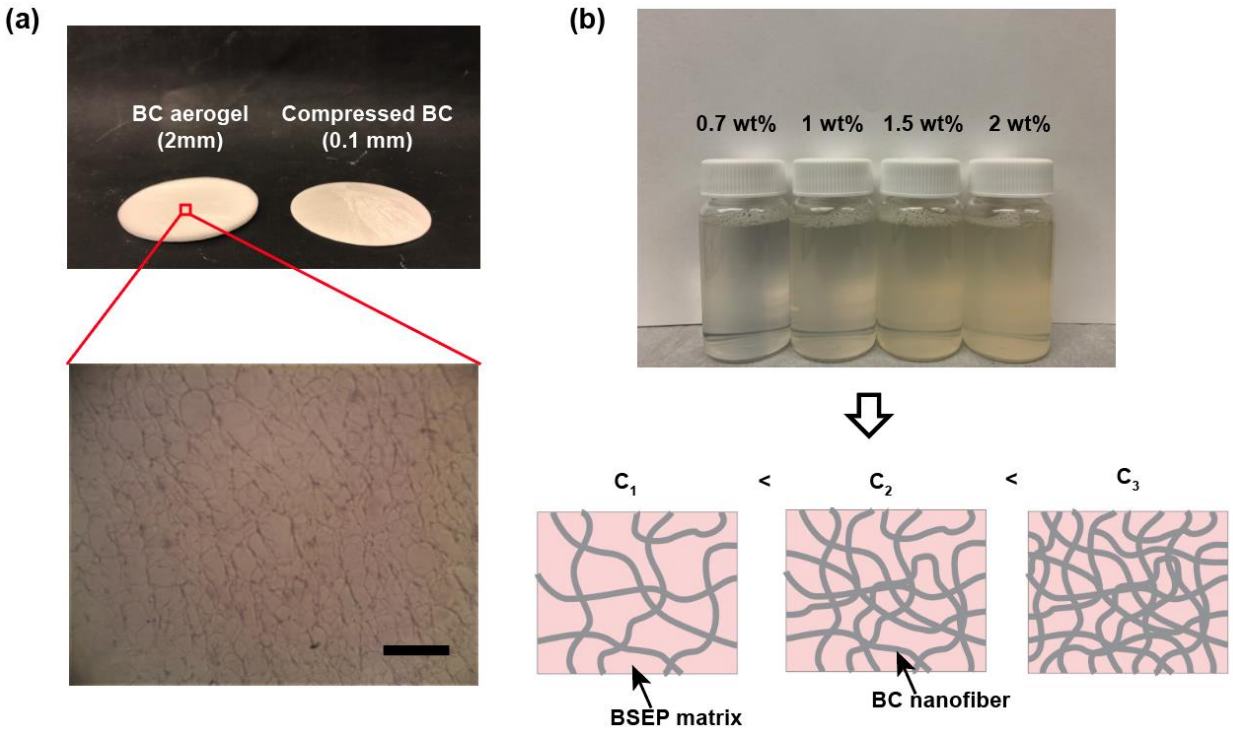

Figure 2-8. (a) Picture demonstration of a as fabricated BC aerogel and a compressed BC film (upper), and a microscopic image showing the porous structure of the BC aerogel (lower). The scale bar is 200 µm. (b) Pictures of BC aqueous solutions with different concentrations (upper), and an illustration of resulting BC aerogels having different cavity percentages (lower).

Storage modulus temperature ramp was performed on a pure condensed BC film to test its mechanical strengthening effect it can bring to the BSEP matrix. The BC exhibits a storage modulus as high as 10 GPa at room temperature. As the temperature increases, the modulus remains relatively constant due to the little temperature effect on bacterial cellulose (Figure 2-9). When the film is immersed in water, it dissolves right away, indicating drastic modulus decrease to 0 Pa.

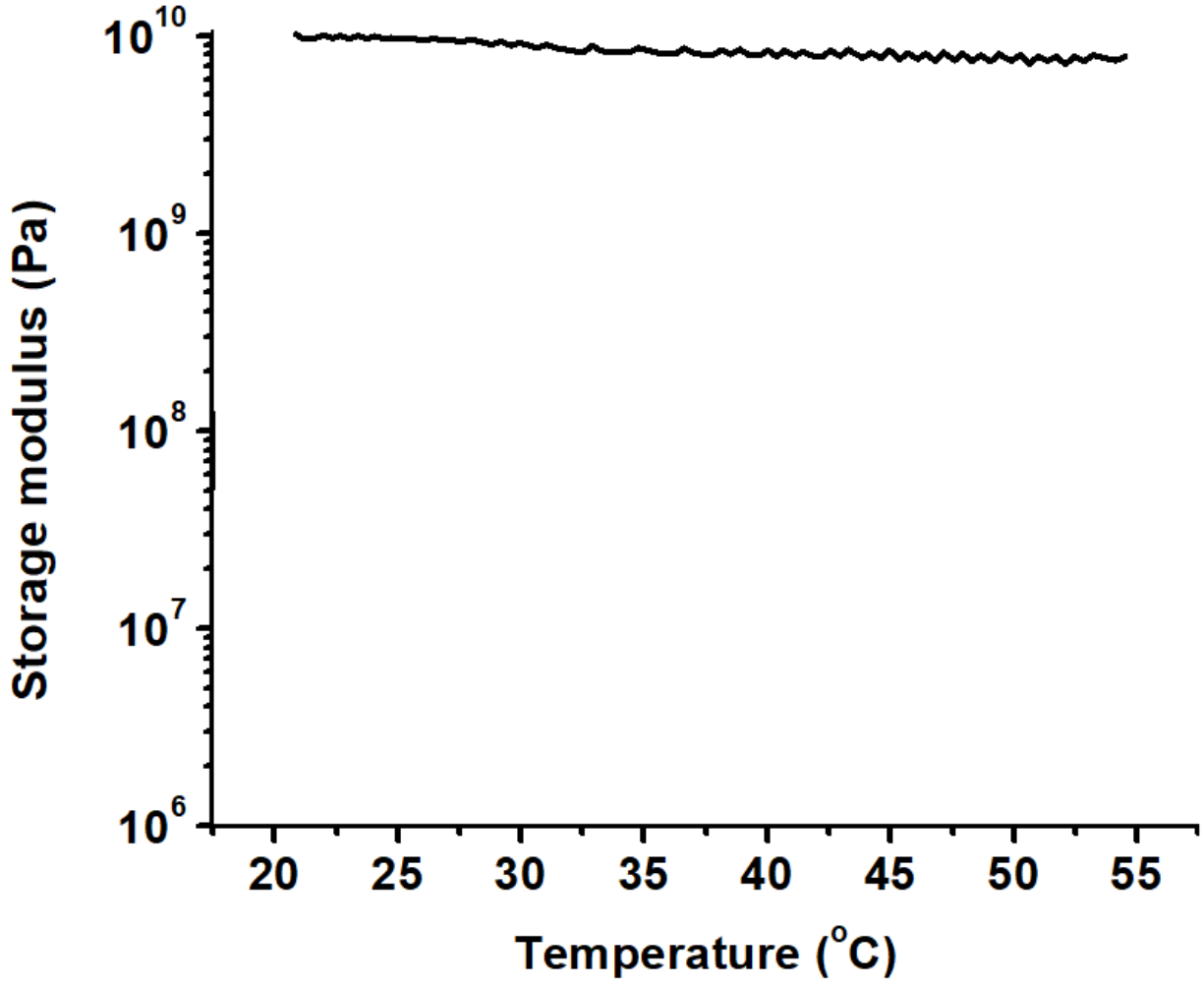

Figure 2-9. Storage modulus temperature profile of a condensed BC film.

2.3.4 BC-BSEP composite

The BC-BSEP composite materials with different filler content were fabricated based on the aforementioned procedure. The composites consist uniformly distributed BC nanofiber percolating network in the BSEP matrix (Figure 2-10a). Because of the "immerse-vacuum" in the fabrication step, the BC nanofibers are well-embedded in the BSEP matrix (Figure 2-10b). The filler content is determined by

the density, or the cavity percentage, of the BC aerogel and can be calculated from the increase in the weight after the BSEP infiltration. Based on the calculation, the BC aqueous solutions (BC_{sol} 1-4) led to BC-BSEP composites with filler content of around 4.7 wt% (BC-BSEP-1), 8.2 wt% (BC-BSEP-2), 16.7 wt% (BC-BSEP-3), and 23 wt% (BC-BSEP-4) respectively.

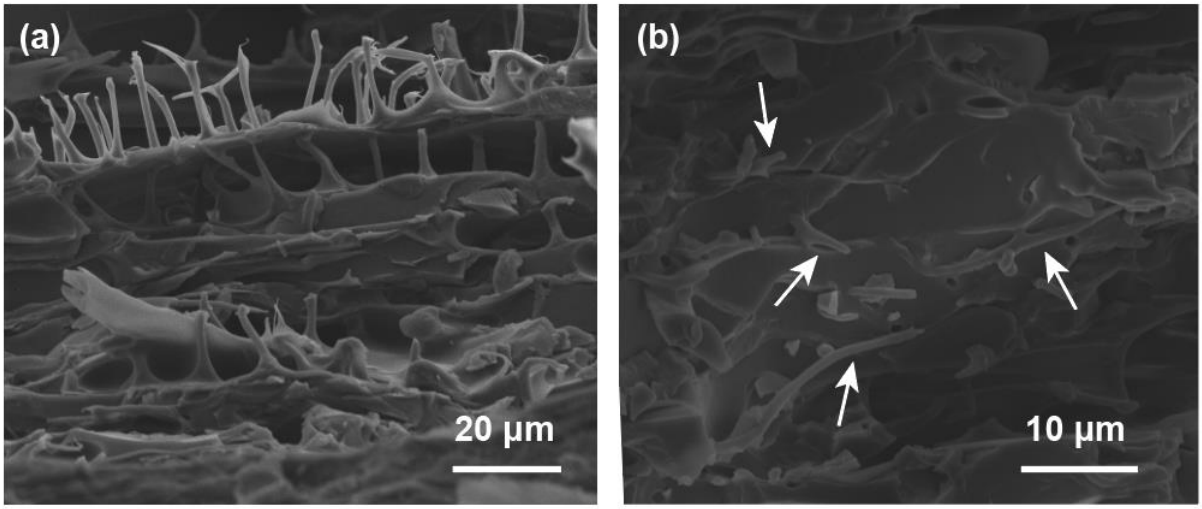

Figure 2-10. (a) SEM images of the cross section from a BC-BSEP composite. (b) A closer view of the cross section demonstrating the BC nanofibers are embedded in the BSEP matrix.

The stress-strain tensile tests were carried out on fully softened (immersed in water at high temperature) BC-BSEP composite materials (Figure 2-11). Due to the low stress-bearing property of BC, the composite materials exhibited decreased maximum elongation and tensile strength compared to neat BSEP polymer. The BC-BSEP-1 showed a tensile strength and strain at break of 0.32 MPa and 974% respectively. As the BC content increases to 23 wt% for BC-BSEP-4, the stress and strain decreased to 0.24 MPa and 313% respectively. The decrease in mechanical toughness may be due to the incompatibility between hydrophilic BC filler and hydrophobic BSEP matrix. Despite the weakened mechanical properties, BC-

BSEP-1, BC-BSEP-2, and BC-BSEP-3 still exhibit excellent stretchability with sufficiently high tensile strength due to the hydrogen bond coupling between CEA in BSEP and hydroxyl groups on BC.

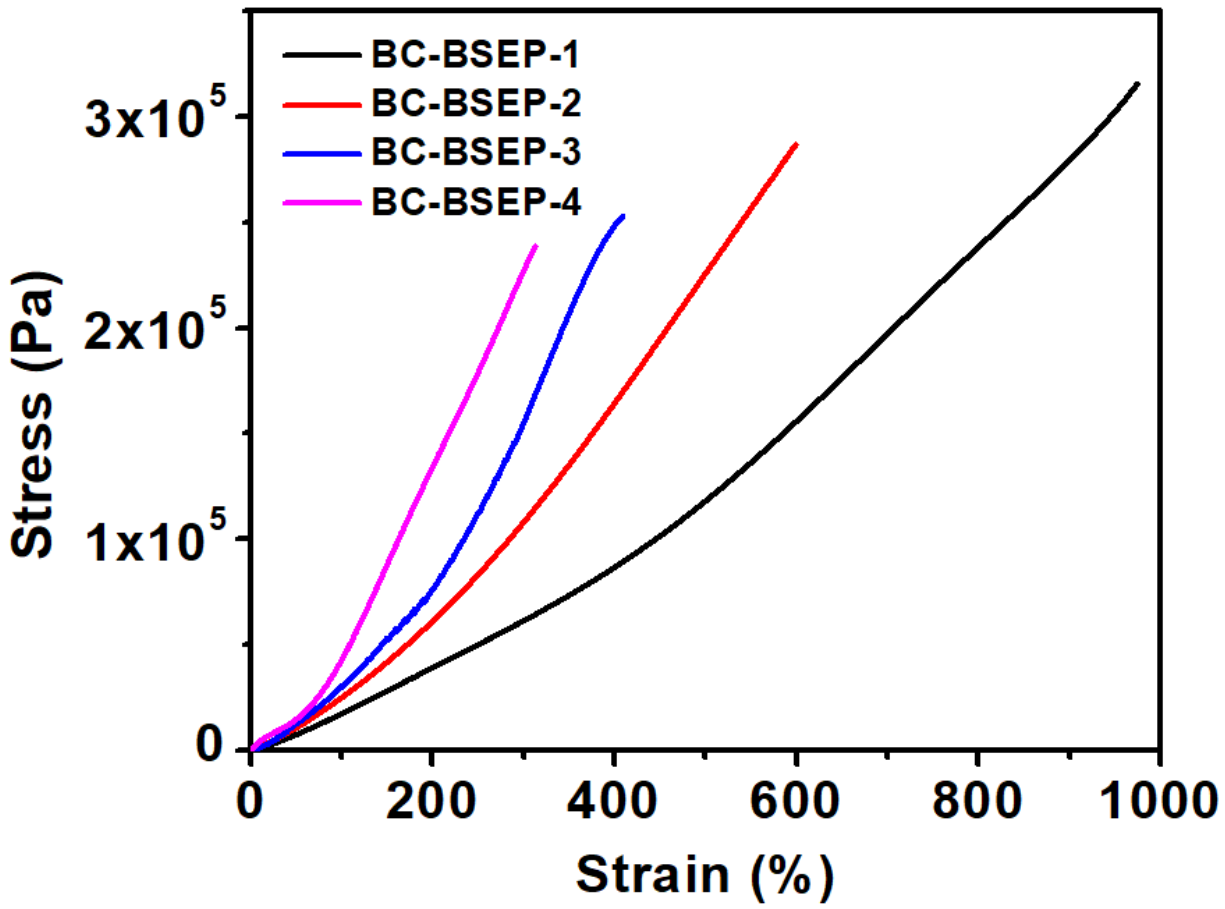

Figure 2-11. Tensile mechanical properties of BC-BSEP composites with different BC content.

The storage modulus was characterized for the composites to test the strengthening effect BC brought to the system. Due to the formation of a percolating network of strongly interacting bacterial cellulose, the storage modulus of the composite was largely influenced by the BC content. Both in the rigid state and soft state, the stiffness increases with increased BC content (Figure 2-12). For example, the storage

modulus of rigid material increased from 200 MPa for neat BSEP to 1.5 GPa for BC-BSEP-4. The 5-fold increase in modulus is resulted from the strong hydrogen bond interactions among BC nanofibers. In the soft state, where the composite was immersed in hot water (50 °C) for 10 min, storage modulus also exhibited an increase from 14 kPa (neat BSEP) to 69 kPa (BC-BSEP-4). The reason behind the increase in the soft end modulus might be the incomplete hydration of BC nanofiber network due to the hydrophobic nature of BSEP matrix. The stiffness of the composite is proved to be responsive to both temperature and water. As demonstrated in Figure 2-13, in the rigid state (RT-dry), the BC-BSEP-3 composite possesses a storage modulus of 900 MPa. With water treatment only (RT-wet), the modulus decreases to 114 MPa due to the hydration of BC nanofibers. With temperature treatment only (HT-dry), the modulus is 77 MPa due to the phase transition of BSEP matrix. With the combination of water and temperature treatment, the modulus drastically reduces to 38 kPa.

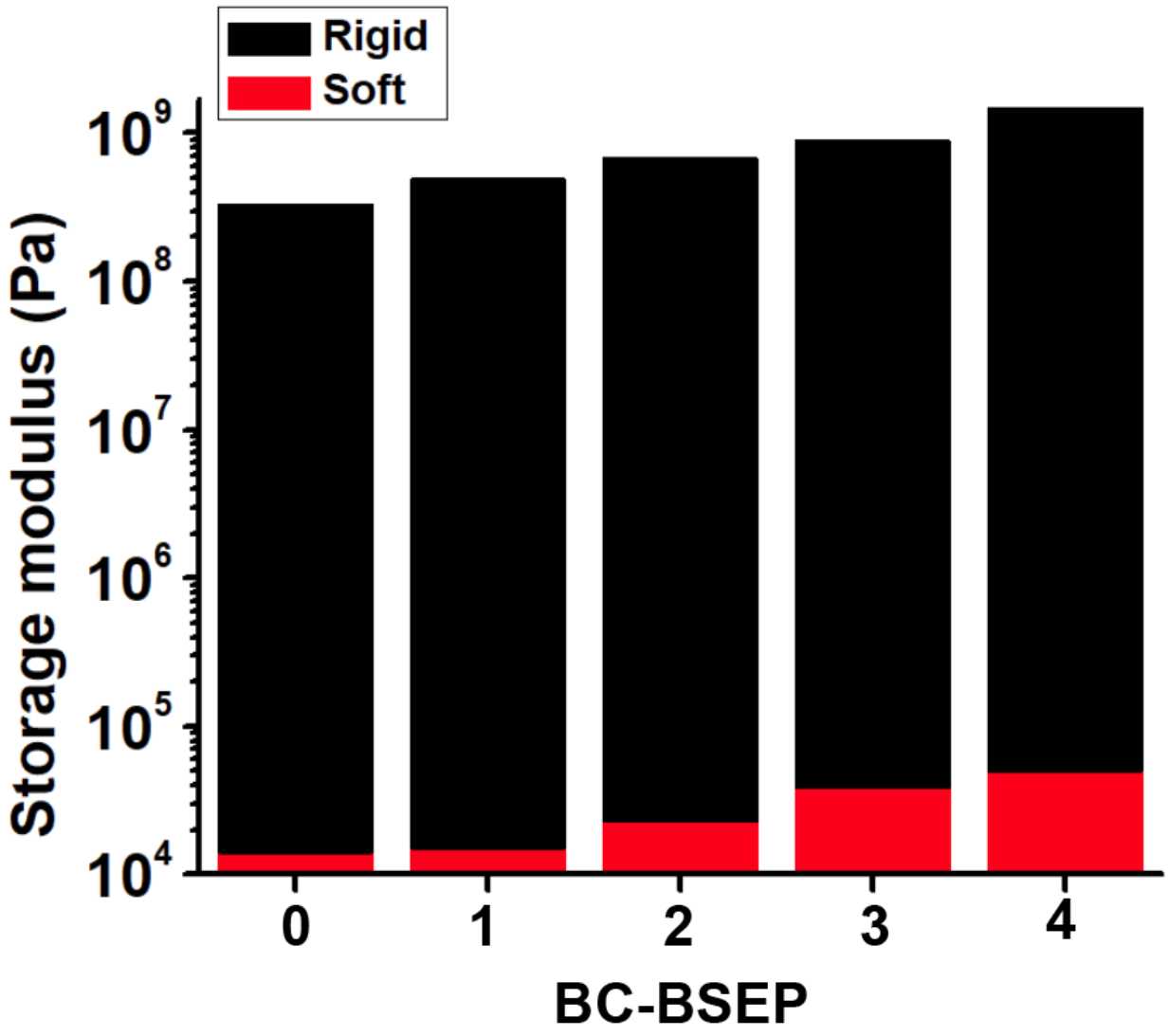

Figure 2-12. Storage modulus comparison of BS-BSEP composites in the rigid (dry and low temperature) and soft (wet and high temperature) state.

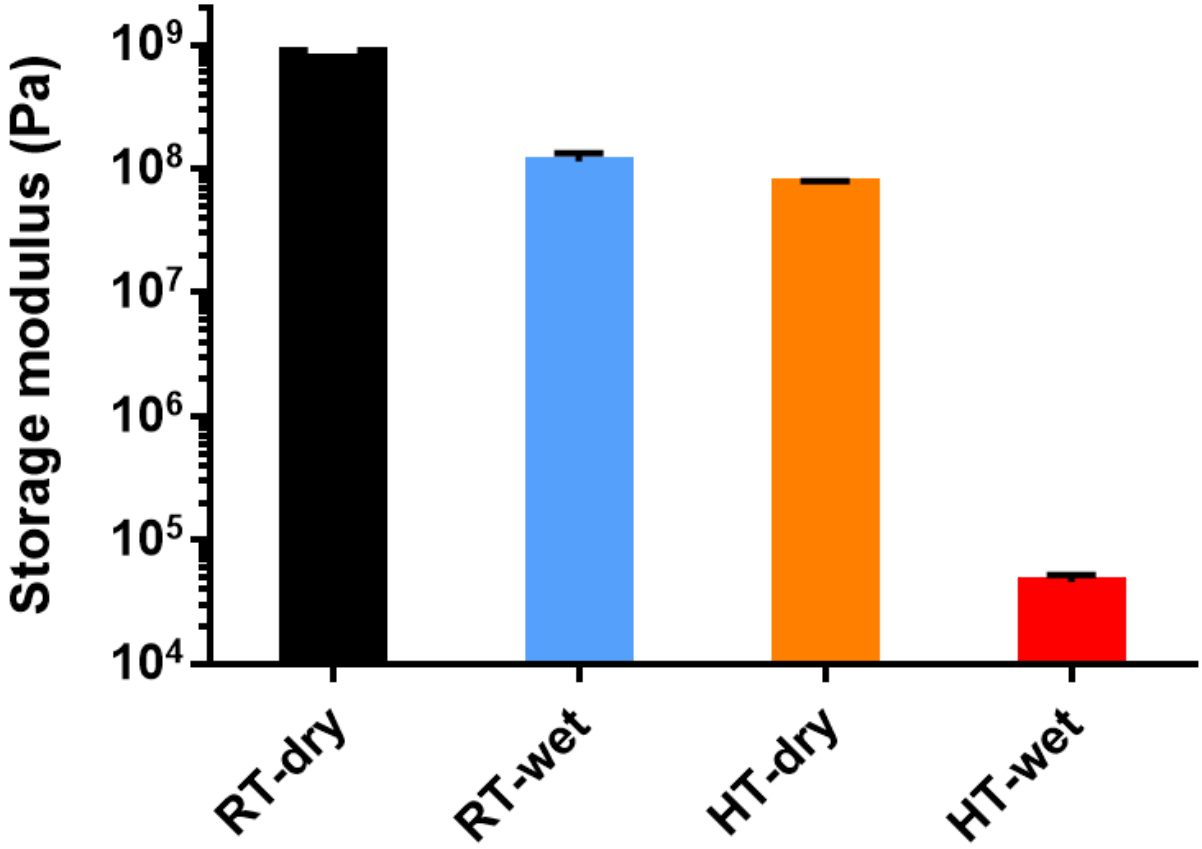

Figure 2-13. The storage modulus measurement of BC-BSEP-3 in room temperature-dry state, room temperature-wet state, high temperature-dry state, and high temperature-wet state.

2.3.5 Biocompatibility of BC-BSEP composite

For the application in biomedical area, the biocompatibility of the BC-BSEP composite is characterized. Since bacterial cellulose is a well-known biosafe material, the tests were only conducted on BSEP matrix (Figure 2-14a) and BC-BSEP composite material (Figure 2-14b). Both materials showed vivid cell growth after seeding. The existence of the dead cells is due to the natural cell growth cycle, which can also be observed in other biocompatible materials. The biocompatibility grants the BC-BSEP composite the

opportunity to be used in biomedical applications. One possible application is to substitute traditional cortical probes which are made from intrinsically rigid materials like silicon or polyimide for easy penetration into brain. The traditional probe has the risk of causing inflammation, long term damage, and scar tissue generation due to the high stiffness. A material like BC-BSEP, which has large-range stiffness tunability and is biocompatible, is ideal for use in neural implants. The dual-stimuli responsive nature is suitable for human body environment when the transition temperature of BSEP matrix is set to body temperature. In the rigid state, the BC-BSEP composite based cortical probe can be stiff enough to penetrate through the brain tissues. The physiological environment of human body will then soften the probe to match the mechanical property of brain, which reduces immune response and makes for more stable chronic recording.

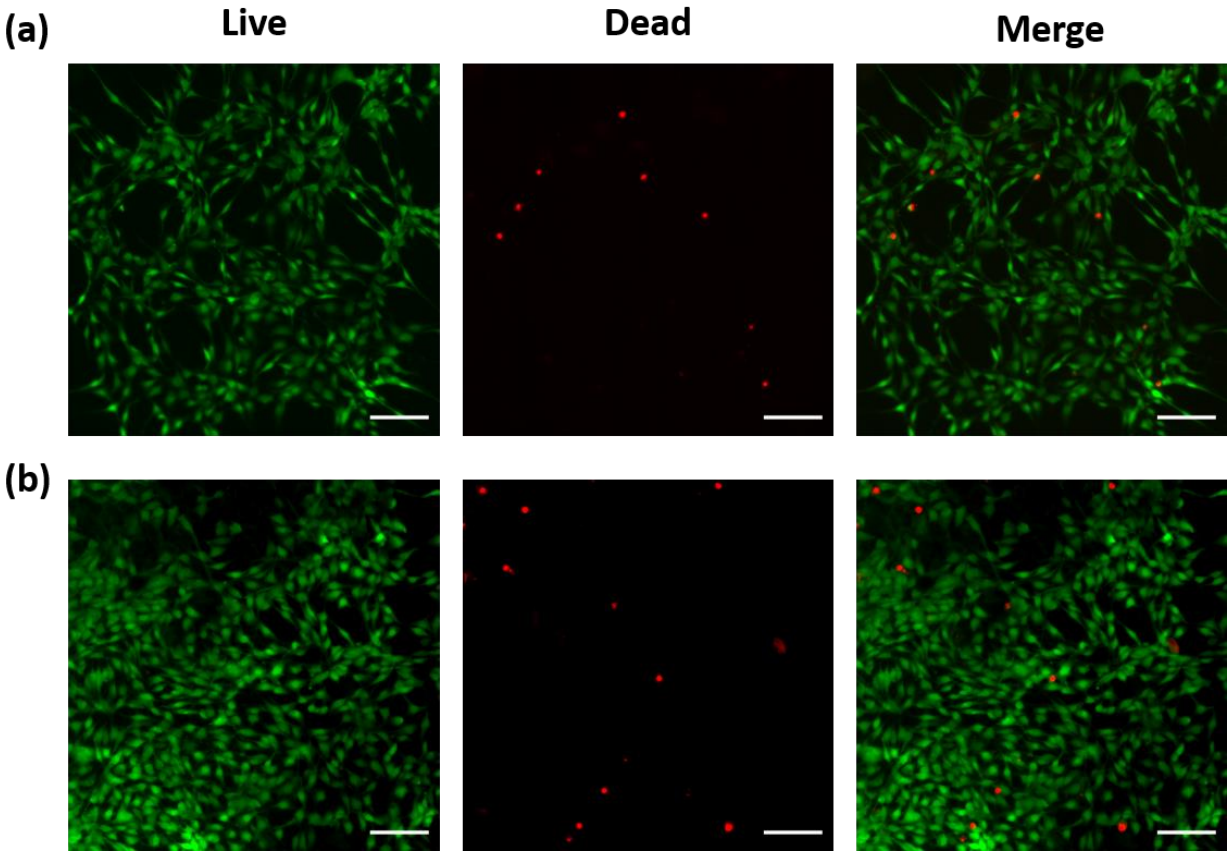

Figure 2-14. Representative fluorescent staining images of live (green) and dead (red) assay of NIH3T3 cells 3 days after cell seeding on BSEP matrix (a) and BC-BSEP composite (b). Scale bar = 100 μm.

2.4. Conclusion

A series of dual-stimuli responsive composite materials with ultra-wide stiffness variation range was fabricated. The material consists of a phase-changing BSEP matrix and a percolating bacterial cellulose network filler. The resulting composite adjust its stiffness via temperature induced phase transition by BSEP matrix and moisture induced water channels by cellulose network. With the augmentation of the twofold stiffness adjustment, the modulus of BSEP composite can be modulated by 25,000 times from nearly 1 GPa to around 40 kPa. The composite exhibits excellent mechanical strechability with maximum elongation of over 600% and tensile strength of 0.3 MPa. The composite also passes the biocompatibility test and can be used in biomedical applications.

2.5. Reference

(1) Li, J. J.; Liang, J.; Li, L.; Ren, F.; Hu, W.; Li, J. J.; Qi, S.; Pei, Q. Healable Capacitive Touch Screen Sensors Based on Transparent Composite Electrodes Comprising Silver Nanowires and a Furan/Maleimide Diels-Alder Cycloaddition Polymer. *ACS Nano* **2014**, *8* (12), 12874–12882.

(2) Niu, X.; Yang, X.; Brochu, P.; Stoyanov, H.; Yun, S.; Yu, Z.; Pei, Q. Bistable Large-Strain Actuation of Interpenetrating Polymer Networks. *Adv. Mater.* **2012**, *24* (48), 6513–6519.

(3) Qiu, Y.; Lu, Z.; Pei, Q. Refreshable Tactile Display Based on a Bistable Electroactive Polymer and a Stretchable Serpentine Joule Heating Electrode. *ACS Appl. Mater. Interfaces* **2018**, *10*,

24807–24815.

(4) Capadona, J. R.; Shanmuganathan, K.; Tyler, D. J.; Rowan, S. J.; Weder, C. Stimuli-Responsive Polymer Nanocomposites Inspired by the Sea Cucumber Dermis. *Science.* **2008**.

(5) Shanmuganathan, K.; Capadona, J. R.; Rowan, S. J.; Weder, C. Stimuli-Responsive Mechanically Adaptive Polymer Nanocomposites. *ACS Appl. Mater. Interfaces* **2010**, *2* (1), 165–174.

(6) Shanmuganathan, K.; Capadona, J. R.; Rowan, S. J.; Weder, C. Biomimetic Mechanically Adaptive Nanocomposites. *Progress in Polymer Science (Oxford)*. 2010.

(7) Kroh, A.; Heinzeller, T.; Nebelsick, J. h. *First Fossil Record of the Family Euryalidae (Echinodermata: Ophiuroidea) from the Middle Miocene of the Central Mediterranean.*; Heinzeller, T., Nebelsick, J. H., Eds.; 2004.

(8) Thurmond, F.; Trotter, J. Morphology and Biomechanics of the Microfibrillar Network of Sea Cucumber Dermis. *J. Exp. Biol.* **1996**.

(9) Esa, F.; Tasirin, S. M.; Rahman, N. A. Overview of Bacterial Cellulose Production and Application. *Agric. Agric. Sci. Procedia* **2014**.

(10) Hu, W.; Chen, S.; Yang, J.; Li, Z.; Wang, H. Functionalized Bacterial Cellulose Derivatives and Nanocomposites. *Carbohydr. Polym.* **2014**.

(11) Wallin, R. F.; Arscott, E. F. A Practical Guide to ISO 10993-5: Cytotoxicity. *Med. Device Diagnostic Ind. Mag.* **1998**, *20*, 96–98.

(12) van der Berg, O.; Capadona, J. R.; Weder, C. Preparation of Homogeneous Dispersions of Tunicate Cellulose Whiskers in Organic Solvents. *Biomacromolecules* **2007**.

(13) Dagnon, K. L.; Shanmuganathan, K.; Weder, C.; Rowan, S. J. Water-Triggered Modulus Changes

of Cellulose Nanofiber Nanocomposites with Hydrophobic Polymer Matrices. *Macromolecules* **2012**.

(14) Lewis, C. L.; Stewart, K.; Anthamatten, M. The Influence of Hydrogen Bonding Side-Groups on Viscoelastic Behavior of Linear and Network Polymers. *Macromolecules* **2014**.

Chapter 3. Refreshable Tactile Display Based on a Bistable Electroactive Polymer and Stretchable Serpentine Joule Heating Electrode

3.1. Background of this study

The interests in developing tactile interactive devices have been growing exponentially in recent years thanks to the increasing demands in a wide range of areas from virtual surgery training in medical technology[1–3], haptic controller of virtual reality (VR) headset in entertainment[4,5], and telemanipulation in robotic controls[6,7]. Tactile communication is also indispensable for people who are visually impaired[8]. Unlike audible and visual means, which are restricted to specific body parts, the sense of touch covers the entire body. Thus, by adding the sense of touch, the quality and amount of information one can gain from a machine will be substantially enriched. The most widely studied tactile displays are those that provide normal indentation to user's fingertips by vertically moving miniature pins to reproduce shape, pattern, or textures. Despite the growing needs, the critical technology barriers have resulted in a handful of tactile display products available on the market. In particular, there lacks a suitable actuation mechanism that can produce large deformations with sufficiently high blocking force, can be packaged at high pixel resolution, have compact form factor and light weight, and can be produced at low costs[9].

3.1.1 Current tactile devices in the field

Most of the tactile devices suffer from bulky actuator structures. Piezoelectric bimorph tactile displays exhibit high blocking force at a wide frequency range[10,11]. Unfortunately, these devices are bulky due to the encumbrance of the cantilevers. Tactile shape display using RC servomotors[12] have large displacement

and appropriate actuator density but are also bulky (76 mm × 76 mm × 119 mm) and inconvenient for day to day operation. Shape memory alloy (SMA)[13] have also been implemented in previous tactile displays. The requirement for extensive heating and cooling steps limits the utility of the device, and raises manufacturing costs. Phase changing materials that exhibit volume change over melting[14] or boiling[15,16] point were developed as refreshable Braille cells. These devices, which require miniature Joule heating electrode and thermally insulated chamber for each dot, have complex architecture and usually exert small stroke and force.

3.1.2 Tactile devices based on DE technology

In recent years, dielectric elastomer actuators (DEA) have emerged as a promising compact tactile display technology [17–19]. Their light weight, high actuator density, and high stroke range offered the same performance as previous technologies but in much more compact form factors. However, the translation of the DEA technology to marketplace has been sluggish, due to the high driving voltages which could cause static shocks or even injury. Attempts by researchers to incorporate insulating layers to seal the DEA generally lowered the actuation performance and increased the fabrication complexity.[20–24] We reported an alternative approach to fabricating a refreshable Braille display using a BSEP as an electroactive transducer. [25] The shape memory property of the BSEP allowed for separation of high voltage elements from operators, but the device used an external heater, and the resulting stroke was small. While mitigated in the BSEP designs, the concerns for high voltage were not eliminated entirety.

3.1.3 Pneumatic tactile devices

In comparison to the electric stimuli, pneumatic tactile devices are usually more stable and can provide higher force feedback. However, most pneumatic devices either have complex structures which require individual air streams for each actuator [26], or require electrostatic microvalves for each dot [27]. Scaling up the number of actuators while maintaining compact form factor is challenging. Recently, Besse et al.[28] reported a 32 by 24 actuator pneumatic flexible active skin based on a shape memory polymer (SMP). Each actuator has a diameter of 3 mm, and is placed on a 4-mm pitch. The device was demonstrated as active camouflage and tactile display with a stroke of 0.4 mm. The pitch and the stroke do not match the requirements for Braille text which are typically 2.5 mm and 0.5-0.6 mm respectively.

3.1.4 Compact pneumatic tactile display based on BSEP

Here, we report a high resolution pneumatic tactile display that can exert large stroke and provide high blocking force. The device exploits the large stiffness change of the BSEP polymer and large-strain deformation of the polymer at the softened state. A serpentine-patterned carbon nanotube coating composited on the BSEP membrane surface is used to administer local temperature change and the membrane's stiffness. A single pneumatic reservoir is employed to deform all the softened areas at once. The tactile display can be actuated at low voltage supply (30 V) to obtain large stroke, high blocking force, and safe operation with fast response speed. Potential applications for such a tactile display are numerous, such as reproducing surface topography, providing haptic feedback for human-machine interfaces, and electronic Braille readers.

3.2. Experimental section

3.2.1 Raw materials

Urethane diacrylate (UDA, catalog name: CN9021) was obtained from SARTOMER and used as received. Stearyl acrylate (SA), trimethylolpropane triacrylate (TMPTA), acrylic acid (AA), 2,2-Dimethoxy-2-phenylacetophenone (DMPA), benzophenone (BP), and isopropyl alcohol (IPA) were purchased from Sigma-Aldrich and used as received. Single-walled carbon nanotubes (catalog name: P3-SWNT) were purchased from Carbon Solutions, Inc.

3.2.2 BS80-AA5 thin film fabrication

The prepolymer solution was made by mixing 80 parts (by weight) of SA, 20 pats of UDA, 5 parts of AA, 1.5 parts of TMPTA, 0.25 part of DMPA, and 0.125 part of BP at 50 °C. The prepolymer solution was then injected between a pair of glass slides on a hot plate with two strips of tape as spacers. The thickness of the liquid layer was defined by the thickness of the spacers. In the device assembling, 90 μm thick spacers were used to fabricate the BSEP film. Next, the prepolymer was cured through a UV curing conveyor equipped with a Fusion 300S type "H" UV curing bulb for about 3min. Then the film can be gently peeled off the glass slide after it cooled down to room temperature.

3.2.3 Serpentine Patterned Carbon Nanotube (S-CNT) Joule Heating Electrode Fabrication.

The carbon naotube (CNT) dispersion solution was made by mixing 5 mg of P3-SWNT powder, 1 ml water, and 20 ml IPA. The mixture was bath sonicated for 90 min to get a stable dispersion. Large aggregates were disposed using centrifuge at 8500 rpm for 10 min. The resulting supernatant is then ready for spray coating.

The stretchable S-CNT electrode was obtained by first prestretching the softened BSEP film by 100% × 100% biaxially. The prestretched film was then cooled down to room temperature to preserve the deformation. Next, a shadow mask with serpentine pattern cutout was attached to the prestretched rigid BSEP. The prepared CNT dispersion solution was sprayed on BSEP through the mask using an airbrush at an air pressure of 30 psi. Next, a solution of UDA in toluene (10 vol%) was sprayed and cured on top of the entire film without the mask. The thickness of the poly(UDA) layer is around 5 μm. Finally, the film recovered to its original size by heating and releasing the prestretch.

3.2.4 Device assembling

The resulting film of BSEP with S-CNT was attached to the chamber cover (17 mm × 17 mm) with a double-sided Kapton^{TM} tape as adhesive layer in between. The double-sided tape was cut with openings that align with the S-CNT matrix. The whole device could be assembled by screwing the chamber cover with the pneumatic chamber.

3.3. Results and discussion

3.3.1 device design and fabrication

The demonstrated tactile device contains a 4 by 4 tactile pixel (taxel) matrix with outer size of 17 mm × 17 mm × 3 mm (Figure 3-1a). Each taxel has 1.5 mm diameter with 2.5 mm distance between the centers of two adjacent taxels (designed according to Braille standard[30]). The device primarily consists of two parts: a pneumatic system and a thin BSEP active film that can be thermally controlled to soften locally. The pneumatic system constitutes a pneumatic chamber and a miniature pump to provide pressurized air

for actuation. The specific BSEP polymer used exhibits stiffness change of three orders of magnitude in a narrow temperature range of less than 10 °C. At room temperature, the BSEP possesses a modulus of several hundred MPa, and behaves as a rigid plastic, capable of providing a blocking force as high as 50 g. Above its transition temperature, the polymer becomes soft and stretchable with its modulus decreasing to 0.1 MPa. The BSEP active film has a thickness of about 90 μm. A matrix of highly compliant single-walled CNT Joule heating electrode patterned in serpentine shape (S-CNT) is formed on the surface of the BSEP film. The thermal stability, mechanical compliancy, and chemical resistance of CNTs made it an ideal choice as the Joule heating electrode [31,32]. The BSEP with S-CNT electrode is attached on the chamber to make the chamber relatively air-tight. The rigid chamber cover is then mounted using an adhesive tape and 4 corner screws. The circular openings on the adhesive tape and the chamber cover aligns with the S-CNT electrode areas, each defining a taxel area. A pin with a flange on one end to prevent it from dropping out of the taxel cell is placed in each taxel. The protruding surface of the pin is the tactile interface of the taxel. As each taxel has an independent S-CNT Joule heating electrode, the modulus of the BSEP can be altered locally, enabling individual taxel control of the display panel. By synchronizing the pneumatic pressure and thermal stimuli, the BSEP can be locally softened and deformed, thereby raising individual pins by 0.7 mm in height (Figure 3-2) and presenting unique configurations to the end user. Upon cooling, the BSEP rigidifies, which takes less than 2 s, no external energy input is then needed. In figure 3-1C, the 4 × 4 tactile display shows “U” “C” “L” “A” on the device, demonstrating the precise control of individual dots. The display can be quickly refreshed by reheating the deformed taxels without applying any pneumatic pressure.

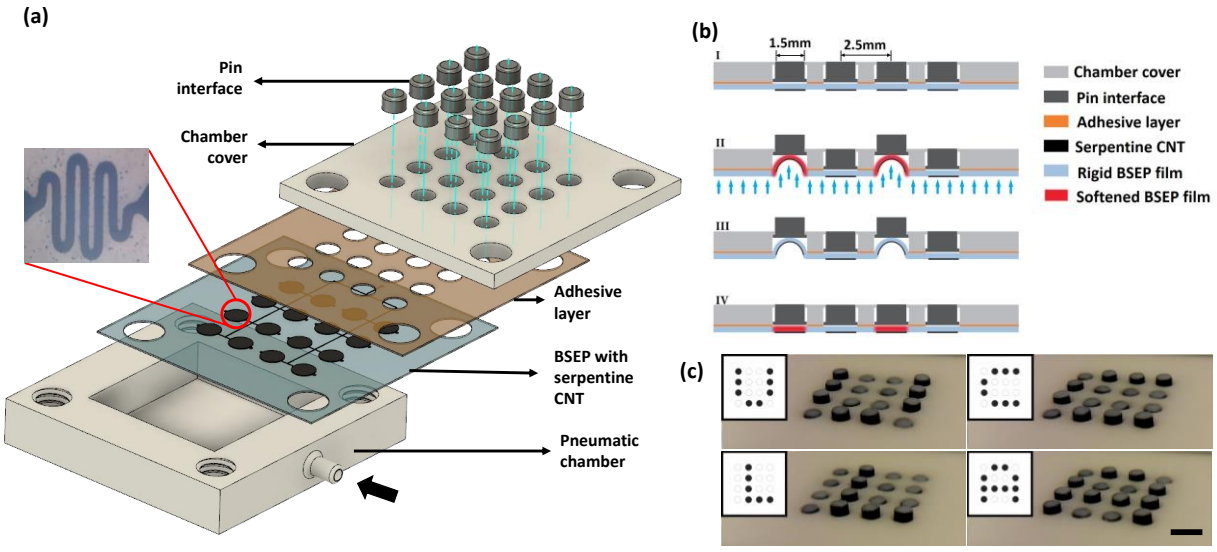

Figure 3-1. A compact tactile display. (a) Schematic of the layered structure of a 4 ×4-pixel array. (b) Cross sectional view of the working mechanism. The taxels, with Braille size (I), is individually actuated by softening (50 °C) and deforming the BSEP in corresponding area (II). The deformation is then maintained without any energy input when the BSEP film cools below 40 °C (III). The original shape is recovered by reheating the BSEP (IV). (c) Demonstration of a 4x4 tactile display showing “U”, “C”, “L”, “A”. The scale bar represents 2 mm.

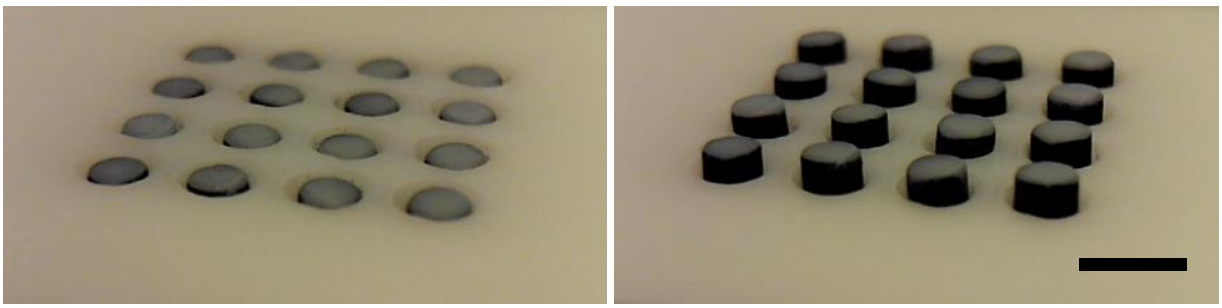

Figure 3-2. Photographs of a 4 × 4 tactile display in the flat state (left) and all actuated state (right). Both states are stable without any external energy input. The scale bar represents 2 mm.

The core component in the pneumatic tactile display is the BSEP film with stretchable Joule heating electrode. To obtain high stretchability, we developed a "P3R" fabrication process: Prestretch-Pattern-Protect-Release (Figure 3-3a). The method starts with prestretching a softened BSEP film biaxialy by 100% × 100%. The prestretched film maintains the stable deformed-shape after it cools down. A dispersion solution of CNTs in an isopropyl alcohol and water mixture solvent is then sprayed on the prestretched BSEP through a shadow mask. The mask has a serpentine shaped cutout pattern formed by laser ablation. Next, a solution of urethane diacrylate (UDA) monomer in toluene is sprayed on top of the CNT-coated BSEP film. Because of its low viscosity, the UDA solution infiltrates into the CNT network, forming an ultra-thin CNT-poly(UDA) interpenetrating composite electrode after the UDA layer is cured. As the CNT network is embedded into the poly(UDA) layer, physical translation of CNTs is largely prevented during the deformation of the BSEP film. Moreover, since the UDA monomer is also one of the co-monomers to form the BSEP, the poly(UDA) layer strongly bonds the BSEP film. When the resulting poly(UDA)/CNT/BSEP composite structure is heated above the BSEP's melting temperature (T_m) to release the prestretch in the BSEP layer, the BSEP matrix along with the S-CNT electrode shrinks 100% × 100% biaxially, while the poly(UDA) layer wrinkles up (Figure 3-3b). The wrinkled topography is shown as a "greasy" surface in the upper microscopic image, whereas the flat surface of the CNT/BSEP electrode prepared without the poly(UDA) shows a "dry" surface. Note that the "greasy" surface is resulted from the surface unevenness that blurs the optical image and imparts the S-CNT electrode with high stretchability. This P3R method and the serpentine shaped pattern of the CNT layer afford an active BSEP film with a highly compliant and stretchable Joule heating electrode.

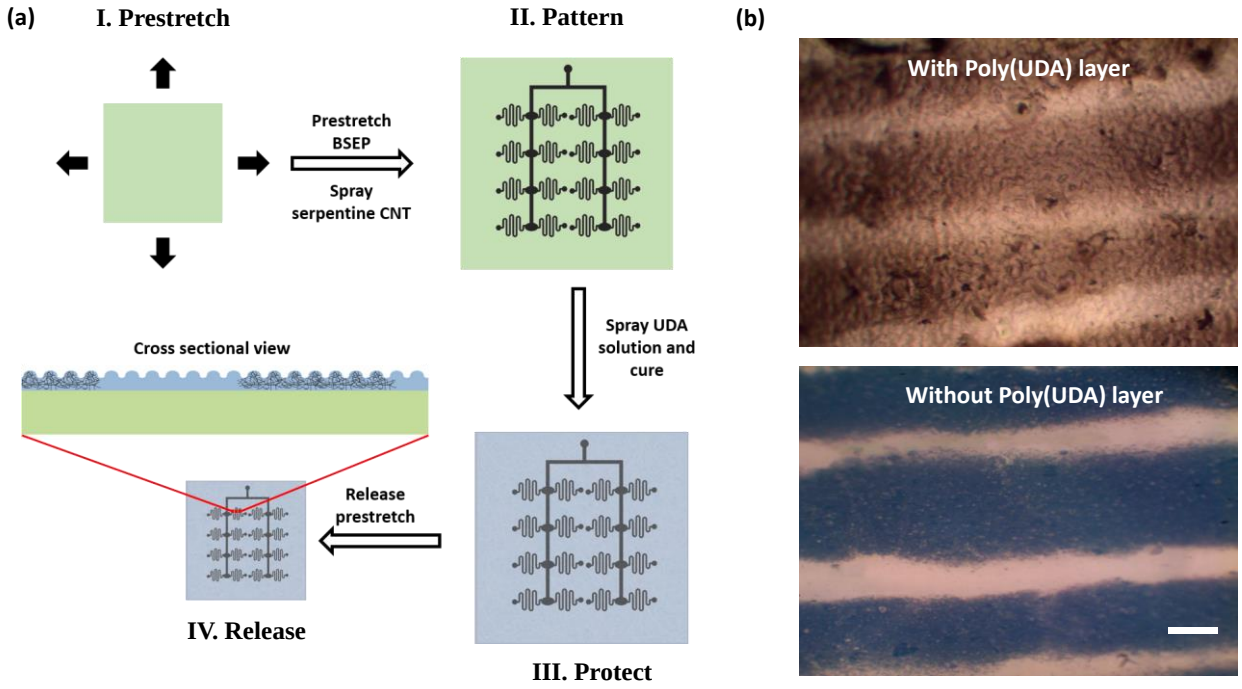

Figure 3-3. (a) Schematic illustration of the "P3R" fabrication process of BSEP film with serpentine CNT Joule heating electrode. (I) Prestretch: the BSEP film is prestretched biaxially at elevated temperature and then cooled down. (II) Pattern: a carbon nanotube solution is spray coated on the prestretched BSEP through a shadow mask. (III) Protect: A monomer (UDA) solution is spray-coated on the CNT electrode and cured, forming a CNT-poly(UDA) interpenetrating composite. (IV) Release: the prestrain is released by softening the BSEP film. (b) Optical microscopic images of the BSEP active layer with (above) and without (bottom) the poly(UDA) layer. The scale bar represents 0.1 mm.

3.3.2 Bistable electroactive polymer (BSEP)

Variable stiffness material has been an actively researched subject for decades because the ability of muscle to adjust its modulus is responsible for the adaptability and dexterity of animals. Shape memory

polymers (SMP), which exhibit a modulus change by a few hundred-fold during glass transition [33,34], can be programed to different rigid shapes via stretching at elevated temperatures[35]. Glass transition typically spans in a broad temperature range of over 20 ºC[25] which limit the utility of these materials. For applications involving human tactile interaction[28], the SMP needs to remain rigid up to around 37 °C to prevent incidental shape changes. The actuation would be conducted above the polymer's glass transition temperature (T_g), or more than 20 °C above body temperature which could induce tissue damage. This limitation is addressed in this work with a phase changing BSEP polymer we recently developed comprising stearyl acrylate (SA) moiety in the polymer that can reversibly crystallize and melt within a narrow temperature range [36] (Figure 3-4). The phase change occurs within 10 °C and induces a modulus change of nearly 1000-fold.

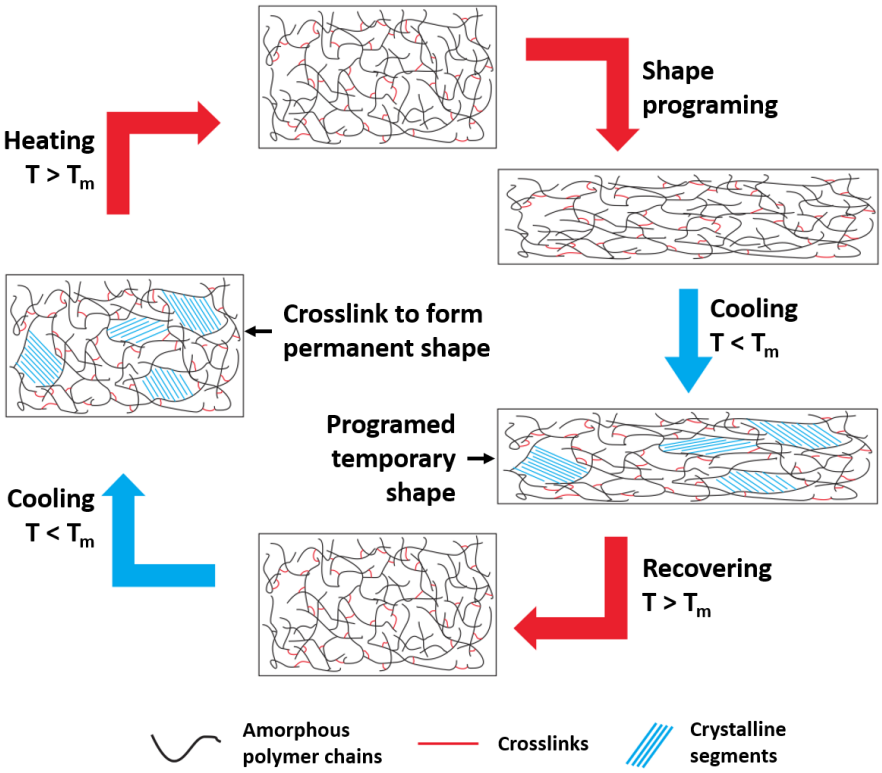

Figure 3-4. Schematic illustration of shape memory mechanism of phase changing BSEP.

The compounds used to synthesize the phase changing BSEP are shown in Figure 3-5, and the synthetic details are found in the experimental section. To obtain the optimal overall performance for tactile display application, the BSEP was formulated to contain 80 parts of SA (by weight), 20 parts of UDA, 5 parts of acrylic acid (AA), 1.5 parts of TMPTA, 0.25 part of DMPA, and 0.125 part of BP, and the polymer is labeled as BS80-AA5. Adding the small amount of acrylic acid was found to help increase the modulus change, mechanical toughness, and electrode bonding.

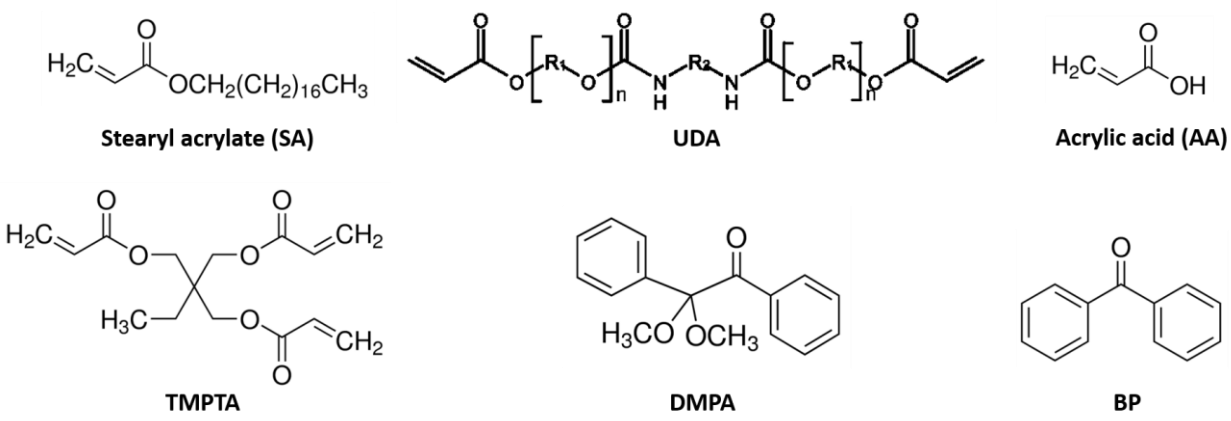

Figure 3-5. Chemical structures of monomers and initiators used for the synthesis of S80-AA5.

Stiffness change is critical for BS80-AA5 to maintain the actuated shape. The hydrogen bonds from the carboxylic acid group in AA helped increase the difference in modulus between room temperature and elevated temperature. At room temperature, the carboxylic acid groups form double hydrogen bonding dimers which help further increase the stiffness.[37] With increasing temperature, the hydrogen bonds weaken, thus have diminished effect on the modulus of the softened BSEP. Dynamic mechanical analysis of the BSEP polymer was conducted at a temperature ramping rate of 2 °C /min from 25 to 55 °C and a mechanical loading frequency of 1 Hz. Figure 3-6a shows that BS80-AA5 possesses a steep stiffness change of 3000 times from about 300 MPa to about 0.1 MPa. The transition occurs from 40 °C to 47 °C. Once the transition is completed, the storage modulus remains constant with further increasing temperature. The ultralow modulus of only 0.1 MPa in the rubbery state is resulted from the presence of large amount of molten stearyl chains which serve as plasticizers to the polymer. The substantial modulus switching leads to high shape memory property (Figure 3-7). In fact, the fixation rate and recovery rate of BS80-AA5 are both close to 100%.

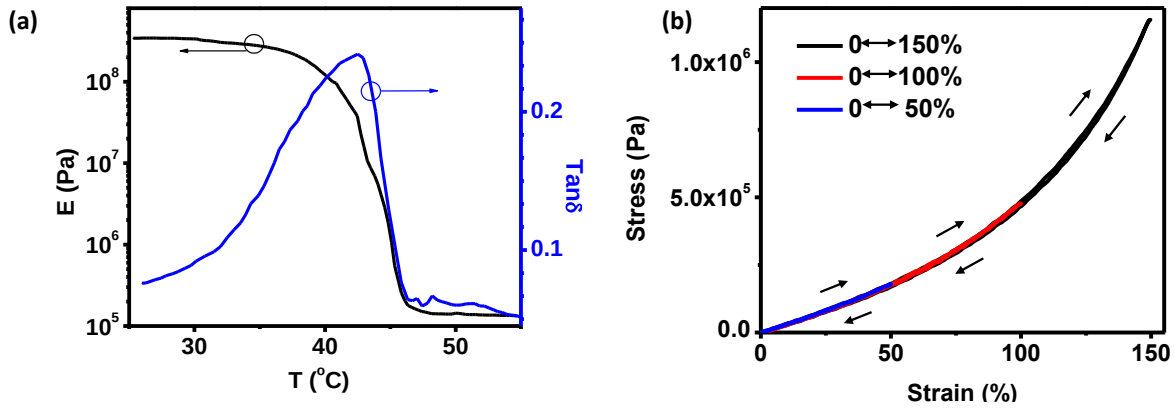

Figure 3-6. Mechanical properties of BS80-AA5. (a) The sharp change of storage modulus and loss factor with respect to temperature. (b) Cyclic tensile loading-unloading tests of BS80-AA5 under different stretch ratio with strain rate of 0.01 /s.

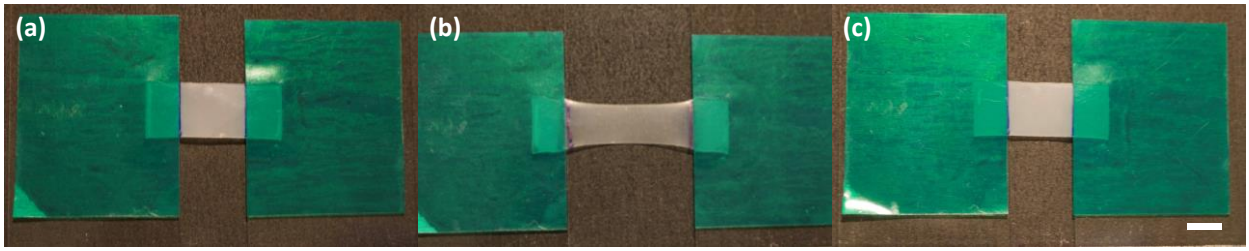

Figure 3-7. Shape memory demonstration of a BS80-AA5 film at its original shape (a), deformed with 100% linear strain via a heating-stretching-cooling procedure (b), and recovered to original shape (c). All shapes are rigid and free-standing. The scale bar represents 1 cm.

An essential requirement for the refreshable tactile display is the reversibility and repeatability of the taxel actuation over many cycles. The elasticity of BS80-AA5 in the rubbery state was thus characterized. The loss factor of the softened BS80-AA5 is around 0.05 (Figure 3-6a), which indicates very low viscoelasticity and thus fast response speed. Cyclic tensile tests were also carried out at 50 °C with a strain rate of 0.01 s^{-1}. The tests consisted of three loading-unloading loops with strain successively up to 50%, 100%, and 150%, respectively, in three separate tests. The resulting stress-strain curves are shown in Figure 3-6b where the loading and unloading curves completely overlap, suggesting that the material behaves elastically with minimal hysteresis, thereby agreeing with the low loss factor measured in dynamic mechanical analysis. Another important requirement for BS80-AA5 to resist fracture during

stretching is high toughness. The hydrogen bonds from acrylic acid act as reversible crosslinks to enhance the toughness. Physical crosslinks have been identified as an essential element to toughen soft gels.[38–40] The non-permanent crosslinks can break and re-form to overcome stress concentration and dramatically enhance crack propagation resistance. The comparison of toughness between BS80-AA5 and BS80 (without acrylic acid) was characterized via uniaxial tensile test at 50 °C (Figure 3-8). The BS80-AA5 has a maximum elongation of 320% with a normal tensile strength of 8 MPa and true tensile strength calculated to be 34 MPa. Without the toughening effect from acrylic acid, BS80 ruptured at 191% strain with a tensile strength of only 0.26 MPa (true stress calculated to be 0.76 MPa). Moreover, the highly stretchable poly(UDA) layer helped further increase the maximum elongation and tensile strength of BS80-AA5/poly(UDA) film without having much impact on the storage modulus of the composite film (Figure 3-9). The high tensile strength of BS80-AA5 is important for the polymer to resist against fracture. Meanwhile, the stress to obtain up to 200% strain is low, i.e., the softened BS80-AA5 is highly compliant, and large deformation could be obtained with low pneumatic pressure. The air pressure needed to actuate a taxel to different heights was measured and the results are shown in Figure 3-10. For a 90 μm thick BSEP film, the pressure to generate an out-of-plain displacement of 0.7 mm (minimum displacement requirement for Braille is 0.5 mm[30]) is only 160 mmHg.

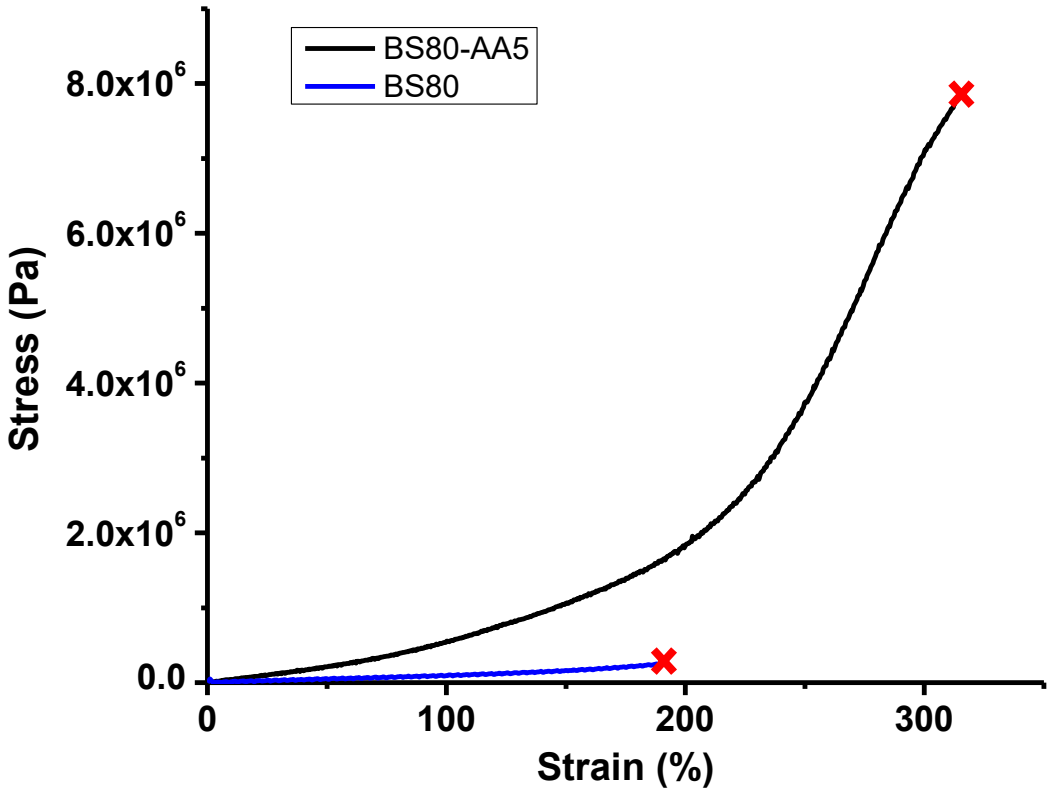

Figure 3-8. Tensile stress-strain response of BS80-AA5 and BS80 at 50 °C. The stretching rate is 0.1 mm/s.

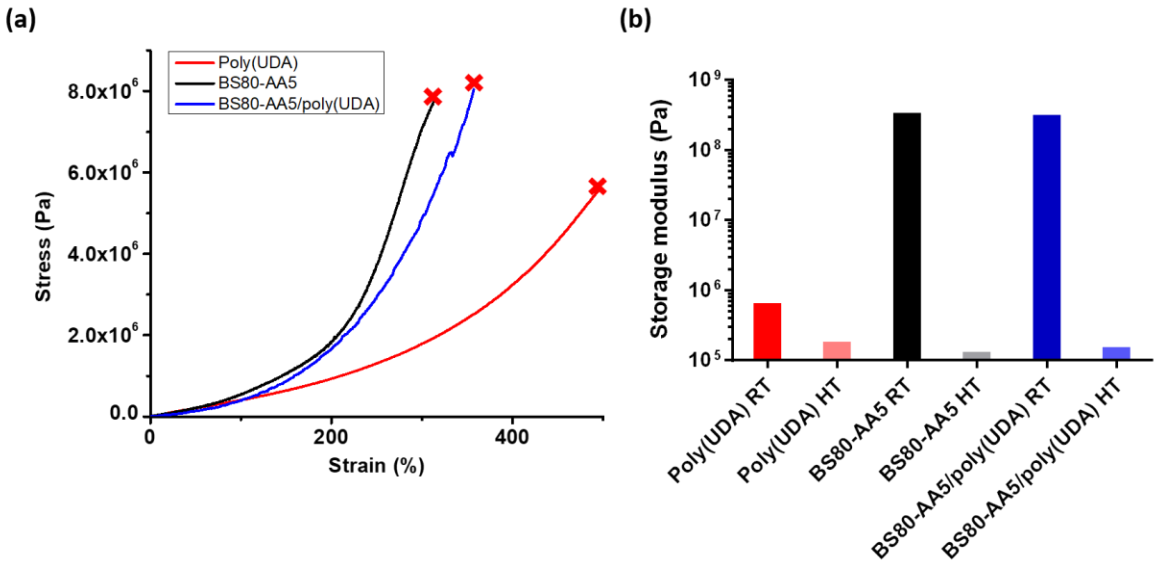

Figure 3-9. (a) Tensile test comparison of poly(UDA), BS80-AA5, and BS80-AA5/poly(UDA) composite. The composite film was made by spraying and curing a thin layer of poly(UDA) (5 μm) on a 90 μm BS80-AA5; (b) Storage modulus measurements of the three materials at room temperature (RT) and 50 °C high temperature (HT).

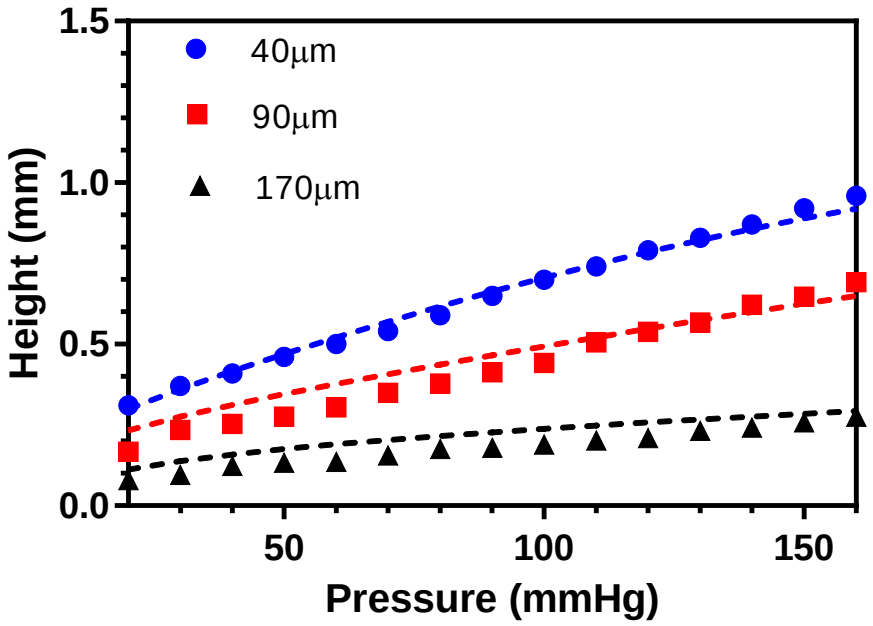

Figure 3-10. Measured (symbols) and simulated (dashed curves) internal air pressure needed to actuate a softened BSEP taxel to different heights. The thickness of the BSEP films ranges from 40 μm to 170 μm.

In the rigid state of the BSEP polymer, the crystalline aggregates of the SA moieties act as hard segments in the polymer, resulting in a storage modulus of 340 MPa. The taxels are thus expected to be able to resist large forces applied to the raised dots. The blocking force, or force required to press down the raised dots to completely overcome the original vertical displacement, was measured for taxels in which the BSEP polymer had originally been actuated into various raised height. Note that raised height of 0.75 mm means the BSEP film was actuated to a half-dome shape with an area expansion of 100%. The results are shown in Figure 3-11a for BS80-AA5 films with undeformed thickness ranging from 40 μm to 170 μm. ANSYS Finite Element Analysis (FEA) was also performed to simulate the blocking force of the taxels based on Yeoh's 3rd hyperelastic model. The FEA simulation results match the experimental data quite well. More

information about FEA simulations can be found in supporting information. For the tactile display panel we fabricated, the BSEP film with un-deformed thickness of 90 μm was used. The rigid taxels with actuated displacement of 0.5 mm have a blocking force of 50 g, which is much greater than the 15 g requirement in typical tactile devices[30].

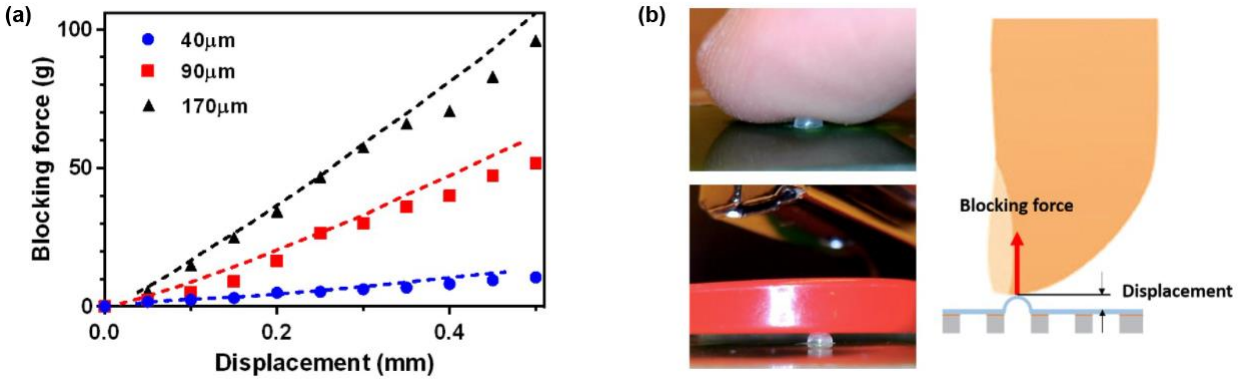

Figure 3-11. (a) Measured (symbols) and simulated (dashed curves) blocking force required to completely press down an actuated BS80-AA5 taxel with different displacement. The thickness of the un-deformed BSEP films ranges from 40 μm to 170 μm. (b) Pictures showing a rigid BSEP taxel with 90 μm thick BSEP capable of deforming a user's fingertip (up left) and supporting a 25 g mini stapler (down left), and a schematic illustration of measured blocking force (right).

3.3.3 Serpentine CNT Joule heating electrode

Mechanical impedance of the Joule heating electrode coated on the BSEP film can alter the actuated strain (raised height) and uniformity (shape of the raised dome structure). It is essential to develop a heating electrode that is both highly compliant and stretchable. In recent years, great efforts have been made to develop stretchable conductors for the next generation of flexible and wearable electronics that can conform to movable and arbitrarily shaped surfaces[41–43]. However, much of these reported stretchable

conductors are too stiff for the present application. We selected carbon nanotube as the Joule heating electrode material thanks to the nanotubes' large length-to-diameter aspect ratio that form highly porous percolation networks and have high thermal and environmental stability. The Joule heating requires a thick coating of CNT to obtain low surface resistance for low-voltage heating, but a thick coating would induce significant mechanical impedance[31] and may delaminate from the polymer matrix. Moreover, with such high resolution, where the closest distance between two adjacent taxels is only 1 mm, it is essential for the Joule heating electrodes to obtain uniform and precise heating to prevent crosstalk. To overcome these issues, the "P3R" fabrication process: Prestretch-Pattern-Protect-Release was employed to obtain simultaneously low surface resistance, low mechanical impedance, and high stretchability.

The carbon nanotubes (P3-SWNT, Carbon Solutions, Inc) we used for the electrode were specifically tailored for dispersion in solvents, and contain 6% carboxylic acid groups (SWNT-COOH) [44]. The SWNT-COOH bonds to BS80-AA5 strongly through the hydrogen bonding interactions between the carboxylic acid groups[37]. Figure 3-12 demonstrates the CNT electrode on a BS80-AA5 film capable of surviving multiple tape peeling tests. A Kapton™ tape with a high peeling strength of 46 oz/in was used to check if the CNT could be removed during peeling. After several peeling processes, the resistance and the color of the CNT electrode on BS80-AA5 didn't change at all, suggesting strong bonding between CNT and BS80-AA5. In comparison, the CNT electrode similarly formed on a BS80 film were almost completely transferred to the tape after one test, and lost surface conductivity.

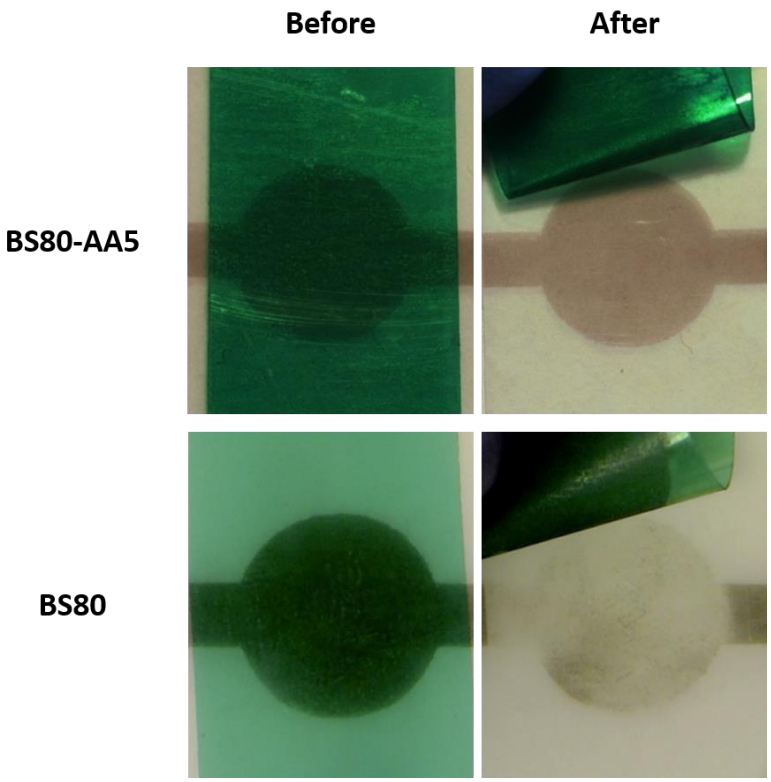

Figure 3-12. Testing of the adhesion of CNT on BS80-AA5 and BS80 film using Kapton^{TM} tape.

The heating process is the most critical step in the operation of the tactile display device. To achieve high-efficiency heating with low mechanical impedance, we fabricated the CNTs into a serpentine shape. The serpentine architecture has been explored by a number of research groups as an effective approach to impart large stretchability to electrodes.[45–49] As Joule heating electrode, a more important character is uniform and rapid heating. With applied voltage, the charge carriers will be restricted within the winding path of the serpentine pattern, resulting in uniform heating over the taxel area (Figure 3-13a and 3-13c). On the other hand, for the conventionally-used round-shaped pattern, the charge carriers tend to travel the shortest distance, causing the current density to mainly distribute along the equatorial area (Figure 3-13b and 3-13d). In our device, the resistance of one S-CNT was kept at around 40-50 kΩ to ensure low voltage

(~ 30 V) activation for the device. As shown in Figure 3-13e, the time needed for the serpentine shaped electrode to reach 47 °C, which is the temperature to soften BS80-AA5, is less than 1 s, while it takes more than 5 s for the round shaped electrode (with same resistance) to reach 40 °C. The unique winding path of the S-CNT increases the heating efficiency, resulting in rapid and uniform heating in a very short time. The short heating duration also prevents excessive heat dissipation which not only consumes more electrical energy, but also could cause thermal crosstalk with neighboring pixels. Moreover, the serpentine pattern is also very effective to retain the compliancy of the Joule heating electrode. Under the same electrode loading per unit area, the storage moduli of the poly(UDA)/CNT/BS80-AA5 films where the CNT electrode is either blanket-coated or serpentine-patterned are 1.9 MPa and 0.36 MPa, respectively, at 50 °C. Both moduli are higher than that of the softened BS80-AA5 film which is 0.13 MPa at 50 °C. Note that PUDA layer has higher stiffness compare to BS80-AA5, which also contributes in the modulus increase (Figure 3-9b). High compliancy of the S-CNT electrode is essential for the low air-pressure actuation.

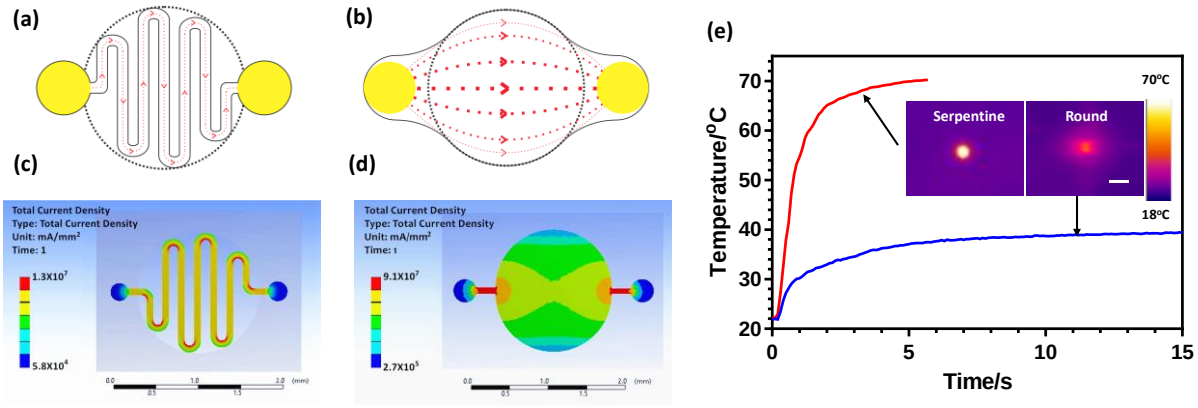

Figure 3-13. Illustration (a,b) and simulated (c,d) results of current density distribution in serpentine shaped and round shaped electrodes. The widths of the red dotted lines in (a) and (b) indicate relative current density. (e) Transient temperature responses of the electrodes at 30 V. Insets in (e) are infrared camera images of the heated electrode areas. The scale bar is 2 mm.

Joule heating characteristics of the S-CNT electrode under different voltages were also investigated, and the results are shown in Figure 3-14. The electrode exhibits high heating rate, considering the high resistance of the S-CNT electrode. Complete softening (above 47 ^{o}C) could be obtained in less than 1 second at 30 V operation. The cooling process to below 40 ^{o}C to stiffen BS80-AA5 requires about 2 seconds. The air flow in the diaphragm configuration induced by the pneumatic pumping could facilitate heat dissipation to further driving down the duration of the cooling step. Thus, a taxel actuation cycle can be completed in 3 seconds. The thermal and pneumatic control sequence of the taxel actuation is illustrated in Figure 3-15. After one second, the Joule heating can be turned off, while the pneumatic pump is turned on. Because of the elastic nature of the BS80-AA5 film, once the pump is on, the pin interface is lifted immediately. Then the pump can be turned off in 2 seconds when the film has cooled down.

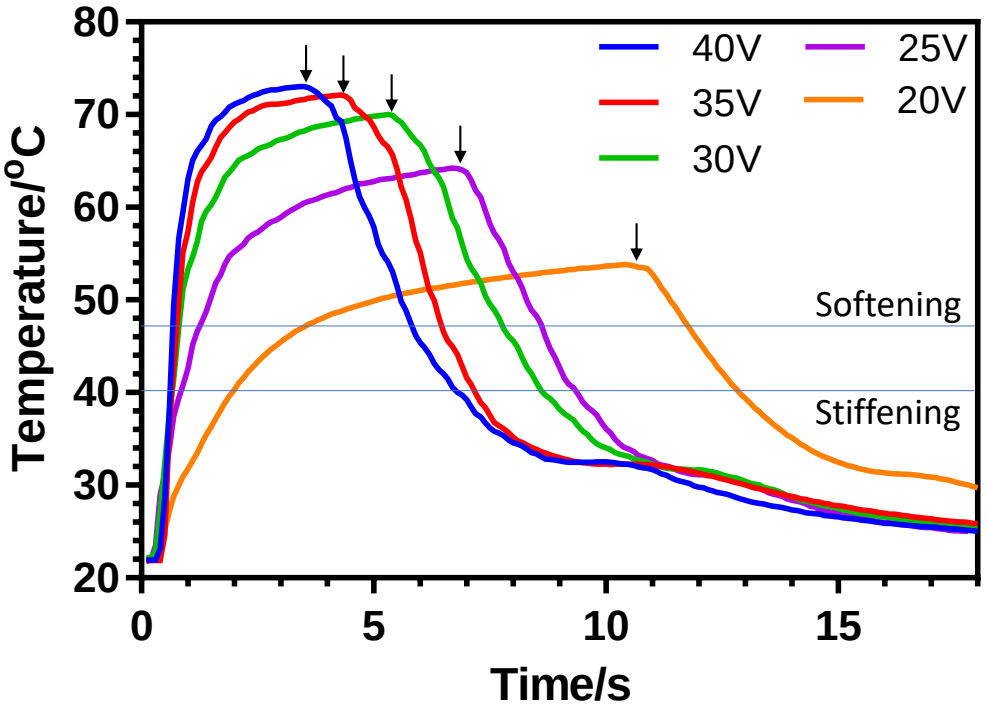

Figure 3-14. Temperature profiles of S-CNT electrode under different voltage supplied. Downward arrows indicate when heating voltage is removed. The "Softening" line indicate the temperature above which the polymer is soft, and the "Stiffening" line the temperature below which the polymer is stiff.

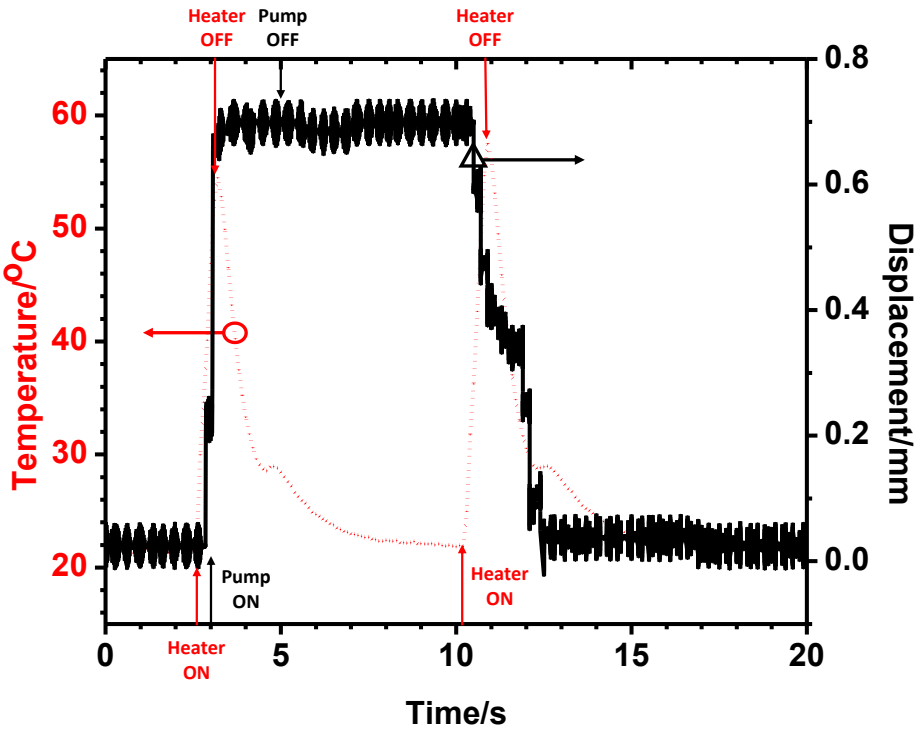

Figure 3-15. Raised height and temperature of a taxel as a function of time during a bistable actuation cycle.

To ensure stable heating during actuation, the resistance of the Joule heating electrode needs to remain constant. In our device, to latch a 0.7 mm displacement, the BSEP active layer needs to expand about 100% area strain to form a half spherical dome. In other words, the Joule heating electrode needs to be compliant enough to be stretched by 100% area strain without much restriction to the polymer matrix, while maintaining a constant resistance to allow for consistent heating steps. Figure 3-16a shows the normalized resistance of a braille sized S-CNT electrode on BS80-AA5 in response to area expansion on a diaphragm. The resistance stays almost constant with area strain up to about 200% and increases dramatically with further increase strain. Such behavior is reasonable because of the "Prestretch-Release" steps in the P3R

fabrication process mentioned above. In the "Prestretch" step, the BSEP film is prestretched to about 100% × 100% biaxial strain (300% area strain). The following "Releasing" step causes the CNT coating embedded in the P(UDA) layer to wrinkle with the P(UDA) layer. Subsequent stretching translates into flattening of the wrinkles without substantial elongation within the CNT coating and thus ensures a relatively constant resistance until the wrinkles has been flattened and further stretching leads to elongation within the S-CNT coating. To obtain high stretchability and durability of the S-CNT electrode, interpenetration of the CNT network within the protecting P(UDA) layer is important to prevent the carbon nanotubes from translational movement during repetitive deforming-recovering cycles.

Cyclic stretching test was also carried out on one taxel. Under induced area strain of 100%, which will exert a displacement over 0.7 mm, the resistance and Joule heating characteristics remain stable for over 100,000 repetitive cycles at a frequency of 0.8 Hz (Figure 3-16b). The upper insets show optical microscope images of a continuous electrode line of the S-CNT electrode before and after the 100,000 cycles of lifetime test. Uniform and precise heating was observed from the infrared thermal images of the electrode before and after the test (lower insets). Figure 3-16c compares heating rate, stretchability, and resistance consistency of S-CNT electrode with other reported compliant and stretchable Joule heating films that can generate uniform heat across the surface. The main efforts of contemporary research activities on stretchable heaters are focused on low dimensional carbon materials (filled symbols)[50–53], metal nanowires: silver based (open symbols) [54–58] and copper based (half-filled symbols)[59–62], and conductive polymers (half-filled pentagon)[63]. The S-CNT electrode can simultaneously perform fast heating rate (31 °C/s), large stretchability (188% area strain), and high resistance consistency (98.9% resistance recovery after one cycle), which can be very challenging for most other reported Joule heating electrodes to fulfill all three-performance metrics at the same time. Figure 3-16d demonstrates a Braille cell device using the S-CNT-BSEP system, which shows "U" "C" "L" "A" in Braille characters. The

insets are the corresponding infrared images of working S-CNT Joule heating electrodes. The heating is precise and uniform without any crosstalk between adjacent dots.

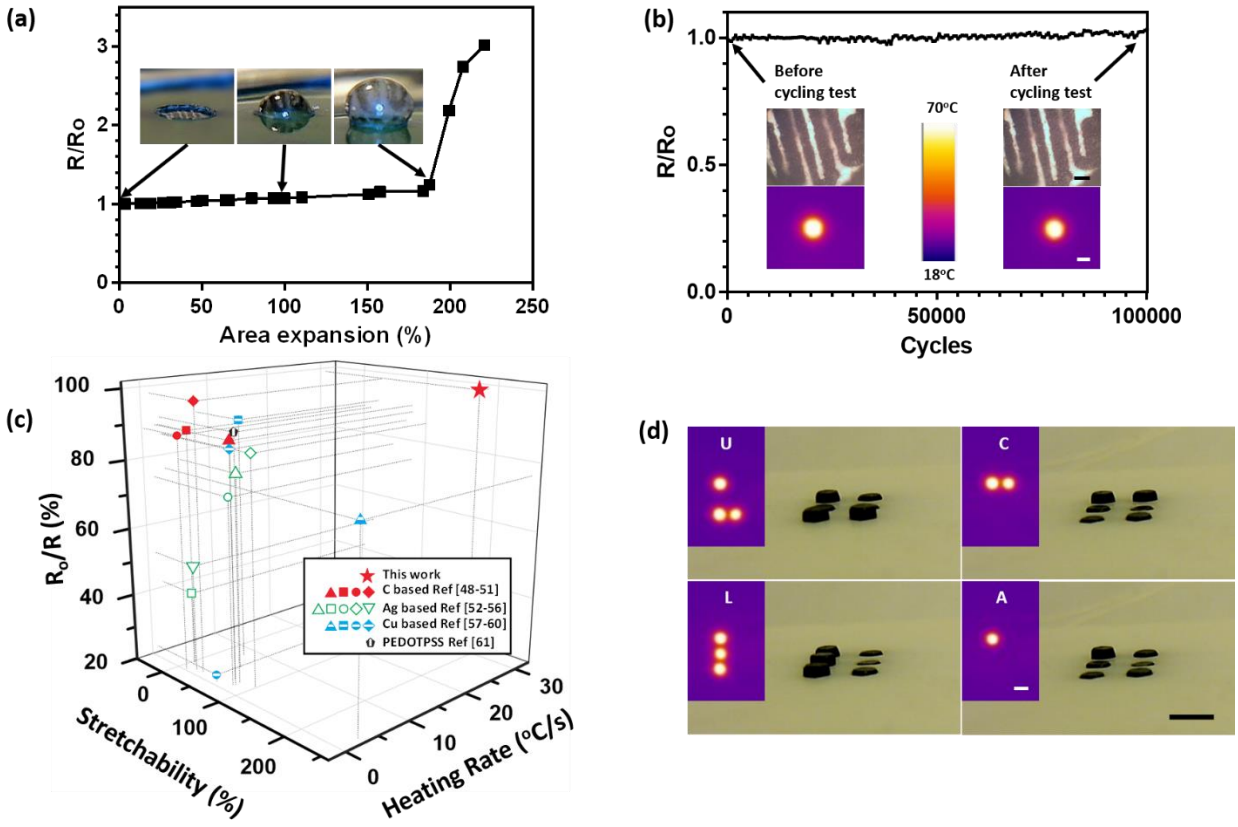

Figure 3-16. Performance of S-CNT Joule heating electrode. (a) Relative resistance variation of a serpentine CNT electrode under different area expansion. (b) Lifetime test on a serpentine CNT Joule heating electrode with 100% area expansion deforming and releasing cycle at a frequency of 0.8 Hz for over 100,000 cycles. The insets show the serpentine CNT electrode retaining the continuous electrode line (up left and up right, scale bar 0.2 mm) and stable heating (down left and down right, scale bar 1 mm) after the cycling test. (c) Comparison of heating performance of important stretchable Joule heating films with respect to heating rate, stretchability, and resistance consistency. Heating rates of the literature films were calculated from reported temperature versus time curve under the highest voltage

provided. If not specified in the literature, stretchability was defined as the stretch ratio when the resistance increases by 20%. The resistance consistency was obtained by initial resistance over the resistance after a stretch-release cycle. (d) Demonstration of a one-cell Braille device showing “U” “C” “L” “A” in Braille characters with infrared images of the corresponding S-CNT Joule heating electrode shown to the left. The scale bars are 2 mm.

High energy consumption is often cited as the key drawback for using shape memory polymers and alloys for shape change. For the proposed tactile display, the Joule heating electrode is patterned directly and only on the active taxel areas. The area being heated is only 1.77 mm^2 per taxel pixel, and the polymer film is 90 μm thickness. In a typical experiment, 30 V was applied to the serpentine CNT electrode of 50 kΩ resistance, it took 1 second to reach 50 °C. The power consumption is calculated to be 18 mW. For a smartphone screen sized panel with 48 × 24 taxels, roughly 50% of the dots are raised during content refreshing, so the total power consumption is 2.16 W. The switching circuit and the pneumatic pump also consume about 1 W during operation. The overall power consumption is thus 3.16 W which is within the useful range for small or portable devices. In comparison, the peak power consumption of iPhone X® is 10.5 W. The power supply required for the Hyperbraille S Display 6240 from Metec® is 48 W.

3.4. Conclusions

A refreshable tactile display with Braille standard resolution has been demonstrated. The steep modulus change of BS80-AA5 over a narrow temperature range grants the device with high blocking force of over 50 g and large displacement of 0.7 mm. The “P3R” fabrication process of Prestretch-Pattern-Protect-Release is effective to form a S-CNT electrode in the wrinkled surface layer with high compliancy and resistance-consistence up to 188% area strain. The electrode can soften the BSEP film at 30 V in less than

1 s. The simple architecture of the tactile display ensures an easy and low-cost fabrication. The demonstrated refreshable tactile display should find a wide range of applications in rehabilitation of people with vision impairment, entertainment, robotics, health care, and so on.

3.5. Reference

(1) Dang, T.; Annaswamy, T. M.; Srinivasan, M. A. Development and Evaluation of an Epidural Injection Simulator with Force Feedback for Medical Training. *Stud. Health Technol. Inform.* **2001**, *81* (August), 97–102.

(2) Langrana, N. A.; Burdea, G.; Lange, K.; Gomez, D.; Deshpande, S. Dynamic Force Feedback in a Virtual Knee Palpation. *Artif. Intell. Med.* **1994**, *6* (4), 321–333.

(3) Vining, D. J.; Liu, K.; Choplin, R. H.; Haponik, E. F. Virtual Bronchoscopy: Relationships of Virtual Reality Endobronchial Simulations to Actual Bronchoscopic Findings. *Chest* **1996**, *109* (2), 549–553.

(4) Maisto, M.; Pacchierotti, C.; Chinello, F.; Salvietti, G.; De Luca, A.; Prattichizzo, D. Evaluation of Wearable Haptic Systems for the Fingers in Augmented Reality Applications. *IEEE Trans. Haptics* **2017**, *10* (4), 1–1.

(5) Bouzit, M.; Burdea, G.; Popescu, G.; Boian, R. The Rutgers Master II - New Design Force-Feedback Glove. *IEEE/ASME Trans. Mechatronics* **2002**, *7* (2), 256–263.

(6) Cortesao, R.; Park, J.; Khatib, O. Real-Time Adaptive Control for Haptic Manipulation with Active Observers. *Proc. 2003 IEEE/RSJ Int. Conf. Intell. Robot. Syst. (IROS 2003) (Cat. No.03CH37453)* **2003**, *3* (October), 2938–2943.

(7) Turner, M. L.; Gomez, D. H.; Tremblay, M. R.; Cutkosky, M. R.; Alto, P. Preliminary Tests of an Arm-Grounded Haptic Feedback Device in Telemanipulation. *Proc. ASME IMECE Haptics Symp.* **1998**, 1–6.

(8) Choi, H. R.; Lee, S. W.; Jung, K. M.; Koo, J. C.; Lee, S. I.; Choi, H. G.; Jeon, J. W.; Nam, J. D. Tactile Display as a Braille Display for the Visually Disabled. *2004 IEEE/RSJ Int. Conf. Intell. Robot. Syst. (IEEE Cat. No.04CH37566)* **2004**, *2*, 1985–1990.

(9) King, H. H.; Donlin, R.; Hannaford, B. Perceptual Thresholds for Single vs. Multi-Finger Haptic Interaction. *2010 IEEE Haptics Symp. HAPTICS 2010* **2010**, 95–99.

(10) Motto Ros, P.; Dante, V.; Mesin, L.; Petetti, E.; Del Giudice, P.; Pasero, E. A New Dynamic Tactile Display for Reconfigurable Braille: Implementation and Tests. *Front. Neuroeng.* **2014**, *7* (April), 6.

(11) Summers, I. R.; Chanter, C. M. A Broadband Tactile Array on the Fingertip. *J. Acoust. Soc. Am.* **2002**, *112* (August), 2118–2126.

(12) Wagner, C. .; Lederman, S. J.; Howe, R. D. Design and Performance of a Tactile Shape Display. *Haptics-e* **2004**, 6.

(13) Velazquez, R.; Pissaloux, E. E.; Hafez, M.; Szewczyk, J. Tactile Rendering with Shape-Memory-Alloy Pin-Matrix. *IEEE Trans. Instrum. Meas.* **2008**, *57* (5), 1051–1057.

(14) Lee, J. S.; Lucyszyn, S. A Micromachined Refreshable Braille Cell. *J. Microelectromechanical Syst.* **2005**, *14* (4), 673–682.

(15) Kwon, H. J.; Lee, S. W.; Lee, S. S. Braille Dot Display Module with a PDMS Membrane Driven by a Thermopneumatic Actuator. *Sensors Actuators, A Phys.* **2009**, *154* (2), 238–246.

(16) Vidal-Verdú, F.; Madueño, M. J.; Navas, R. Thermopneumatic Actuator for Tactile Displays and Smart Actuation Circuitry. *Proc. SPIE - Int. Soc. Opt. Eng.* **2005**, *5836* (July 2005), 484–492.

(17) Koo, I. M.; Jung, K.; Koo, J. C.; Nam, J. Do; Lee, Y. K.; Choi, H. R. Development of Soft-Actuator-Based Wearable Tactile Display. *IEEE Trans. Robot.* **2008**, *24* (3), 549–558.

(18) Matysek, M.; Lotz, P.; Winterstein, T.; Schlaak, H. F. Dielectric Elastomer Actuators for Tactile Displays. *Proc. - 3rd Jt. EuroHaptics Conf. Symp. Haptic Interfaces Virtual Environ. Teleoperator Syst. World Haptics 2009* **2009**, 290–295.

(19) Jungmann, M.; Schlaak, H. F. Miniaturised Electrostatic Tactile Display with High Structural Compliance. *Proc. Conf. Eurohaptics* **2002**, No. August, 12–17.

(20) De Rossi, D.; Carpi, F.; Carbonaro, N.; Tognetti, A.; Scilingo, E. P. Electroactive Polymer Patches for Wearable Haptic Interfaces. *Proc. Annu. Int. Conf. IEEE Eng. Med. Biol. Soc. EMBS* **2011**, No. Section III, 8369–8372.

(21) Lee, H. S.; Phung, H.; Lee, D. H.; Kim, U. K.; Nguyen, C. T.; Moon, H.; Koo, J. C.; Nam, J. Do; Choi, H. R. Design Analysis and Fabrication of Arrayed Tactile Display Based on Dielectric Elastomer Actuator. *Sensors Actuators, A Phys.* **2014**, *205*, 191–198.

(22) Phung, H.; Nguyen, C. T.; Nguyen, T. D.; Lee, C.; Kim, U.; Lee, D.; Nam, J. Do; Moon, H.; Koo, J. C.; Choi, H. R. Tactile Display with Rigid Coupling Based on Soft Actuator. *Meccanica* **2015**, *50* (11), 2825–2837.

(23) Chakraborti, P.; Toprakci, H. A. K.; Yang, P.; Di Spigna, N.; Franzon, P.; Ghosh, T. A Compact Dielectric Elastomer Tubular Actuator for Refreshable Braille Displays. *Sensors Actuators, A Phys.* **2012**, *179* (June), 151–157.

(24) Yu, Z.; Yuan, W.; Brochu, P.; Chen, B.; Liu, Z.; Pei, Q. Large-Strain, Rigid-to-Rigid Deformation of Bistable Electroactive Polymers. *Appl. Phys. Lett.* **2009**, *95* (19), 21–24.

(25) Wu, X.; Kim, S. H.; Zhu, H.; Ji, C. H.; Allen, M. G. A Refreshable Braille Cell Based on Pneumatic Microbubble Actuators. *J. Microelectromechanical Syst.* **2012**, *21* (4), 908–916.

(26) Yobas, L.; Huff, M. A.; Lisy, F. J.; Durand, D. M. A Novel Bulk-Micromachined Electrostatic Microvalve with a Curved-Compliant Structure Applicable for a Pneumatic Tactile Display. *J. Microelectromechanical Syst.* **2001**, *10* (2), 187–196.

(27) Besse, N.; Rosset, S.; Zarate, J. J.; Shea, H. Flexible Active Skin: Large Reconfigurable Arrays of Individually Addressed Shape Memory Polymer Actuators. *Adv. Mater. Technol.* **2017**, *1700102*, 1700102.

(28) Runyan, N. H.; Carpi, F. Seeking the `holy Braille' Display: Might Electromechanically Active Polymers Be the Solution? *Expert Rev. Med. Devices* **2011**, *8* (5), 529–532.

(29) Ren, Z.; Hu, W.; Liu, C.; Li, S.; Niu, X.; Pei, Q. Phase-Changing Bistable Electroactive Polymer Exhibiting Sharp Rigid-to-Rubbery Transition. *Macromolecules* **2016**, *49* (1), 134–140.

(30) Yuan, W.; Hu, L.; Yu, Z.; Lam, T.; Biggs, J.; Ha, S. M.; Xi, D.; Chen, B.; Senesky, M. K.; Grüner, G.; Pei, Q. Fault-Tolerant Dielectric Elastomer Actuators Using Single-Walled Carbon Nanotube Electrodes. *Adv. Mater.* **2008**, *20* (3), 621–625.

(31) Yamada, T.; Hayamizu, Y.; Yamamoto, Y.; Yomogida, Y.; Izadi-Najafabadi, A.; Futaba, D. N.; Hata, K. A Stretchable Carbon Nanotube Strain Sensor for Human-Motion Detection. *Nat. Nanotechnol.* **2011**, *6* (5), 296–301.

(32) Niu, X.; Yang, X.; Brochu, P.; Stoyanov, H.; Yun, S.; Yu, Z.; Pei, Q. Bistable Large-Strain

Actuation of Interpenetrating Polymer Networks. *Adv. Mater.* **2012**, *24* (48), 6513–6519.

(33) Meng, Y.; Jiang, J.; Anthamatten, M. Body Temperature Triggered Shape-Memory Polymers with High Elastic Energy Storage Capacity. *J. Polym. Sci. Part B Polym. Phys.* **2016**, *54* (14), 1397–1404.

(34) Hu, X.; Zhou, J.; Vatankhah-Varnosfaderani, M.; Daniel, W. F. M.; Li, Q.; Zhushma, A. P.; Dobrynin, A. V.; Sheiko, S. S. Programming Temporal Shapeshifting. *Nat. Commun.* **2016**, *7* (May), 1–7.

(35) Dong, J.; Ozaki, Y.; Nakashima, K. Infrared, Raman, and Near-Infrared Spectroscopic Evidence for the Coexistence of Various Hydrogen-Bond Forms in Poly(Acrylic Acid). *Macromolecules* **1997**, *30* (4), 1111–1117.

(36) Sun, J.-Y.; Zhao, X.; Illeperuma, W. R. K.; Chaudhuri, O.; Oh, K. H.; Mooney, D. J.; Vlassak, J. J.; Suo, Z. Highly Stretchable and Tough Hydrogels. *Nature* **2012**, *489* (7414), 133–136.

(37) Haque, M. A.; Kurokawa, T.; Kamita, G.; Gong, J. P. Lamellar Bilayers as Reversible Sacrificial Bonds to Toughen Hydrogel: Hysteresis, Self-Recovery, Fatigue Resistance, and Crack Blunting. *Macromolecules* **2011**, *44* (22), 8916–8924.

(38) Tuncaboylu, D. C.; Sari, M.; Oppermann, W.; Okay, O. Tough and Self-Healing Hydrogels Formed via Hydrophobic Interactions. *Macromolecules* **2011**, *44* (12), 4997–5005.

(39) McCoul, D.; Hu, W.; Gao, M.; Mehta, V.; Pei, Q. Recent Advances in Stretchable and Transparent Electronic Materials. *Adv. Electron. Mater.* **2016**, *2* (5), 1500407.

(40) Trung, T. Q.; Lee, N. E. Recent Progress on Stretchable Electronic Devices with Intrinsically Stretchable Components. *Adv. Mater.* **2017**, *29* (3).

(41) Bauer, S.; Bauer-Gogonea, S.; Graz, I.; Kaltenbrunner, M.; Keplinger, C.; Schwödiauer, R. 25th Anniversary Article: A Soft Future: From Robots and Sensor Skin to Energy Harvesters. *Adv. Mater.* **2014**, *26* (1), 149–162.

(42) Hu, H.; Bhowmik, P.; Zhao, B.; Hamon, M. A.; Itkis, M. E.; Haddon, R. C. Determination of the Acidic Sites of Purified Single-Walled Carbon Nanotubes by Acid-Base Titration. *Chem. Phys. Lett.* **2001**, *345* (1–2), 25–28.

(43) Zhang, Y.; Xu, S.; Fu, H.; Lee, J.; Su, J.; Hwang, K.-C.; Rogers, J. A.; Huang, Y. Buckling in Serpentine Microstructures and Applications in Elastomer-Supported Ultra-Stretchable Electronics with High Areal Coverage. *Soft Matter* **2013**, *9* (33), 8062.

(44) Li, T.; Suo, Z.; Lacour, S. P.; Wagner, S. Compliant Thin Film Patterns of Stiff Materials as Platforms for Stretchable Electronics. *J. Mater. Res.* **2005**, *20* (12), 3274–3277.

(45) Gonzalez, M.; Axisa, F.; Bulcke, M. Vanden; Brosteaux, D.; Vandevelde, B.; Vanfleteren, J. Design of Metal Interconnects for Stretchable Electronic Circuits. *Microelectron. Reliab.* **2008**, *48* (6), 825–832.

(46) Lu, N.; Lu, C.; Yang, S.; Rogers, J. Highly Sensitive Skin-Mountable Strain Gauges Based Entirely on Elastomers. *Adv. Funct. Mater.* **2012**, *22* (19), 4044–4050.

(47) Gutruf, P.; Walia, S.; Nur Ali, M.; Sriram, S.; Bhaskaran, M. Strain Response of Stretchable Micro-Electrodes: Controlling Sensitivity with Serpentine Designs and Encapsulation. *Appl. Phys. Lett.* **2014**, *104* (2), 1–5.

(48) Li, Y.; Zhang, Z.; Li, X.; Zhang, J.; Lou, H.; Shi, X.; Cheng, X.; Peng, H. A Smart, Stretchable Resistive Heater Textile. *J. Mater. Chem. C* **2017**, *5* (1), 41–46.

(49) Kang, J.; Kim, H.; Kim, K. S.; Lee, S.-K.; Bae, S.; Ahn, J.-H.; Kim, Y.; Choi, J.; Hong, B. H. High-Performance Graphene-Based Transparent Flexible Heaters. *Nano Lett.* **2011**, 5154–5158.

(50) Li, Y. Q.; Zhu, W. Bin; Yu, X. G.; Huang, P.; Fu, S. Y.; Hu, N.; Liao, K. Multifunctional Wearable Device Based on Flexible and Conductive Carbon Sponge/Polydimethylsiloxane Composite. *ACS Appl. Mater. Interfaces* **2016**, *8* (48), 33189–33196.

(51) Zhou, R.; Li, P.; Fan, Z.; Du, D.; Ouyang, J. Stretchable Heaters with Composites of an Intrinsically Conductive Polymer, Reduced Graphene Oxide and an Elastomer for Wearable Thermotherapy. *J. Mater. Chem. C* **2017**, *5*, 1544–1551.

(52) Yoon, S. S.; Khang, D. Y. Facile Patterning of Ag Nanowires Network by Micro-Contact Printing of Siloxane. *ACS Appl. Mater. Interfaces* **2016**, *8* (35), 23236–23243.

(53) Hong, S.; Lee, H.; Lee, J.; Kwon, J.; Han, S.; Suh, Y. D.; Cho, H.; Shin, J.; Yeo, J.; Ko, S. H. Highly Stretchable and Transparent Metal Nanowire Heater for Wearable Electronics Applications. *Adv. Mater.* **2015**, *27* (32), 4744–4751.

(54) Hu, H.; Wang, Z.; Ye, Q.; He, J.; Nie, X.; He, G.; Song, C.; Shang, W.; Wu, J.; Tao, P.; Deng, T. Substrateless Welding of Self-Assembled Silver Nanowires at Air/Water Interface. *ACS Appl. Mater. Interfaces* **2016**, *8* (31), 20483–20490.

(55) Choi, S.; Park, J.; Hyun, W.; Kim, J.; Kim, J.; Lee, Y. B.; Song, C.; Hwang, H. J.; Kim, J. H.; Hyeon, T.; Kim, D. H. Stretchable Heater Using Ligand-Exchanged Silver Nanowire Nanocomposite for Wearable Articular Thermotherapy. *ACS Nano* **2015**, *9* (6), 6626–6633.

(56) Ko, E.-H.; Kim, H.-J.; Lee, S.-M.; Kim, T.-W.; Kim, H.-K. Stretchable Ag Electrodes with Mechanically Tunable Optical Transmittance on Wavy-Patterned PDMS Substrates. *Sci. Rep.* **2017**,

7 (March), 46739.

(57) Jo, H. S.; An, S.; Lee, J.-G.; Park, H. G.; Al-Deyab, S. S.; Yarin, A. L.; Yoon, S. S. Highly Flexible, Stretchable, Patternable, Transparent Copper Fiber Heater on a Complex 3D Surface. *NPG Asia Mater.* **2017**, *9* (2), e347.

(58) Li, P.; Ma, J.; Xu, H.; Xue, X.; Liu, Y. Highly Stable Copper Wire/Alumina/Polyimide Composite Films for Stretchable and Transparent Heaters. *J. Mater. Chem. C* **2016**, *4* (16), 3581–3591.

(59) Ding, S.; Jiu, J.; Gao, Y.; Tian, Y.; Araki, T.; Sugahara, T.; Nagao, S.; Nogi, M.; Koga, H.; Suganuma, K.; Uchida, H. One-Step Fabrication of Stretchable Copper Nanowire Conductors by a Fast Photonic Sintering Technique and Its Application in Wearable Devices. *ACS Appl. Mater. Interfaces* **2016**, *8* (9), 6190–6199.

(60) An, B. W.; Gwak, E. J.; Kim, K.; Kim, Y. C.; Jang, J.; Kim, J. Y.; Park, J. U. Stretchable, Transparent Electrodes as Wearable Heaters Using Nanotrough Networks of Metallic Glasses with Superior Mechanical Properties and Thermal Stability. *Nano Lett.* **2016**, *16* (1), 471–478.

(61) Yeon, C.; Kim, G.; Lim, J. W.; Yun, S. J. Highly Conductive PEDOT:PSS Treated by Sodium Dodecyl Sulfate for Stretchable Fabric Heaters. *RSC Adv.* **2017**, *7* (10), 5888–5897.

Chapter 4. A Self-Conformable Smart Skin with Sensing and Variable Stiffness Functions

4.1. Introduction

Skin provides our body with protection, regulation, sensation, and is highly adaptive. [1,2] As the interface for the outside world, skin can be regarded as an ultra-compliant sensor for our body. It is, thus, inspiring for the engineering field to build compliant sensor skins with apparent simplicity and complex functionalities. The current electronic skin devices have shown the ability to detect touch[3,4], stretch[5,6], bend[7], and pressure[8]. For continuous and more precise sensing, several approaches have been explored to achieve high compliancy which often involve electronics tattoos[9] and soft elastomer electronics[10].

Electronic tattoos usually consist of ultrathin polymeric membranes with printed electrodes. The polymer membranes, with thicknesses ranging from nanometers to a few micrometers, are subsequently laminated onto the skin by soft contact via van der Waals forces resulting in an intimate contact for precise sensing. [11] The systems are usually attached to the skin via assistant transfer by a water soluble liner[12] or direct printing on skin[13]. Electronic tattoos demonstrated promising results in terms of mobility, comfort, and continuous long-term precision monitoring in biomedicine applications.[9] However, the devices lack the flexibility of repetitive mounting and dismounting. Additionally, the safety concern of having such long-term intimate contact on skin remains controversial.[14]

Soft elastomer-based smart skin electronics are soft, curvilinear, and deformable. The epidermis has an elastic modulus ranging from ten to a few hundred kP, coinciding with the modulus range of most soft elastomers.[15] The use of a soft elastomer ensures matched form factors and mechanical properties with epidermis resulting in compliant bioelectronic interfaces.[16–18]Soft elastomer electronics act as

conformable artificial electronic skins eliminating the concern of leaving a nonremovable trace on epidermis and minimizing irritation caused by contact between the skin and certain metals.[14,19] However, most soft elastomer electronics are difficult to handle due to the soft-adhesive nature of soft materials.[20,21] During transfer or lamination the soft elastomer membrane, especially a thin film elastomer with thickness under 500 μm, may adhere to other objects or itself, and the printed electrodes or control elements could delaminate by stretching. Increasing the elastomer membrane thickness may ease the concern of crumpling, but it also weakens the compliancy of the device. Thus, a material with adjustable stiffness that can be both compliant for conformal lamination and rigid for easy handling, such as variable stiffness polymer (VSP), is desired in the field of conformable thin film electronics.

Phase-changing bi-stable electroactive polymers (BSEPs) emerge as novel VSPs that can adjust the stiffness from rigid to soft state.[22,23] The phase-changing BSEP is a thermal stimulus variable stiffness polymer that exhibits stiffness change of three orders of magnitude in a narrow temperature band slightly above room temperature. In the rigid state, the BSEPs behave like plastics and possess modulus of several hundred of MPa. In the softened state the modulus decreases to kPa range and the BSEPs can be treated as soft elastomers. The stiffness tunability is realized by reversible crystallization and melting of nanocrystalline phase in the polymer network which grants the BSEP with compliancy in a controllable manner. Unlike most glass transition shape memory polymers[24,25], which have a broad transition temperature band of over 30 °C, phase-changing BSEP possesses a sharp phase transition within 10 °C and a tunable inflection point below 50 °C. Such narrow transition band and low inflection point reduces thermal energy consumption during heating and ensures the use of BSEP in human-contact applications.[23]

Here, we design and fabricate a self-conformable smart skin sensor comprised of a highly sensitive capacitive touch sensor matrix on a stiffness variable BSEP substrate. The smart skin sensor has the ability to accommodate irregular surfaces and demonstrates excellent sensing performance in imitate contact to

human skin. The embedded, compliant Joule heating electrode controls the device stiffness conforming to nearly any surface topography.

4.2. Experimental section

4.2.1 Raw materials

AgNWs (catalog name: Agnw-L30) were purchased from ACS Material, LLC. The average diameter and length of the AgNWs are 30 nm and 100-200 μm. Urethane diacrylate (UDA, catalog name: CN9021) was obtained from SARTOMER and used as received. Stearyl acrylate (SA), acrylic acid (AA), 2,2-Dimethoxy-2-phenylacetophenone (DMPA), benzophenone (BP), and isopropyl alcohol (IPA) were purchased from Sigma-Aldrich and used as received. Screen-printable silver ink (catalog name: PE873) was purchased from DUPONT and used as received. Single-walled carbon nanotubes (catalog name: P3-SWNT) were purchased from Carbon Solutions, Inc.

4.2.2 BSEP prepolymer solution preparation and thin film fabrication

The prepolymer solution was made by mixing 80 parts (by weight) of SA, 20 parts of UDA, 10 parts of AA, 0.25 part of DMPA, and 0.125 part of BP at 50 °C. The prepolymer solution was then injected between a pair of glass slides on a hot plate with two strips of tape as spacers, forming a "sandwich" structure. The thickness of the liquid layer was defined by the thickness of the spacers. In the experiments, BSEP film with thickness varied from 30 to 90 μm were fabricated. Next, the prepolymer was cured in a Dymax UV light-curing chamber equipped with ECE 5000 flood-lamp for one minute. The film can be gently peeled off the glass substrate upon cooling to room temperature.

4.2.3 Capacitive touch sensor fabrication

Sensor electrodes were made by first spray coating a dispersion of AgNW (concentration of 1.5 mg/mL) in IPA on two glass substrates through shadow masks. The shadow masks have antenna-shaped and strip-shaped cutouts formed by laser ablation. BSEP film was fabricated using the AgNW-patterned glass slides following aforementioned "sandwich" method. In the "sandwich" structure, the AgNW electrodes were facing each other and embedded into the BSEP film.

4.2.4 Joule heating electrode fabrication

The carbon nanotube (CNT) dispersion was made by mixing 5 mg of P3-SWNT powder, 1 ml water, and 20 ml IPA. The mixture was tip sonicated for 40 min to obtain a stable dispersion. The solution was then kept overnight to settle large aggregates. The resulting supernatant is then ready for spray coating.

The interdigitated silver electrode (ID-Ag) was obtained by screen printing the silver paste electrode on a glass substrate. Screen-printing tests were performed on a semi-automatic screen printer (Asys E2), and a 12 × 12 inch precision stainless-steel screen mesh (200 mesh count, 40 µm wire diameter, 29 N/cm mesh tension and 15 µm emulsion thickness) purchased from Sefar Inc. The print speed was 100 mm/s and printing force 1 N. The printed ID-Ag pattern was annealed at 110 °C for 30 min to evaporate the solvent. Then, a layer of CNT electrode was blanket-coated on top of silver electrode through spray printing.

4.2.5 Device assembly

The device can be integrated by first taking off the top glass substrate (the one close to R_X) of the as fabricated sensor "sandwich" structure. The remaining sensor structure was used as the substrate to form

another “sandwich” structure with a new glass slide and a new pair of spacers (70 µm thickness) to fabricate the top BSEP layer. The above-mentioned process was then repeated to fabricate bottom BSEP layer (70 µm thickness) by taking off the bottom glass slide (the one close to T_X) and use ID-Ag/CNT patterned glass to form new “sandwich” structure. The resulting device comprises, from top to bottom, a 70 µm thick BSEP top layer, a R_X sensor electrode, a 90 µm thick BSEP dielectric layer, a T_X sensor electrode, a 70 µm thick BSEP bottom layer, and a Joule heating electrode layer.

4.3. Results and discussion

4.3.1 Device design and fabrication

The self-conformable sensor contains an 8 by 8 tactile pixel (taxel) sensor matrix combined with an embedded resistive heater (Figure 4-1a). The device has an active area of 40 × 40 mm with a thickness of 230 µm. It comprises four main components: (i) top and bottom BSEP layer (thickness 70 µm); (ii) top and bottom silver nanowire (AgNW) sensor electrodes (R_X: receiver and T_X: transmitter); (iii) BSEP sensor dielectric layer (thickness 90 µm); (iv) bottom heater electrode comprised of an interdigitate-patterned silver combined with carbon nanotubes (ID-Ag/CNT). The bottom heater layer also serves as the ground electrode to eliminate electrical noises caused by the surface charge on human skin or other electronic devices.

The top sensor electrodes are patterned into antenna-shaped electrodes (ASEs) with 5 mm pitch. The bottom electrodes are parallel lines with 0.5 mm width and 5 mm pitch capacitively coupled with ASEs through the BSEP dielectric layer. Fringing fields are generated from the ASE pattern be used to couple with and enable detection of a nearby finger (C_F). As shown in Figure 4-1b, an approaching finger leads to a reduction of the charge stored between the two adjacent electrodes, resulting in decrease of measured

capacitance (C_S). A layer of compliant ID-Ag/CNT Joule heating electrode is formed at the bottom to administrate the stiffness of the BSEP matrix through thermal stimuli. Conductive silver ink is patterned into interdigitated shape to uniformly deliver charge carriers over the active area. Highly compliant CNTs are chosen based on their thermal stability, mechanical compliancy, and chemical resistance.[23] The resulting ASE-patterned sensor combined with ID-Ag/CNT heater can effectively work as a capacitive touch sensor with an ability to adapt to different surfaces (Figure 4-1c-f).

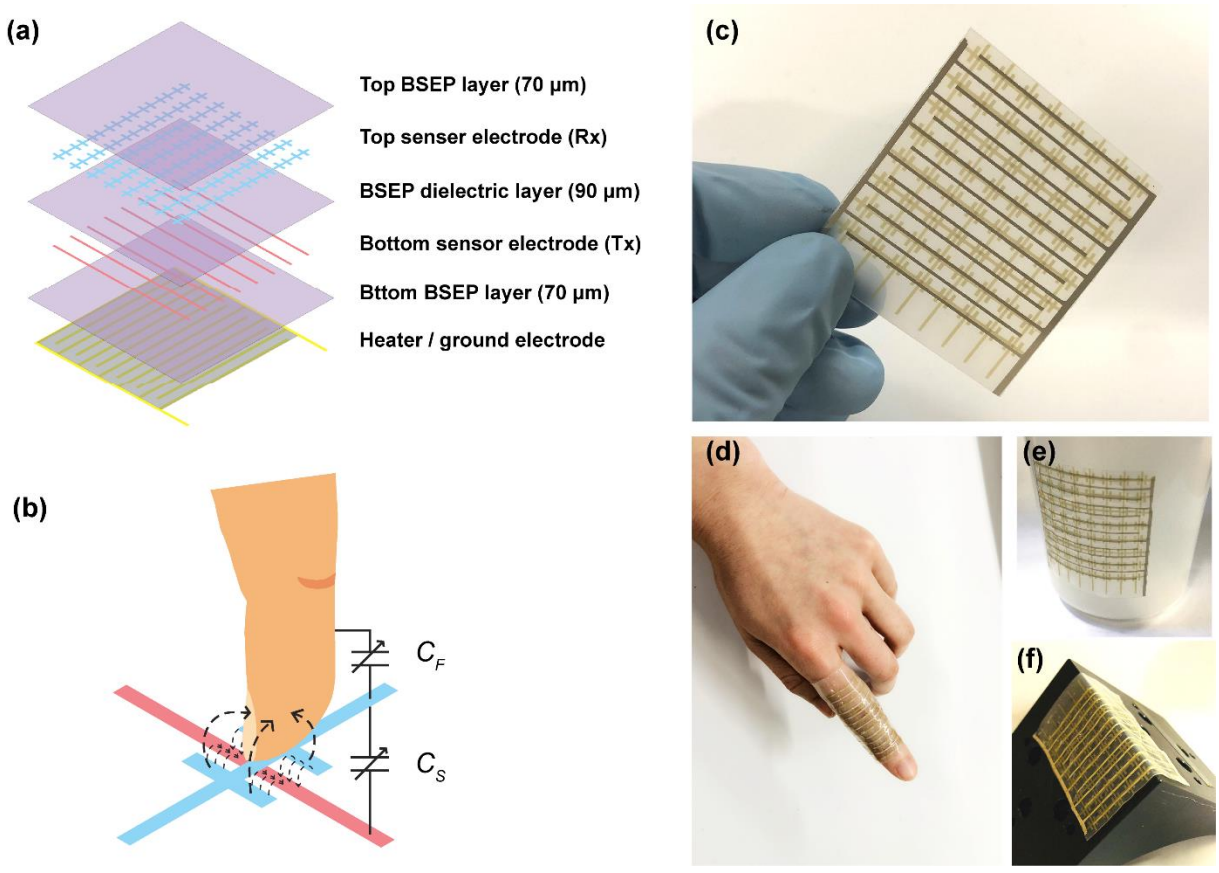

Figure 4-1. Self-conformable capacitive touch sensor. (a) Schematic of the layered structure of the device. (b) Finger approaching a pair of antenna-shaped electrodes. The finger reduces the coupling

between the sensor electrodes (C_S) by coupling itself with the fringing field (C_F increases). (c) Representative image of the smart electronic skin with capacitive sensing and shape memory function. (d-f) Demonstration of the device's conformity by wrapping around a finger, laminating to the wall of a cup, and conforming on a sharp edge.

Phase-changing BSEP was formulated to contain 80 parts (by weight) of stearyl acrylate (SA), 20 parts of urethane diacrylate (UDA), 10 parts of acrylic acid (AA), 0.25 part of 2,2-dimethoxy-2-phenylacetophenone (DMPA), and 0.125 part of benzophenone (BP). This formulation is optimized based on our previous work[23] to achieve high compliancy in the soften state. The use of SA and UDA forms bottlebrush polymer network results in ultralow stiffness of 45 kPa in the soften state. The addition of AA introduces hydrogen bonds to the polymer system, which can help increase the mechanical toughness and electrode bonding.[23,26] The synthetic details are found in the Experimental Section.

Fabrication of self-conformable sensor device comprises of three primary steps: (1) fabrication of the sensor; (2) fabrication of the Joule heating electrode (ID-Ag/CNT); (3) alignment of the sensor and heater (Figure 4-2). The process starts with spray-printing AgNW electrodes (R_X and T_X) on shadow masked glass substrates. The two glass substrates are then stacked together with two stripes of tape as spacers (90 μm thick). The electrode sides are facing each other and perfectly aligned to form R_X and T_X electrodes. Next, the BSEP prepolymer solution is injected between two glass substrates to encapsulate the AgNWs and cured under UV. The top glass substrate is be gently taken off. The BSEP top layer (70 μm) is formed above the R_X electrode using the same stack-inject method. Fabrication of ID-Ag/CNT electrode starts

with screen-printing of interdigitated silver on a glass substrate. Then, the CNT solution is blanket-sprayed on top of ID-Ag. The glass substrate is aligned and stacked underneath the sensor structure to form the bottom BSEP layer (70 μm thick). The thin film electronic device can be gently peeled off from the glass substrates and works as a self-conformable capacitive touch sensor. A more detailed fabrication process can be found in the experimental section.

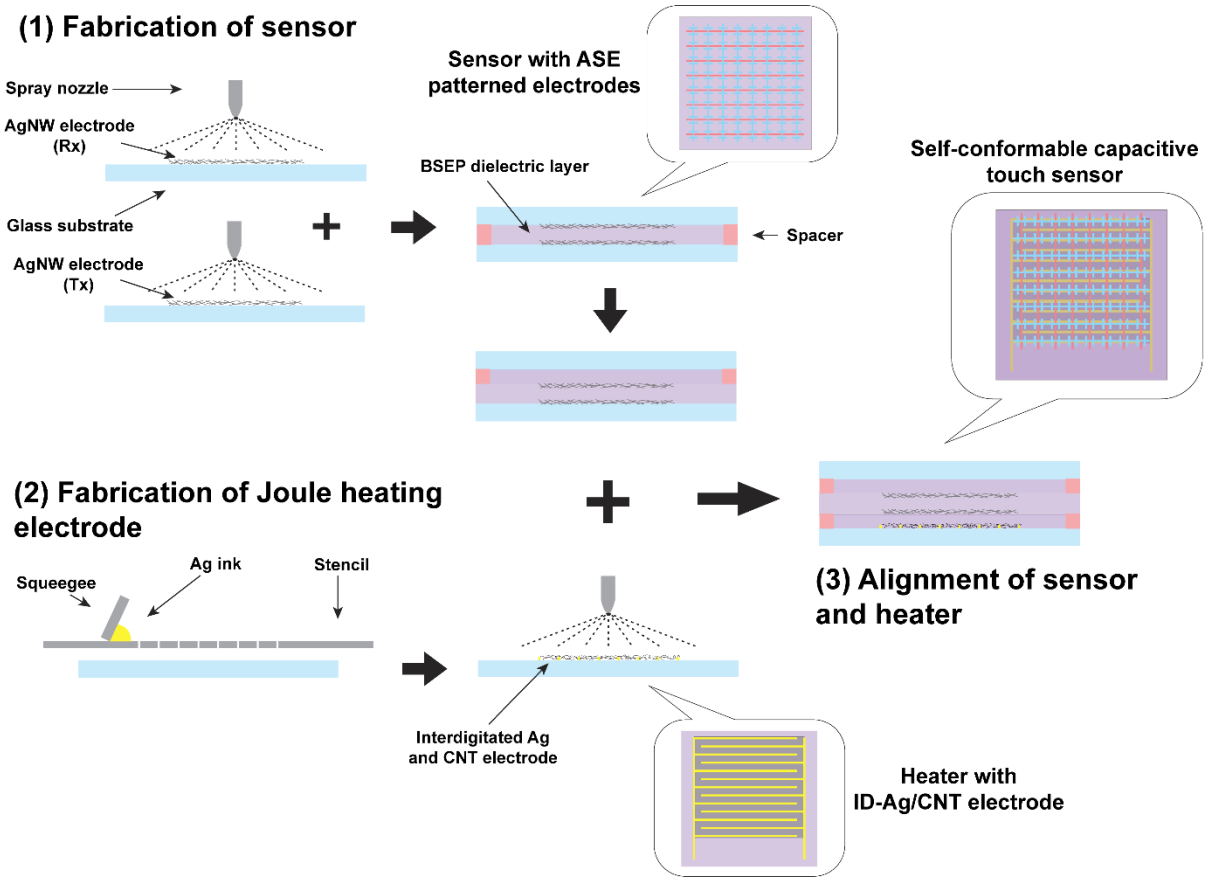

Figure 4-2. Schematic illustration of the fabrication process of self-conformable capacitive touch sensor (not to scale).

4.3.2 Capacitive touch sensor

The rapid growth of capacitive touch sensor in commercial products is mainly attributed to their high working sensitivity, good mechanical robustness, and structural simplicity.[27] A self-conformable smart skin sensor requires not only a deformable dielectric substrate but also compliant electrodes. Low resistance electrode are desirable in sensor devices to enable fast circuit measuring time and high signal-to-noise ratio.[27,28] Sliver nanowires with a high length-to-diameter aspect ratio (Figure 4-3a,b) have shown promise in low sheet resistance and high compliancy for flexible electronics.[3,29,30] We used spray printing to produce high quality AgNW patterns resulting in a sheet resistance as low as 18 Ω/sq (Figure 4-4). The AgNW patterns were embedded in the BSEP substrate, physical translation of nanowires is largely prevented during deformation (Figure 4-3c,d). Moreover, strong bonding is formed between AgNWs and BSEP substrate due to the existence of large amount of acrylic acid in the polymer system.[31] The combination of AgNWs and BSEP affords a capacitive touch sensor with high compliancy and good sensing performances.

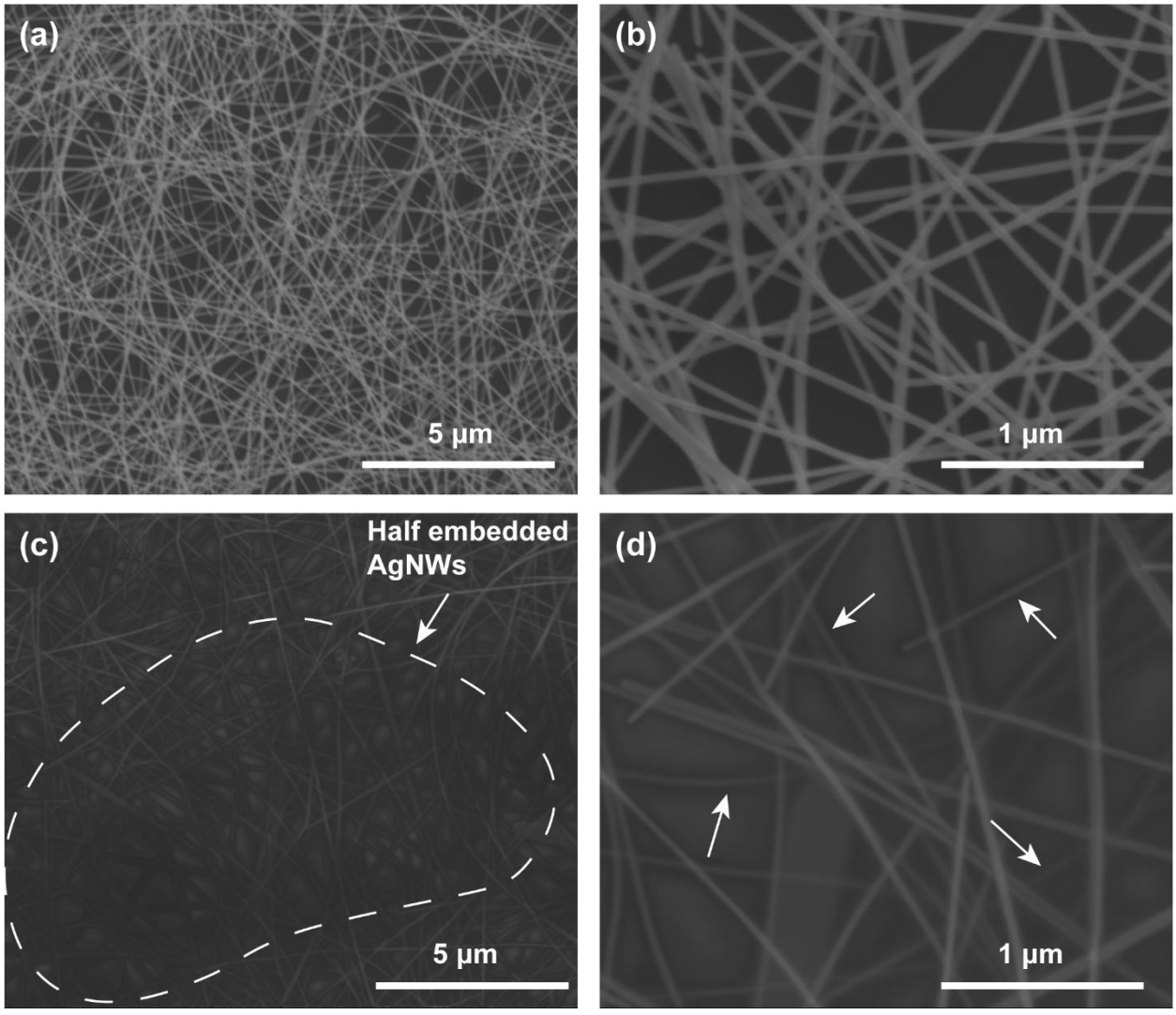

Figure 4-3. SEM image of spray-printed AgNW electrode on a glass substrate (a,b) and being embedded in BSEP substrate (c,d). The arrows in (d) indicate representative AgNWs that are half-embedded in BSEP.

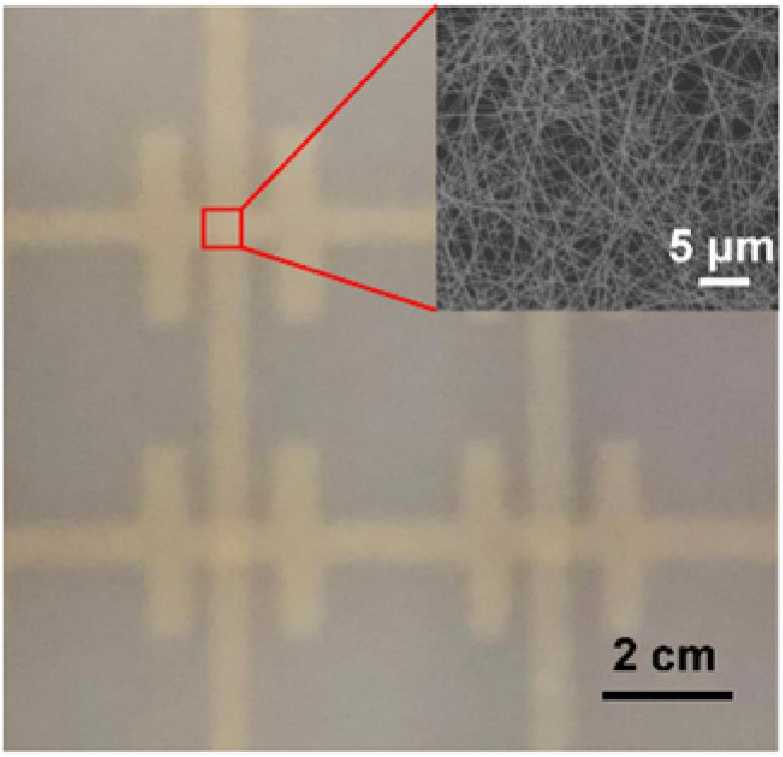

Figure 4-4. An optical microscope image of silver nanowires patterned into antenna-shaped electrode by spray-printing. The inset is the SEM image showing AgNW network structure.

The ANSYS finite element analysis (FEA) was performed to seek and optimize vital structural parameters of the sensor device. The 3D structural model was generated using computer aided design software SolidWorks. After inputting the model to ANSYS Electronics Desktop suite and assigning corresponding materials properties, ANSYS Q3D analysis module was executed to calculate capacitance between adjacent electrodes. Briefly, the calculation process involves the following steps: (1) set a 1 volt potential on one of the conductive bodies and set all other conductive bodies to 0 volt (ground); (2) calculate spatial potential using Laplace's equation; (3) find electrical field from the calculated potential using gradient operation; (4) find total charges between each electrode pair using Gauss' law; (5) find capacitance value

based on C=Q/V; (6) Repeat steps 1-5 for all conductive bodies to compute full capacitance matrix. We evaluated influences of electrode pattern design, BSEP layer thickness and simulated human finger on capacitance values, and compared simulation results to experimentally measured values.

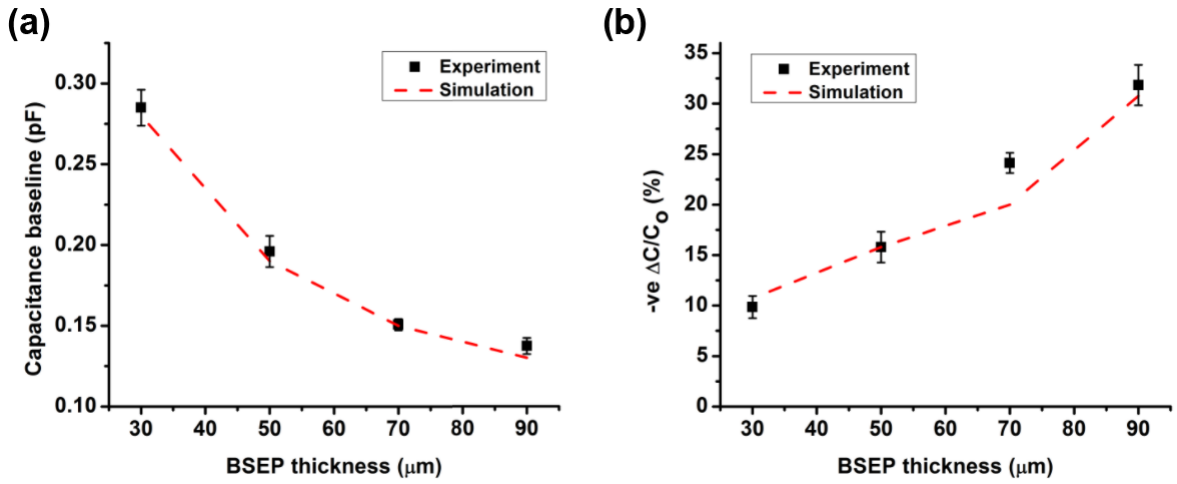

Figure 4-5. Capacitance baseline (a) and touching sensitivity (b) comparison of devices with different BSEP dielectric layer thickness (30 – 90 μm).

As a capacitive touch sensor, one of the most important parameters that impacts sensing performance is the thickness of the BSEP dielectric layer between R_X and T_X electrodes. Thus, sensor devices with BSEP thickness varied from 30 to 90 μm were fabricated, their capacitances were characterized with an LCR meter (E4980A, Agilent, Technologies, Santa Clara, CA). Figure 4-5a and 4-5b show the experiment data and simulation results of capacitance baseline (C_o) and change in the device capacitance as a function of thickness. Experimental results match the simulation data extremely well. When the ASE is untouched, the C_o decreases with increasing BSEP thickness (t), which can be explained by the less charges shared between R_X and T_X for thicker BSEPs.[27] The sensitivity (-ve $\Delta C/C_o$), however, increases with increasing t. This is due to the amount of charge transferred remaining stable for different t. Co is inversely proportional to t. Thus, the sensitivity, equal to the change in capacitance divided by the capacitance

baseline, increases with increasing *t*. Theory is verified by the simulation results shown in Figure 4-6, in which the changes in capacitance with touch (C_o - C) of sensors with different BSEP thicknesses are characterized. For different *t*, the value of $C_o - C$ remains constant. Based on the above-mentioned results, we have chosen 90 μm thick BSEP layer to fabricate the device. We chose not to increase *t* for even higher sensitivity due to our desire to ease the Joule heating challenge during the softening process (thermal mass at reasonably small value to achieve fast heating rate). The representative sensor highly sensitive device possesses a C_o of 0.13 pF and a change of 31% in capacitance.

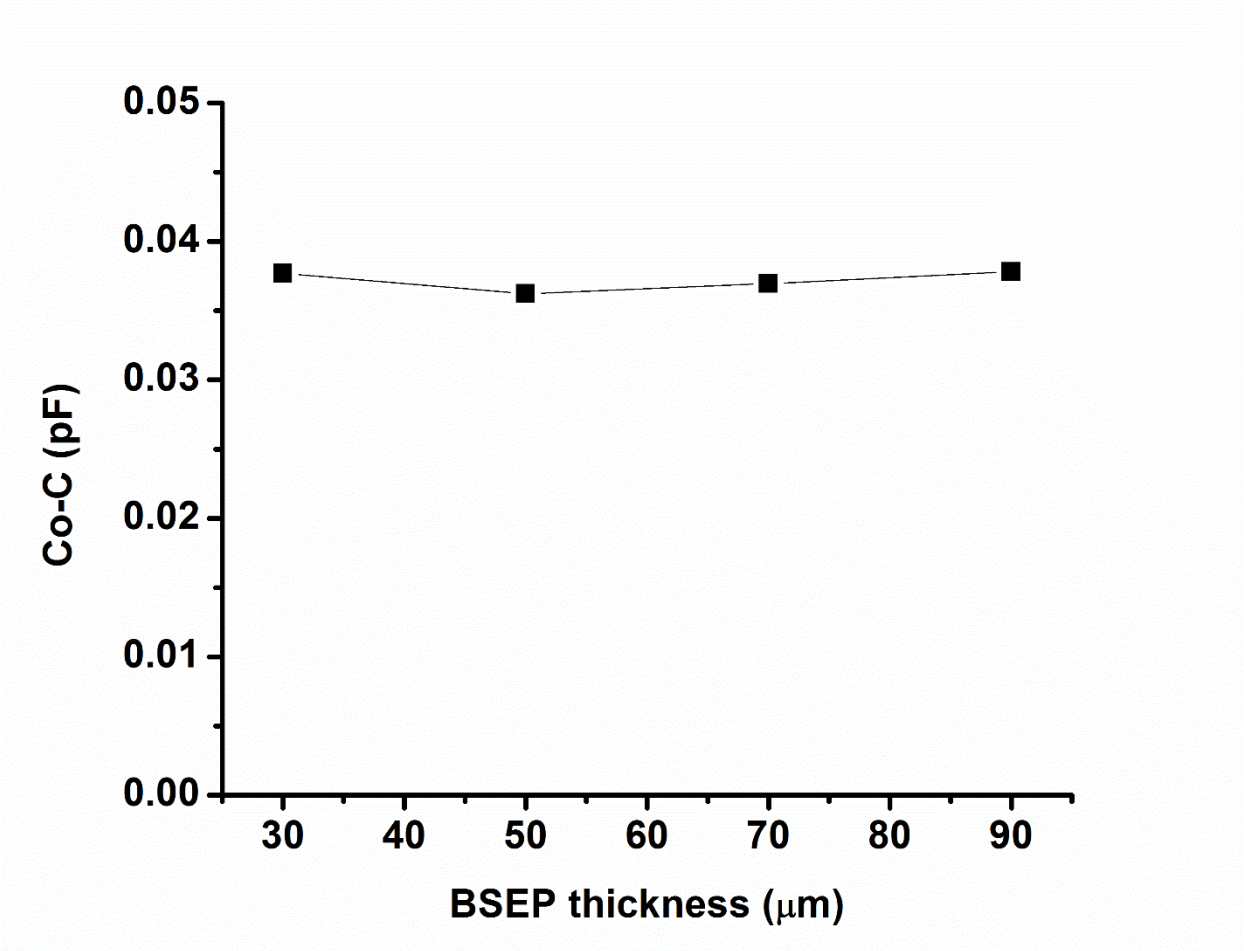

Figure 4-6. The change of capacitance with touch for sensors with different BSEP thicknesses.

Contactless sensing is important for devices that require remote control. One way to characterize that is through proximity detection. As shown in Figure 4-7 inset, measurements were carried out by vertically moving the finger through an elevator stage with the sensor at a fixed position with the corresponding device capacitances as a function of BSEP thicknesses recorded. Figure 4-7 shows the sensitivity as a function of distance between finger and device surface. Sensors with 70 μm and 90 μm BSEP thickness demonstrate sensitivity greater than 10% at hovering distance smaller than 0.5 cm. The changes in capacitances fall off significantly when the finger moves further than 1 cm from the surface. As the BSEP thickness increases, the sensitivity increases as well, which corresponds with the previous results shown in Figure 4-5. For the 90 μm BSEP device, the most sensitive of all thicknesses, the change in capacitance is still significant with a value of 10%, even at a 2 cm distance.

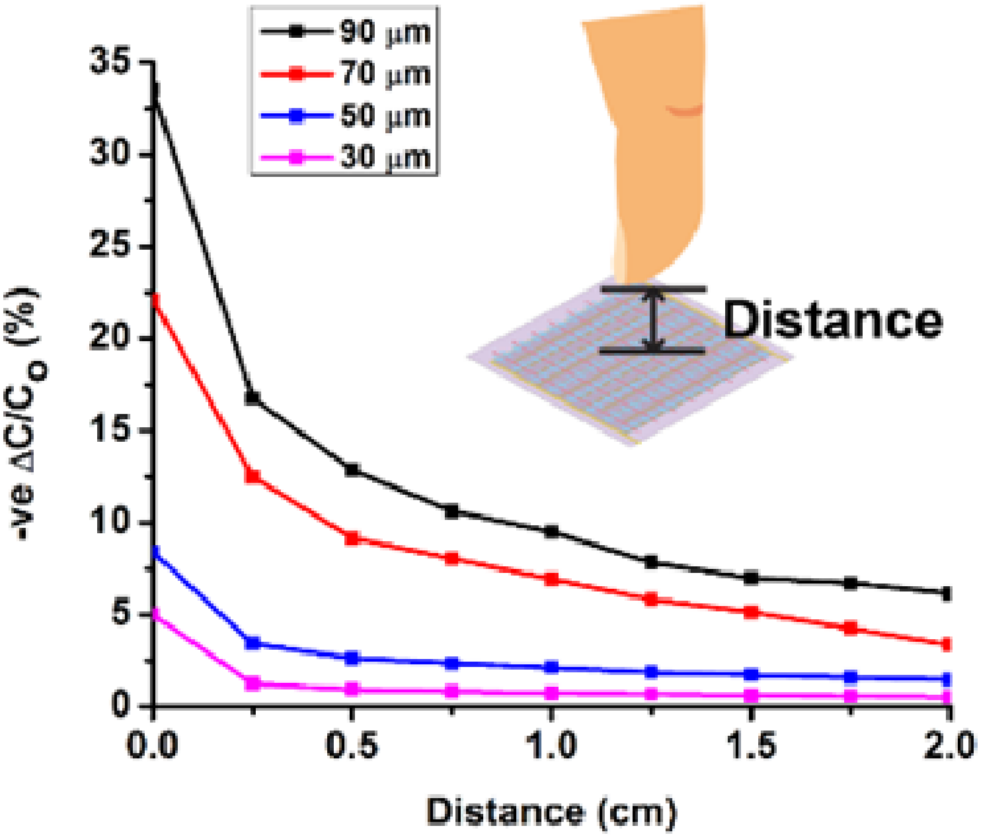

Figure 4-7. Proximity test of sensor devices with different BSEP thickness.

As a conformable touch sensor, the device may conform to surfaces with different curvatures; for example, the surface of a cup, a forearm, and a pen. To determine the stability of sensing to bending we measured the capacitance of the device with different bending radii (Figure 4-8). As shown in the Figure 4-8 inset, the BSEP sensor was softened and wrapped around metal bars with the radius varying from 10 to 1 mm. Then, the capacitance was recorded after the BSEP cooled down to room temperature. The device displayed a very consistent capacitance and sensitivity curve with various bending radii, which guarantees a reliable performance when conformed to arbitrary surfaces. After the tests, the capacitance perfectly recovered after BSEP returned to its original flat state. Moreover, the Joule heating electrode is used as ground plane, which shields electrical field coupling between sensor electrode and substrate materials.

Therefore, our sensor shows identical properties, which are independent when different substrate materials area used.

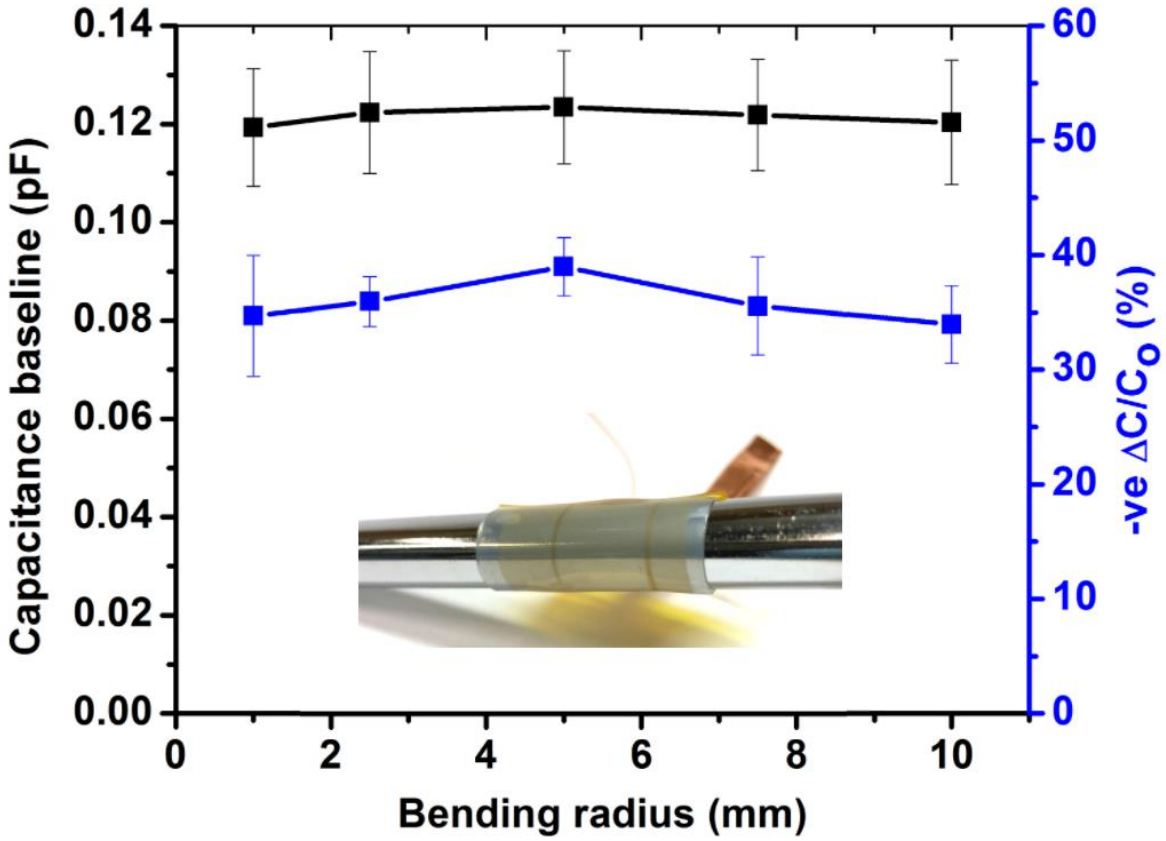

Figure 4-8. Sensing performance behavior of the device with 90 μm BSEP thickness under different bending radii.

A capacitive touch sensor with good sensibility and reliability, structured as an 8 × 8 matrix, was then fabricated for touch-sensing visualization. The lateral position of a finger can be detected on the basis of the capacitance changes observed in the sensor matrix (as shown in Figure 4-9). When a finger approaches the surface of the sensor, the fringing electric field generated from the ASE design is absorbed resulting in capacitance reduction. Such local capacitance change can be measured individually at each taxel. When

the finger reaches the interface, it yields up to 30% decrease in capacitance at the taxels being activated (Figure 4-9).

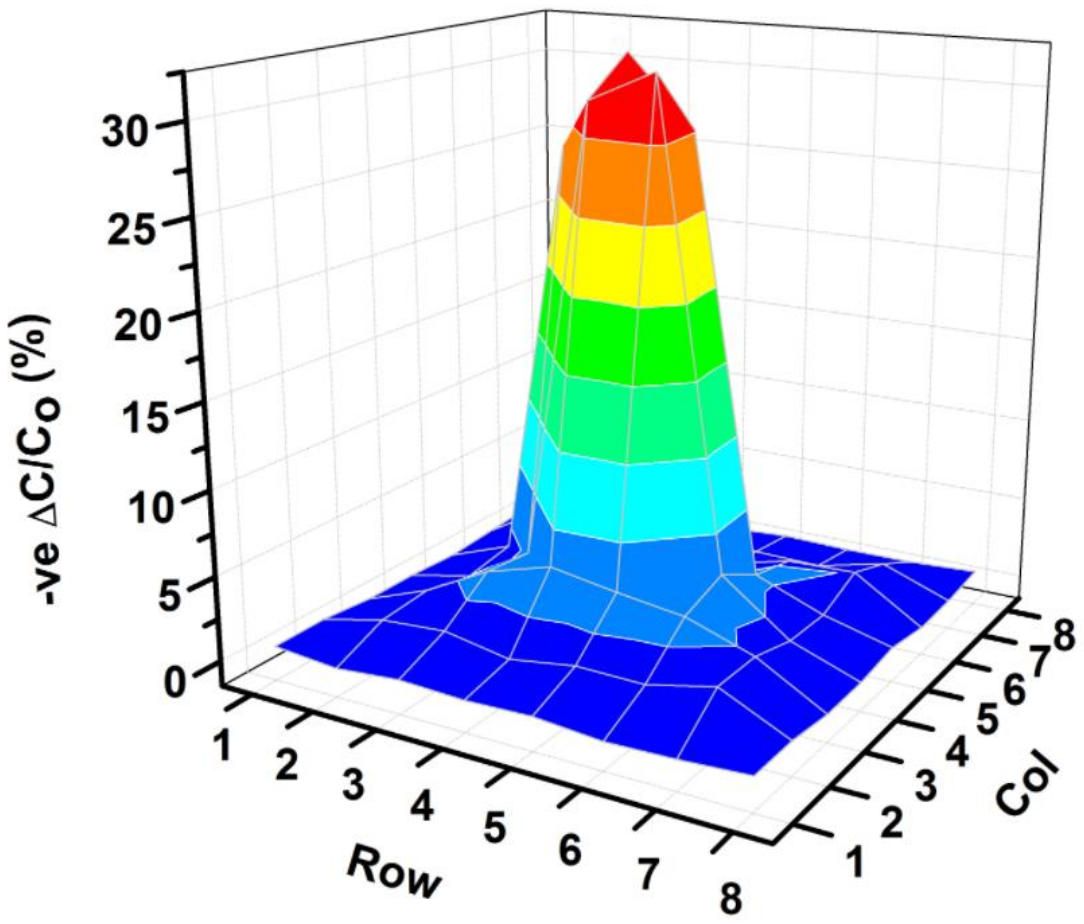

Figure 4-9. Capacitance map showing the localized change in capacitance due to local finger touch input.

4.3.3 Joule heating electrode

Ununiform heating and stiffness impedance of the Joule heating electrode can affect the compliancy of the smart skin sensor. It is essential to develop a heating electrode that is compliant and can generate uniform heat over a relatively large area. We selected CNT as the main Joule heating electrode material, thanks to the nanotube's large length-to-diameter aspect ratio that forms highly compliant networks. Traditional blanket-coated Joule heating requires a thick layer of CNT to obtain low surface resistance for low-voltage activation, but a thick coating would induce significant stiffness increase and impede electrode deformation.[32] Serpentine architecture is widely explored as an effective approach to impart electronic device compliance.[17,23] However, in a Joule heating electrode with active area as large as 40 × 40 mm the total length of the serpentine path may be too long to achieve low resistance for low voltage activation. Moreover, uniform heating often requires a high quality CNT coating that can increase the fabrication difficulty.[33,34] To overcome these issues, we combined the screen-printed interdigitated silver electrode with CNT for low surface resistance, low mechanical impedance, and uniform heating (Figure 4-10a). The combination of an interdigitated silver electrode with blank-coated CNT largely reduces the difficulty in fabrication and increases reproducibility of the Joule heating electrode to generate uniform heating over a large area.

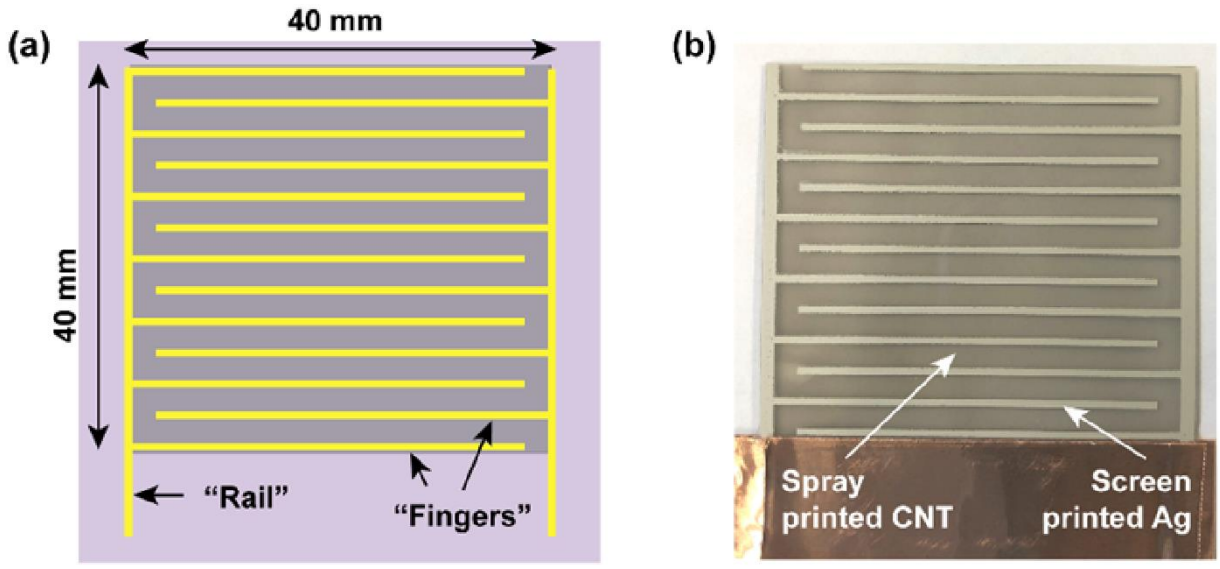

Figure 4-10. Schematic (a) and picture (b) of an ID-Ag/CNT electrode.

The electrode pattern design is critical for efficient Joule heating. To achieve uniform and high-efficiency heating with low stiffness constraint, we fabricated the ID-Ag/CNT electrode. Using the silver electrode with interdigitated pattern results in uniform heating over large surface area (Figure 4-10a). This is due to interdigitated pattern forming a uniform gap between neighbored "fingers" resulting in highly controlled potential difference across each pair. This approach effectively overcomes the current crowding phenomenon that can significantly deteriorate heating uniformity. The screen-printed ID-Ag electrodes contain sharp edges and have uniform and well-defined line widths (Figure 4-10b). The printed lines were continuous with no voids. The resistances of the ID-Ag electrode from the end of the "rail" to the end of "fingers" were measured to be relative consistent with value of $3 \pm 0.2\ \Omega$. This value determines uniform heating if the CNT resistance between two adjacent Ag "fingers" is much larger than $3\ \Omega$, which is easily achieved for carbon-based electrode materials. The ID-Ag only covers 20% of the active area, which limits the stiffness impedance it may bring due to the relatively rigid silver electrode. The storage modulus of the BSEP substrate with embedded ID-Ag/CNT increases from 142 to 322 MPa in the rigid state and 46

to 108 kPa in the soft state (Figure 4-11), which is still small for targeted applications. The use of ID-AG/CNT, however, decreases the amount of CNT used to four times less (compare to serpentine-patterned electrode[23]), resulting in a resistance below 50 Ω. The interdigitated silver may possess anisotropic mechanical stiffness. However, due to the small thickness of ID-Ag/CNT as well as the small difference in anisotropy, it won't have much impact on the device compliance. As demonstrated in Figure 4-1d-f, the device was conformed on surfaces with different orientations.

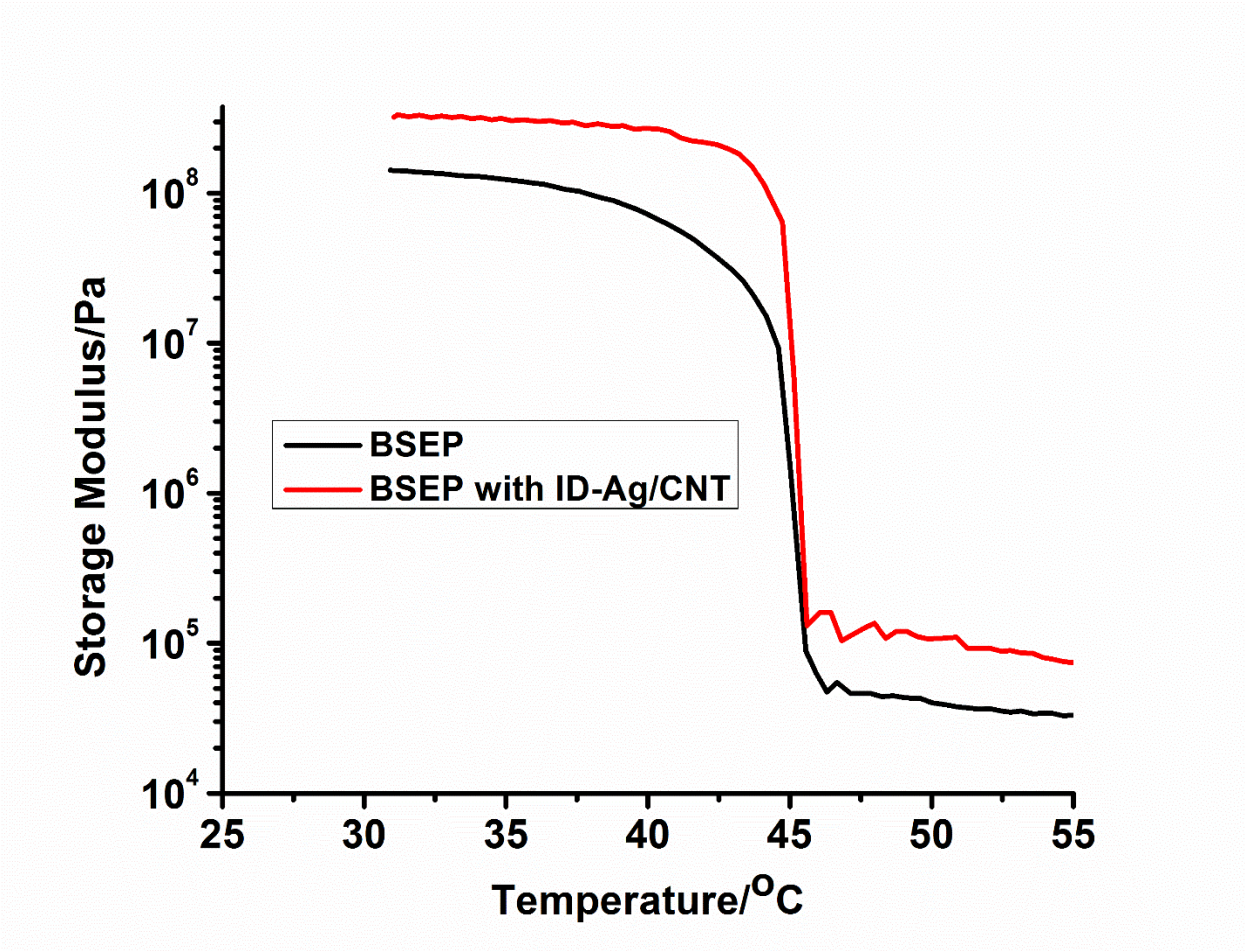

Figure 4-11. Storage modulus versus temperature curves of pristine BSEP and BSEP with ID-Ag/CNT electrode. The temperature was scanning from 30 to 55 °C at 2 °C/min.

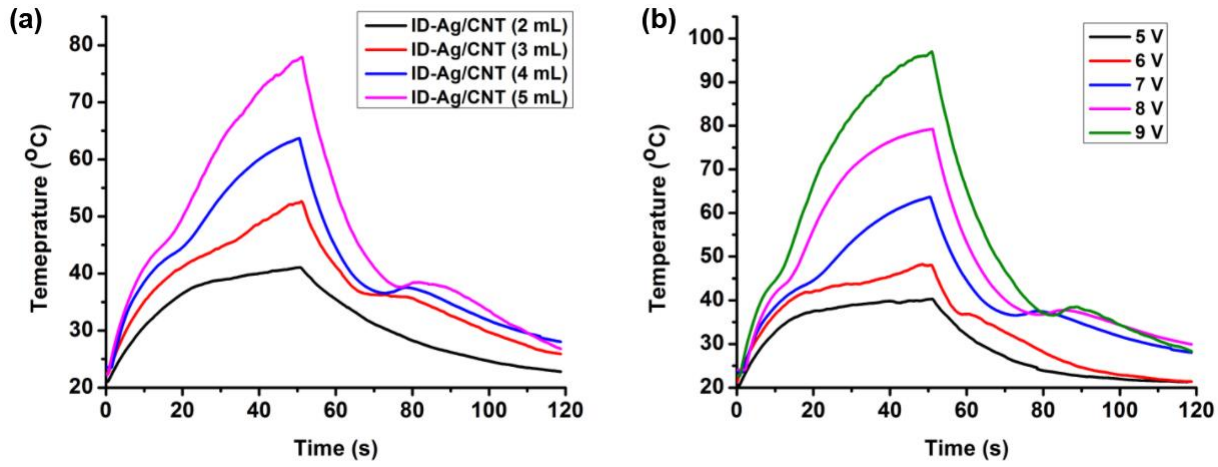

Figure 4-12. (a) Temperature as a function of time for devices with different amount of spray-printed CNT under applied voltage of 7 V. The temperature was characterized as an average temperature of the electrode active area (40 × 40 mm). (b) Temperature profile of ID-Ag/CNT (4 mL) under different voltage supplied.

A key parameter determining ID-Ag/CNT electrode heating performance is the amount of CNT sprayed on ID-Ag. Thus, electrodes with different CNT concentrations were fabricated and their Joule heating characteristics under 7 volts DC were investigated (Figure 4-12a). The temperature was recorded as the average temperature of the device active area. During the tests, the voltage was on for 50 s, then turned off. The temperature vs time profiles were captured by IR camera (FLIR T640). As the amount of CNT increases, resistance decreases and the heating rate increases. Based on the temperature profiles, the efficiency of the device heating performance (E) can be calculated as

$$E = \frac{Q_{out}}{W_{in}} \quad (1)$$

where Q_{out} is the thermal energy generated by ID-Ag/CNT, W_{in} is the electrical energy input. The results were shown in Table 4-1. Q_{out} is defined as

$$Q_{out} = m \times c \times \Delta T \quad (2)$$

where m is the mass of the device (230 μm thick BSEP with ID-Ag/CNT electrode), c is the specific heat of BSEP, ΔT is the change in temperature during the heating process. BSEP specific heat was calculated from differential scanning calorimetric (DSC) curves by integrating the area under the endothermic curve (Figure 4-13), 3.17 $Jg^{-1}\,°C^{-1}$. The electric energy input W_{in} was calculated by

$$W_{in} = \frac{U^2}{R} \times t \quad (3)$$

where U is the applied voltage (7 V), R is the resistance of the corresponding ID-Ag/CNT electrode, t is the working time (50 s). Based on the aforementioned calculations, the ID-Ag/CNT (4 mL) demonstrates highest efficiency of 67.2%, so it was chosen to be used in following experiments.

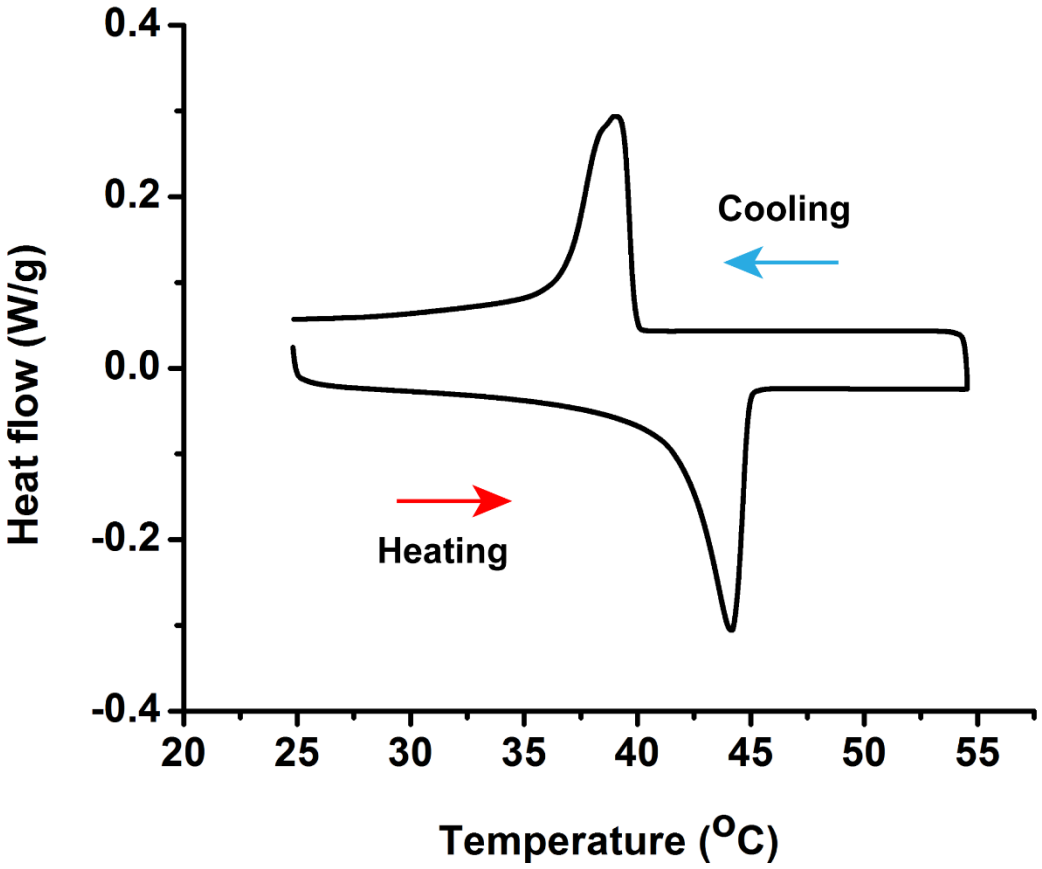

Figure 4-13. DSC diagram of phase-changing BSEP during heating and subsequent cooling. The scanning rate was 1 °C/min.

Table 4-1. Heating performances of ID-Ag/CNT electrodes with different amount of CNT.

	ID-AG/CNT (2 ML)	**ID-AG/CNT (3 ML)**	**ID-AG/CNT (4 ML)**	**ID-AG/CNT (5 ML)**
R [Ω]	46.71	34.25	26.13	15.95
W_{IN} [J]	53.2	73	94.7	157.1
T_R [°C/MIN]	23.7	35.3	47.7	65.3
Q_{OUT} [J]	31.7	47.6	63.6	88.1
EFFICIENCY [%]	59.6	65.2	67.2	56.1

Joule heating characteristics of the ID-Ag/CNT (4 mL) electrode under different voltages were investigated and the results are illustrated in Figure 4-12b. The electrode appears at a high heating rate, considering the large active area and thick BSEP substrate. During heating, most of the curves (7 - 9 V) exhibit an inflection point at approximately 45 °C, the nanocrystalline melting point of BSEP. The complete softening (above 47 °C) could be obtained in less than 15 s at voltage as low as 7 V. In the cooling step, an inflection point appears at similar temperature range for those curves, indicating recrystallization of the BSEP. Stiffening of the device can be completed within 30-40 s depending on the maximum temperature or the activation voltage. We have chosen 7 V to be the activation voltage to drive the device because it is the lowest voltage required to efficiently soften the BSEP while producing a gentle upward-temperature within the comfort of human perception.

The heating uniformity of ID-Ag/CNT was also characterized by recording the temperature profiles of five different spots (1 in the center of device and 4 on device corners) in the active area (Figure 4-14a). The 5 spots show similar heating profile with negligible differences. The heating and cooling performance of ID-Ag/CNT on BSEP substrate can be seen in Figure 4-14b.

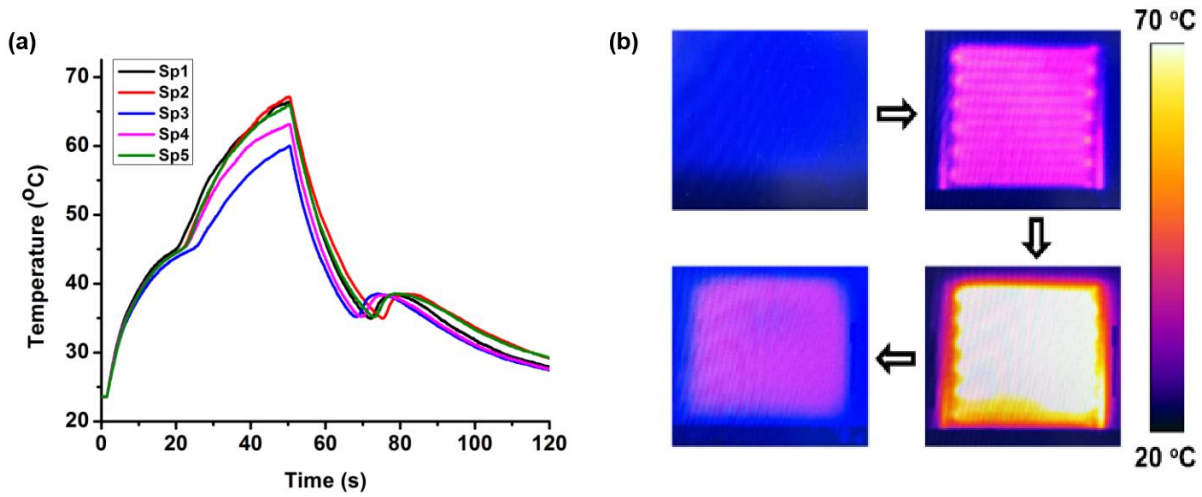

Figure 4-14. (a) Heating uniformity infrared camera characterization of ID-Ag/CNT (4 mL) under 7 V by recording temperature profiles of 5 different spots on the electrode. The spots are shown as cross marks in the IR image inset. (b) Infrared images of ID-Ag/CNT (4 mL) electrode in the heating and cooling steps.

4.4. Conclusions

In summary, a highly sensitive capacitive touch sensor with the ability to self-conform was designed and fabricated. The sensor electrodes comprise highly conductive AgNWs patterned in antenna shape for effective fringing field coupling. The resulting sensor device exhibits large capacitance change of 31% with touch and good proximity detection with 10% of capacitance change at distance of 2 cm. Due to the strong bonding between AgNW electrodes and BSEP substrate, the device demonstrates stable sensing performance at bend radii to 1 mm. The compliant ID-Ag/CNT Joule heating electrode shows stable and uniform heating over an active area of 40 × 40 mm. The low active voltage of 7 V and fast heating rate of 47.7 °C/min produces an ID-Ag/CNT electrode with efficiencies as high as 67.2%. The developed process demonstrates a low-cost, repeatable, and efficient method of fabricating multi-layer electronics. The

integrated multifunctional device mimics the sensing and adaptiveness of human skin and has the potential to be used in areas such as wearable electronics and smart skin for next generation robotics.

4.5. Reference

(1) Tobin, D. J. Biochemistry of Human Skin - Our Brain on the Outside. *Chemical Society Reviews*. 2006.

(2) Dahiya, R. S.; Metta, G.; Valle, M.; Sandini, G. Tactile Sensing-from Humans to Humanoids. *IEEE Trans. Robot.* **2010**.

(3) Hu, W.; Niu, X.; Zhao, R.; Pei, Q. Elastomeric Transparent Capacitive Sensors Based on an Interpenetrating Composite of Silver Nanowires and Polyurethane. *Appl. Phys. Lett.* **2013**, *102* (8), 0–5.

(4) Kang, M.; Kim, J.; Jang, B.; Chae, Y.; Kim, J. H.; Ahn, J. H. Graphene-Based Three-Dimensional Capacitive Touch Sensor for Wearable Electronics. *ACS Nano* **2017**.

(5) Yamada, T.; Hayamizu, Y.; Yamamoto, Y.; Yomogida, Y.; Izadi-Najafabadi, A.; Futaba, D. N.; Hata, K. A Stretchable Carbon Nanotube Strain Sensor for Human-Motion Detection. *Nat. Nanotechnol.* **2011**, *6* (5), 296–301.

(6) Pang, C.; Lee, G. Y.; Kim, T. Il; Kim, S. M.; Kim, H. N.; Ahn, S. H.; Suh, K. Y. A Flexible and Highly Sensitive Strain-Gauge Sensor Using Reversible Interlocking of Nanofibres. *Nat. Mater.* **2012**.

(7) Park, S.; Kim, H.; Vosgueritchian, M.; Cheon, S.; Kim, H.; Koo, J. H.; Kim, T. R.; Lee, S.; Schwartz, G.; Chang, H.; et al. Stretchable Energy-Harvesting Tactile Electronic Skin Capable of Differentiating Multiple Mechanical Stimuli Modes. *Adv. Mater.* **2014**.

(8) Lipomi, D. J.; Vosgueritchian, M.; Tee, B. C. K.; Hellstrom, S. L.; Lee, J. A.; Fox, C. H.; Bao, Z.

Skin-like Pressure and Strain Sensors Based on Transparent Elastic Films of Carbon Nanotubes. *Nat. Nanotechnol.* **2011**.

(9) Liu, Y.; Pharr, M.; Salvatore, G. A. Lab-on-Skin: A Review of Flexible and Stretchable Electronics for Wearable Health Monitoring. *ACS Nano* **2017**, *11* (10), 9614–9635.

(10) Chen, D.; Pei, Q. Electronic Muscles and Skins: A Review of Soft Sensors and Actuators. *Chemical Reviews*. 2017.

(11) Kim, D. H.; Rogers, J. A. Stretchable Electronics: Materials Strategies and Devices. *Adv. Mater.* **2008**.

(12) Kim, D. H.; Lu, N.; Ma, R.; Kim, Y. S.; Kim, R. H.; Wang, S.; Wu, J.; Won, S. M.; Tao, H.; Islam, A.; et al. Epidermal Electronics. *Science (80-.).* **2011**.

(13) Yeo, W. H.; Kim, Y. S.; Lee, J.; Ameen, A.; Shi, L.; Li, M.; Wang, S.; Ma, R.; Jin, S. H.; Kang, Z.; et al. Multifunctional Epidermal Electronics Printed Directly onto the Skin. *Adv. Mater.* **2013**.

(14) Suzuki, H. Nickel and Gold in Skin Lesions of Pierced Earlobes with Contact Dermatitis. A Study Using Scanning Electron Microscopy and x-Ray Microanalysis. *Arch. Dermatol. Res.* **1998**.

(15) Rus, D.; Tolley, M. T. Design, Fabrication and Control of Soft Robots. *Nature*. 2015.

(16) Gao, W.; Emaminejad, S.; Nyein, H. Y. Y.; Challa, S.; Chen, K.; Peck, A.; Fahad, H. M.; Ota, H.; Shiraki, H.; Kiriya, D.; et al. Fully Integrated Wearable Sensor Arrays for Multiplexed in Situ Perspiration Analysis. *Nature* **2016**.

(17) Lu, N.; Lu, C.; Yang, S.; Rogers, J. Highly Sensitive Skin-Mountable Strain Gauges Based Entirely on Elastomers. *Adv. Funct. Mater.* **2012**, *22* (19), 4044–4050.

(18) Araromi, O. A.; Rosset, S.; Shea, H. R. High-Resolution, Large-Area Fabrication of Compliant Electrodes via Laser Ablation for Robust, Stretchable Dielectric Elastomer Actuators and Sensors. *ACS Appl. Mater. Interfaces* **2015**.

(19) Huang, X.; Liu, Y.; Chen, K.; Shin, W. J.; Lu, C. J.; Kong, G. W.; Patnaik, D.; Lee, S. H.; Cortes, J. F.; Rogers, J. A. Stretchable, Wireless Sensors and Functional Substrates for Epidermal Characterization of Sweat. *Small* **2014**.

(20) Shull, K. R. Contact Mechanics and the Adhesion of Soft Solids. *Materials Science and Engineering: R: Reports*. 2002.

(21) Style, R. W.; Hyland, C.; Boltyanskiy, R.; Wettlaufer, J. S.; Dufresne, E. R. Surface Tension and Contact with Soft Elastic Solids. *Nat. Commun.* **2013**.

(22) Ren, Z.; Hu, W.; Liu, C.; Li, S.; Niu, X.; Pei, Q. Phase-Changing Bistable Electroactive Polymer Exhibiting Sharp Rigid-to-Rubbery Transition. *Macromolecules* **2016**, *49* (1), 134–140.

(23) Qiu, Y.; Lu, Z.; Pei, Q. Refreshable Tactile Display Based on a Bistable Electroactive Polymer and a Stretchable Serpentine Joule Heating Electrode. *ACS Appl. Mater. Interfaces* **2018**, *10*, 24807–24815.

(24) Yu, Z.; Yuan, W.; Brochu, P.; Chen, B.; Liu, Z.; Pei, Q. Large-Strain, Rigid-to-Rigid Deformation of Bistable Electroactive Polymers. *Appl. Phys. Lett.* **2009**, *95* (19), 21–24.

(25) Besse, N.; Rosset, S.; Zarate, J. J.; Shea, H. Flexible Active Skin: Large Reconfigurable Arrays of Individually Addressed Shape Memory Polymer Actuators. *Adv. Mater. Technol.* **2017**, *1700102*, 1700102.

(26) Yun, S.; Niu, X.; Yu, Z.; Hu, W.; Brochu, P.; Pei, Q. Compliant Silver Nanowire-Polymer Composite Electrodes for Bistable Large Strain Actuation. *Adv. Mater.* **2012**.

(27) Baxter, L. K. *Capacitive Sensors: Design and Applications*; 1996.

(28) Ma, S.; Ribeiro, F.; Powell, K.; Lutian, J.; Møller, C.; Large, T.; Holbery, J. Fabrication of Novel Transparent Touch Sensing Device via Drop-on-Demand Inkjet Printing Technique. *ACS Appl. Mater. Interfaces* **2015**.

(29) Liang, J.; Li, L.; Niu, X.; Yu, Z.; Pei, Q. Elastomeric Polymer Light-Emitting Devices and Displays. *Nat. Photonics* **2013**, *7* (10), 817–824.

(30) Lee, P.; Lee, J.; Lee, H.; Yeo, J.; Hong, S.; Nam, K. H.; Lee, D.; Lee, S. S.; Ko, S. H. Highly Stretchable and Highly Conductive Metal Electrode by Very Long Metal Nanowire Percolation Network. *Adv. Mater.* **2012**.

(31) Yun, S.; Niu, X.; Yu, Z.; Hu, W.; Brochu, P.; Pei, Q. Compliant Silver Nanowire-Polymer Composite Electrodes for Bistable Large Strain Actuation. *Adv. Mater.* **2012**, *24* (10), 1321–1327.

(32) Yuan, W.; Hu, L.; Yu, Z.; Lam, T.; Biggs, J.; Ha, S. M.; Xi, D.; Chen, B.; Senesky, M. K.; Grüner, G.; et al. Fault-Tolerant Dielectric Elastomer Actuators Using Single-Walled Carbon Nanotube Electrodes. *Adv. Mater.* **2008**, *20* (3), 621–625.

(33) Yoon, Y. H.; Song, J. W.; Kim, D.; Kim, J.; Park, J. K.; Oh, S. K.; Han, C. S. Transparent Film Heater Using Single-Walled Carbon Nanotubes. *Adv. Mater.* **2007**.

(34) Jung, D.; Kim, D.; Lee, K. H.; Overzet, L. J.; Lee, G. S. Transparent Film Heaters Using Multi-Walled Carbon Nanotube Sheets. *Sensors Actuators, A Phys.* **2013**.

Chapter 5. Conclusions and future directions

5.1. Summary of the dissertation

This dissertation focuses on the research of bistable electroactive polymer, a unique phase changing VSP that possesses sharp modulus change within narrow temperature band. The study covers important work on BSEP mechanical property optimization and novel devices based on BSEPs.

The work of material property exploration focuses on BSEP mechanical property and variable stiffness range improvement. It was achieved by incorporating bacterial cellulose nanofibers into BSEP matrix. The resulting dual-stimuli responsive composite adjust its stiffness via temperature induced phase transition by BSEP matrix and moisture induced water channels by cellulose network. With the augmentation of the twofold stiffness adjustment, the modulus of BSEP composite can be modulated by 25,000 times from nearly 1 GPa to 40 kPa. The stress strain response of the BC-BSEP composite was also engineered by introducing hydrogen bond interactions in the polymer network. The hydrogen bonds act as reversible crosslinkers that can significantly improve the toughness of the material.

BSEP finds its phenomenal application opportunity in refreshable dynamic tactile devices. A pneumatic tactile display with Braille standard resolution using a BSEP thin film and serpentine-patterned carbon nanotube (S-CNT) electrode was fabricated. The tactile pixels are diaphragm actuators that can be individually controlled to produce 0.7 mm out of plain deformation and greater than 50 g of blocking force by application of local heating and pneumatic pressure. The device can operate under low voltage supply (30 V) and has a lifetime of over 100,000 cycles without much performance degradation. This work could open a path to building compact, user friendly, and cost-effective tactile devices for a variety of important applications.

Another use of BSEP was proved as a highly sensitive capacitive touch senor with self-conformability function. The device combines the properties of shape memory polymer and touch sensor, which grants the sensor the ability of adapting on various surfaces and in different working conditions. The unique electrode pattern enables the sensor to have a capacitance change of 31% when touched with a baseline of 0.13 pF. The BSEP provides stiffness tunability via an embedded compliant heater. The stiffness of the device can be adjusted from several hundred MPa, for easy handling, to several tens of kPa, for conformal lamination. The efficient resistive heater provides uniform and stable heating over an area of 40 by 40 mm with a rate of 52 °C/min at voltage input as low as 7 V. The BSEP smart skin affords great working flexibility. This research strides forward on the road of merging intelligent polymeric systems into thin film electronics.

5.2. Future directions

The modified BSEP shows broad stiffness variation range from several tens of kPa to several GPa, which grants the material more application opportunities in areas like biomedicine, human-machine interface, and wearable electronics. As summarized in Table 1-1, most synthetic VSPs have their variable stiffness range cover the flexible (MPa) to rigid (GPa) region. The work depicted in this dissertation widened the stiffness range for synthetic VSP to cover the soft region, which may bring the BSEP more application opportunities in biomedical area.

An example would be a BSEP based cortical probe. Bio-inspired, dynamic smart materials have become the forefront of innovation for many medical devices. Traditional cortical probes are made from intrinsically rigid materials like silicon or polyimide for easy penetration into brain, which may cause inflammation, long term damage, and scar tissue generation. A material like BSEP, which has stiffness

tunability and is biocompatible, is ideal for use in neural implants. In the rigid state, the BSEP based cortical probe can be stiff enough to penetrate through the brain tissues. The physiological environment of human body will then soften the probe to match the mechanical property of brain, which reduces immune response and makes for more stable chronic recording.

Another possible direction would be utilizing BSEP as dielectric elastomer actuator (DEA). The biggest challenge of using DEA technology in any commercialized product is the high driving voltage of several kV. The improved BSEP system possesses ultra-low stiffness and high stretchability in the softened state, which shows the potential of lowering the driving voltage while obtaining large actuation strain. Thus, BSEP based DEA would be an interesting direction worth exploring.